

Development of Highly Water Permeable Robust PSQ-RO  
Membranes for Water Separation

(高透水性有機シリカ逆浸透水分離膜の開発)

September, 2022

Dian Zhang

Hiroshima University



## Contents

	Page
Chapter 1 General Introduction	1-15
Chapter 2 Development of PSQ-RO membranes for water desalination from tris[(ethoxysilyl) alkyl]amines by SG process and IP process	16-38
Chapter 3 Preparation of PSQ-RO membranes with hydroxyl groups by copolymerization of bis[3-(triethoxysilyl)propyl]amine and triethoxy(3-glycidyoxypropyl)silane	39-54
Chapter 4 Preparation of high water permeable PSQ-RO membranes by introducing hydroxyethylurea-based hydrophilic water channels	55-78
Chapter 5 Preparation of robust and high RO performance PSQ-RO membranes modified by SiO <sub>2</sub> nanoparticles	79-94
Chapter 6 Conclusions	95-96
List of Publication	97-98
Acknowledgments	99



## **General Introduction**

Water is a vital resource and the Earth's surface is covered by water to the tune of 71%. However, ninety-nine percent of that water are ground water, which is hard to utilize. Of the remaining 1%, surface water is considered to constitute 0.0067% of total water, which can be used as a water resource [1]. The global demand for freshwater is increasing and the freshwater usage from 1900 to 2015 was summarized in Figure 1.1 (Data from Global International Geosphere-Biosphere Programme (IGB)). As shown in Figure 1.1, global water use has increased approximately eight-fold in the last hundred years. However, limited water resources are becoming increasingly scarce, the most obvious manifestation of water scarcity is the fact that there are 785 million people who lack even basic access to clean drinking water. According to the statistics, there are approximately two billion people whose drinking water is contaminated with feces, which may cause diseases (2019, WHO). In addition, water supply systems are already challenged by climate change, increasing water scarcity, population growth, demographic changes, and urbanization. According to WHO, half of the world's population will live in lacking water areas by 2025. Except for drinking water, the lack of freshwater for irrigation is also a very serious issue. For example, producing one ton of rice need more than 1000 m<sup>3</sup> of water for irrigation. Therefore, developing effective tools for water purification is very important.

The development of efficient tools for water desalination is essential. Nowadays, various approaches for seawater desalination have been reported so far such as reverse osmosis (RO), electro dialysis (ED), multi-effect distillation (MED), etc. And RO process is the most effective and advanced technology which accounts for most desalination processes with 64% [2-4].

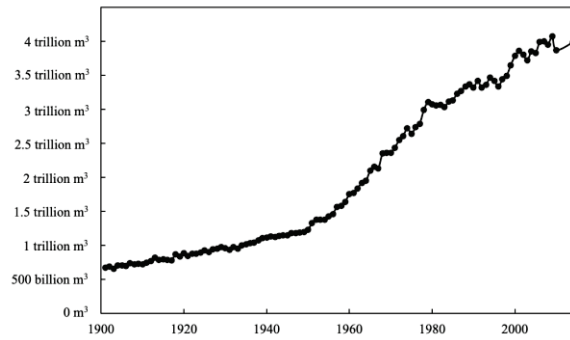


Figure 1.1. Global freshwater usage per year from 1900 to 2015, data from Global International Geosphere-Biosphere Programme (IGB)

The membrane separation is a technique for selectively separating molecules of different particle sizes at the molecular level through semi-permeable membranes, also known as a separation membrane or filter membrane. According to the pore size from large to small, membranes can be classified into microfiltration membrane (MF), ultrafiltration membrane (UF), nanofiltration membrane (NF), reverse osmosis membrane (RO). The applicable separation ranges of these membranes are shown in Figure 1.2. For water desalination applications, RO technology was widely used, in which reverse osmosis technology can be used to separate water from salt aqueous solution or remove atoms or some small organic molecules to yield pure water. In this work, the author will focus on the RO membrane separation technology.

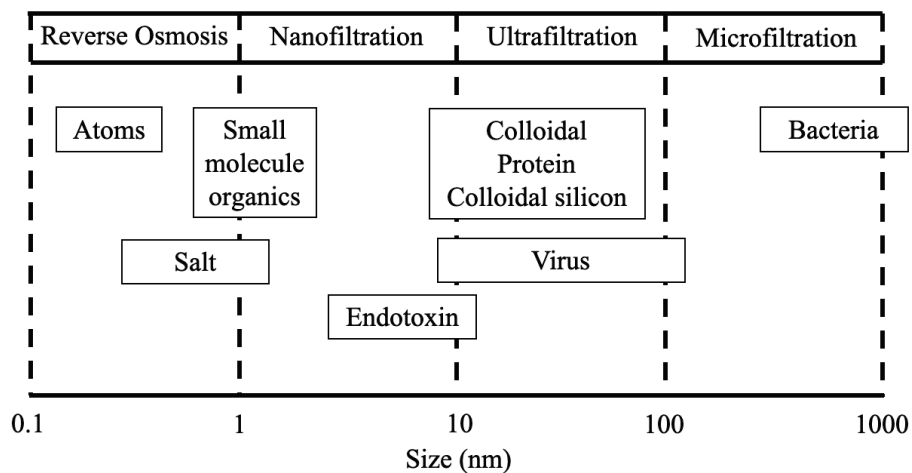


Figure 1.2. Applicable separation ranges of MF, UF, NF, RO technologies.

Reverse osmosis is a leading technology to purified water by using a semi-permeable membrane to remove salt ions and/or macromolecular, which works by using a high feed pressure on the saltwater side of the semi-permeable RO membrane and force the water across the membrane to yield pure water, as illustrated in Figure 1.3. Nowadays, Polyamide-based reverse osmosis membranes, which were prepared by interfacial polymerization with *m*-phenylene diamine and trimesoyl chloride. RO membranes based on polyamide is widely used for the industrial applications because of their high RO performance of high water permeability (water flux) and high salt rejection (salt selectivity). By 2000, the amount of desalinated water generated by reverse osmosis process was 65.5 million m<sup>3</sup>/day, which is 69 % of the volume of total amount. [5]

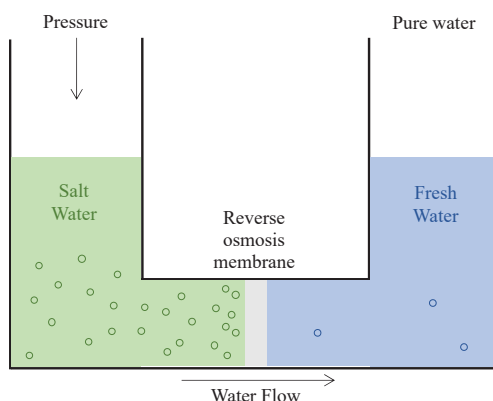


Figure 1.3. A simple diagram of the reverse osmosis process.

Although polyamide-based reverse osmosis membranes exhibit excellent separation properties, these membranes still present some problems, as illustrated in Figure 1.4. For example, because chlorine easily attacks the N-H group in the amide group [6-8], polyamide-based membranes commonly show poor chlorine resistance. However, the chlorine-containing solution (such as NaOCl aqueous solution) is conveniently used as an anti-fouling reagent to remove bacteria on the membranes. Therefore, the service life of polyamide-based RO membranes was limited. In addition, polyamide-based RO membranes generally exhibit low thermal stability, which has

limited their operation temperature (up to 45 °C) [9]. It has been demonstrated that many strategies have been developed to increase the thermal stability and chlorine resistance of polyamide-based membranes. For example, Ge and coworkers prepared polyamide-based membranes with high thermal stability and chlorine resistance by using g-C<sub>3</sub>N<sub>4</sub> nanosheets as nanofiller [10]. Zhang *et al.* prepared high chlorine-resistant polyamide-based RO membranes by modification with natural occurring  $\epsilon$ -poly-l-lysine [11]. Although many strategies have been reported to enhance the stability of polyamide-based membranes, improvement of their stability is still desired. Thus, the development of RO membranes with high thermal stability and high chlorine resistance is essential.

Polysilsesquioxanes (PSQs) with the chemical formula of [RSiO<sub>1.5</sub>], have been considered as robust materials due to the inorganic siloxane Si-O-Si networks possessing basic robustness, thus increasing the robustness and stability of PSQ-based materials [12-14]. A simple schematic of hydrolysis/condensation reactions of bridged trialkoxysilane precursors is shown in Figure 1.5. Organically bridged PSQs can be readily prepared via hydrolysis/condensation reactions of bridged trialkoxysilanes in the sol-gel (SG) process, to form a robust three-dimensional Si-O-Si network. Many applications of PSQ-based material have been reported. For example, Maeda and coworkers demonstrated that materials prepared by copolymerization of poly(3-aminopropyl)silsesquioxane and poly(3-(2-aminoethylaminopropyl)silsesquioxane) exhibited excellent antifogging ability [15]. Tsuru and coworkers developed PSQ gas separation membranes that exhibited high selectivity and excellent permeance [16-18]. In addition, other applications such as adsorbents, catalysts, and heat insulators were also explored [19-23].

Attributable to the robust and porous structure of PSQ-based materials, PSQ-based materials are suitable for RO membranes preparation and the studies of PSQ-RO membranes have been well examined and reported. Previously, Tsuru and coworkers first demonstrated that PSQ-RO membranes prepared by polymerized bis(triethoxysilyl)ethane (BTESE) via SG process exhibited a good salt rejection of



approximately 98 %. Although BTESE-based RO membranes exhibit low water permeability on the order of  $10^{-13}$   $\text{m}^3/\text{m}^2\text{sPa}$ . These membranes exhibit favorable stability that both treatments of these membranes with water bath at 90 °C for 3 hours, and 10 hours exposure by using 1000 ppm NaOCl aqueous solution resulted in no obvious changes in separation property, indicating the high robustness of these membranes [24]. In addition, it was reported that the PSQ-RO membranes of bis[(triethoxysilyl)propyl]amine (BTESPA) exhibited salt rejection of 96 %, and low water permeability of  $1.1 \times 10^{-13}$   $\text{m}^3/\text{m}^2\text{sPa}$  [25]. However, those PSQ-RO membranes exhibited water permeability on the order of  $10^{-13}$   $\text{m}^3/\text{m}^2\text{sPa}$ , which is approximately 10-folds lower than the average value of commercially available polyamide RO membranes ( $10^{-12}$   $\text{m}^3/\text{m}^2\text{sPa}$ ), although salt rejection was close to the polyamide-based membranes.

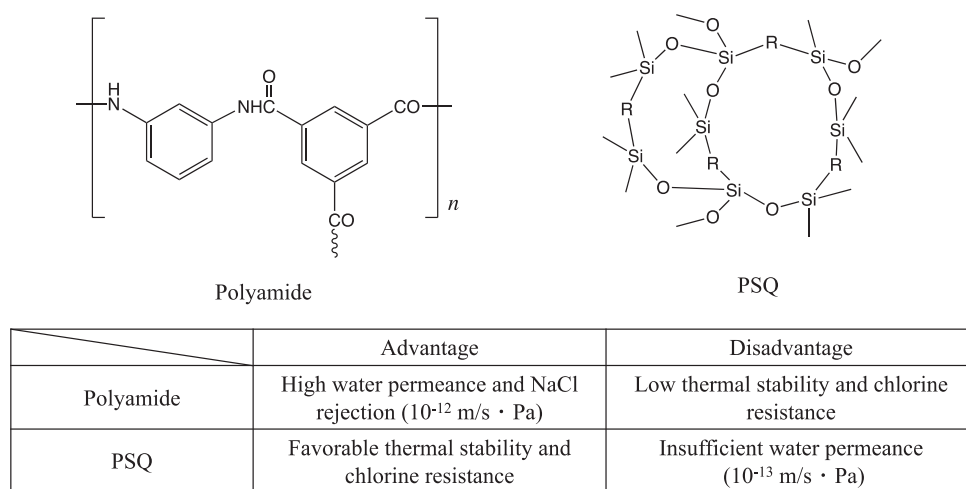


Figure 1.4. Advantages and disadvantages of polyamide-based RO membranes and PSQ-based RO membranes.

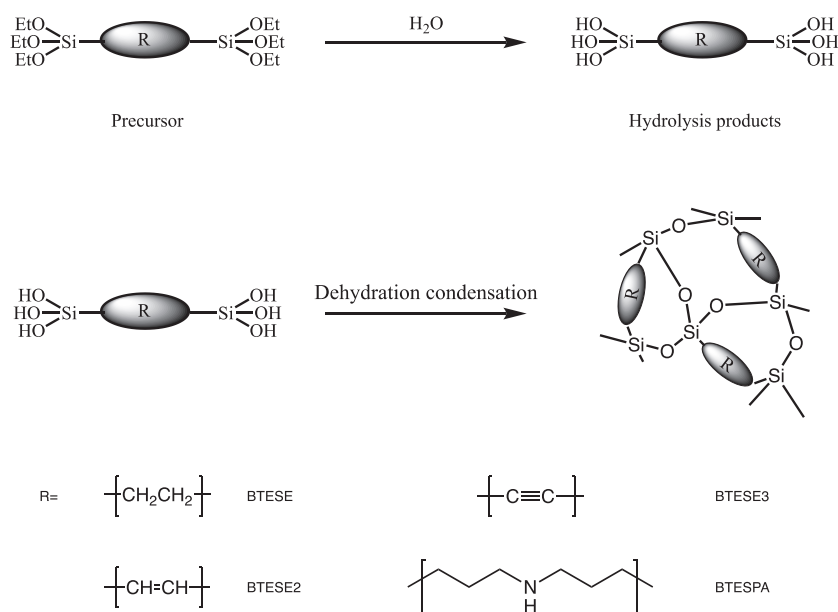


Figure 1.5. The hydrolysis/condensation reactions of bridged trialkoxysilanes.

Although organically bridged PSQ-RO membranes demonstrated favorable thermal stability and chlorine resistance, these membranes have remained insufficient for practical industrial use due to their poor water permeability. For improving the water permeability of PSQ-RO membranes, several strategies have been proposed in our previous works. It has been demonstrated that the introduction of rigid and polar bridged groups PSQ-RO membranes increases water permeability [14, 25, 26]. In contrast to BTESE-based membranes, bis(triethoxysilyl)ethene (BTESE2)- and bis(triethoxysilyl)ethyne (BTESE3)-based PSQ-RO membranes via the SG process exhibited higher water permeability, although salt rejection slightly decreased [27]. In addition, the other strategies to improve the water permeability of PSQ-RO membranes by the synthesis of polar and rigid bridged trialkoxysilane precursors has also been proposed in the past work (Figure 1.6 (a)). For example, Yamamoto *et al* synthesized 1,4-bis(triethoxysilylmethyl)1,2,3-triazole (BTESMAz) to introduce rigid and polar bridging units, and the BTESMAz-based membranes prepared by the SG process of this compound exhibited water permeability of  $3.7 \times 10^{-13} \text{ m}^3/\text{m}^2\text{sPa}$  and salt rejection of 95% [26], of which water permeability was approximately 3-fold higher than that of BTESE-based membranes. It was also demonstrated that RO membranes based on (2Z,4Z)-1,6-diacetoxy-3,4-bis(triethoxysilyl)hexa-2,4-diene (BTES-EAc) with a polar

acetoxymethyl group, exhibited water permeability of  $3.5 \times 10^{-13} \text{ m}^3/\text{m}^2\text{sPa}$  and salt rejection of 96% [28]. In addition, PSQ-RO membranes prepared from BTES-ED exhibited water permeability of  $1.7 \times 10^{-13} \text{ m}^3/\text{m}^2\text{sPa}$  and salt rejection of 98.5 % [29]. BTES-MOU- and BTES-POU-based RO membranes exhibited water permeability of  $2.6 \times 10^{-13} \text{ m}^3/\text{m}^2\text{sPa}$  and  $7.8 \times 10^{-14} \text{ m}^3/\text{m}^2\text{sPa}$ , and salt rejection of 90 % and 85 %, respectively [26].

Improvements in RO performance can also be achieved by copolymerization (Figure 1.6 (b)). For example, compared with BTESE-homo-based membranes, RO membranes prepared by copolymerizing precursors BTESE and hydroxymethyl(triethoxy)silane (HMTES) showed approximately three times improvement in water permeability [30]. The improvement in water permeability can be attributed to the introduction of hydroxyl groups, thereby increasing the hydrophilicity. Moreover, the copolymerization of BTESE2 with HMTES produced membranes with approximately seven times higher water permeability than those based on BTESE2 [31]. In addition, it has been reported that copolymer-based PSQ-RO membrane prepared from the copolymerization of BTESE and BTESPA, exhibited water permeability of  $1.3 \times 10^{-12} \text{ m}^3/\text{m}^2\text{sPa}$  and salt rejection of 92 % [32], and the copolymer RO membrane which prepared from BTESE and octakis(triethoxysilylethyl)-substituted POSS exhibited high water permeability of  $1.6 \times 10^{-12} \text{ m}^3/\text{m}^2\text{sPa}$  but low salt rejection of 86 %. However, the RO performance, especially the permeability, is still insufficient for practical applications. In this thesis, the author describes the preparation of new PSQ-based RO membranes for further improving the permeability with keeping the salt rejection at the level of practical applications, by applying new strategies including the design and synthesis of new precursors, the introduction of hydroxyl groups by in-situ ring opening reaction of epoxide and hydrophilic water channels, and the composite formation with  $\text{SiO}_2$  nanoparticles.

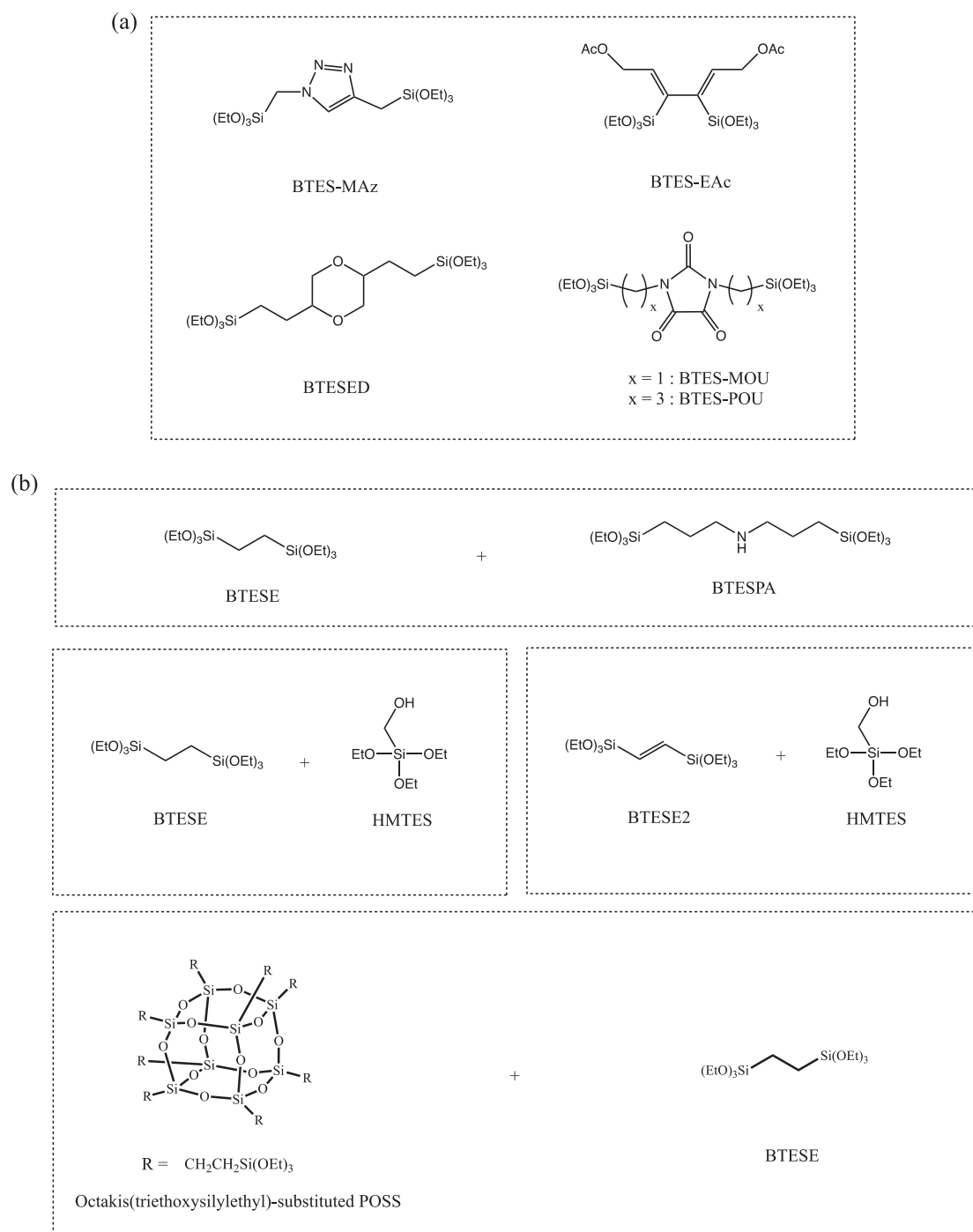


Figure 1.6. Structure of precursors for the preparation of (a) homopolymer-based RO membranes (b) copolymer-based RO membranes in the previous work.

In Chapter 2, the author examined tris[3-(triethoxysilyl)propyl]amine (TTESPA), tris[3-(diethoxymethylsilyl)propyl]amine (TDEMSPA), tris[(triethoxysilyl)methyl]amine (TTESMA) tris[(triethoxysilyl)propenyl]amine (TTESP2A), and tris[3-(triethoxysilyl)prop-2-ynyl]amine (TTESP3A) as new precursors for PSQ-RO membrane preparation by the sol-gel process and interfacial polymerization. It was found that a dense separation layer was formed by precursors with three reactive ethoxysilyl units. Of these, TTESPA-homo-based membranes which prepared by the interfacial polymerization gave the best RO performance of water permeance and salt rejection of  $7.3 \times 10^{-13} \text{ m}^3/\text{m}^2\text{sPa}$  and 95.6% respectively, which were close to the best RO performance of BTESE3-based membranes ( $8.5 \times 10^{-13} \text{ m}^3/\text{m}^2\text{sPa}$  and 95 %) in our previous work.

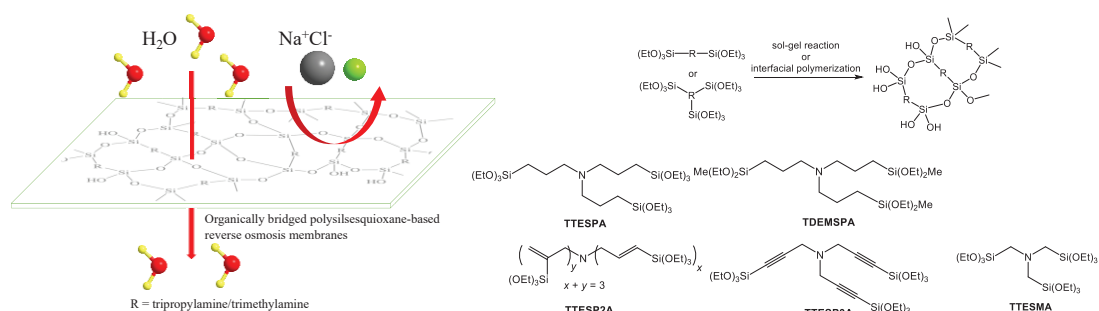


Chart 1.1. Schematic diagram of PSQ-RO membrane and precursors for membranes preparation, described in Chapter 1.

In Chapter 3, the copolymerization of BTESPA with triethoxy(3-glycidyloxypropyl)silane (TEGPS) for membrane preparation is described. It is demonstrated that epoxy groups in TEGPS would undergo a ring-opening reaction with the attack by the amine unit of BTESPA and form hydroxyl groups, which will significantly improve the water permeability. The RO experiments clearly indicated that the introduction of epoxy-containing monomer significantly improved RO performance, yielding excellent water permeability and high salt rejection of  $1 \times 10^{-12} \text{ m}^3/\text{m}^2\text{sPa}$  and 98%, respectively.

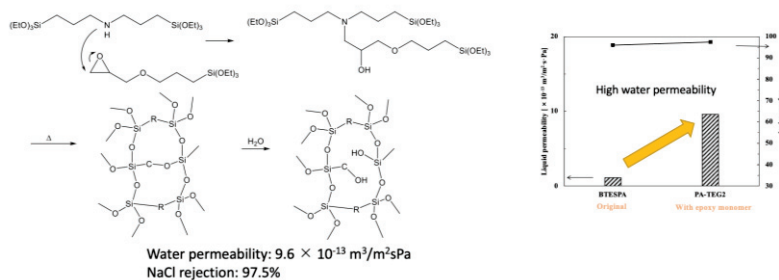


Chart 1.2. Schematic diagram of works described in Chapter 2.

In Chapter 4, the author copolymerized BTESPA with N-(2-hydroxyethyl)-N'-[3-(triethoxysilyl)propyl]urea (HETESPU), the RO results indicated that the water permeability was extremely improved approximately 19 times comparing to BTESPA homo based membrane ( $1.86 \times 10^{-12} \text{ m}^3/\text{m}^2\cdot\text{sPa}$ ), with salt rejection nearly unchanged (96%), which is the highest water permeability so far obtained from PSQ membranes that show higher than 90% salt rejection. The extreme improvement of water permeability is attribute to the aggregation of hydroxyethylurea units through hydrogen bonding in the PSQ layer to form hydrophilic water channels.

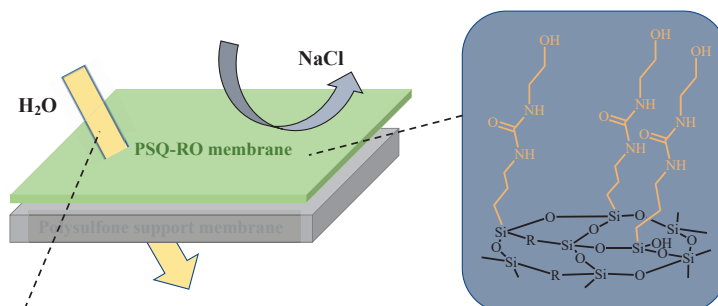


Chart 1.3. Schematic diagram of the aggregation of hydroxyethylurea units through hydrogen bonding, described in Chapter 3.

In Chapter 5, mixed matrix membranes (MMMs) were prepared by the introduction of nanoparticles into the PSQ separation layer. It was demonstrated that  $\text{SiO}_2$  nanoparticles provides additional surface area and micropores in the PSQ layer by filler effects, thus increasing the porosity and improving water permeability. It has been also demonstrated that the rigidity of the PSQ polymer chain was increased by the

interaction between SiO<sub>2</sub> nanoparticles and polymer, which results in the improvement of thermal stability. The author anticipated that the introduction of the robust and rigid inorganic SiO<sub>2</sub> nanoparticles would stabilize the PSQ chain by immobilization, thereby increasing the thermal stability of RO membranes.

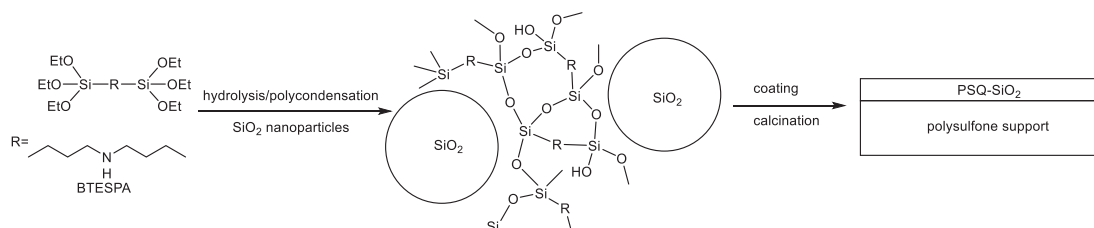


Chart 1.4. Preparation of SiO<sub>2</sub> nanoparticles modified PSQ-RO membranes, described in Chapter 4.

## Reference

- [1] C. Arqueros, F. Zamora, C. Montoro, A Perspective on the Application of Covalent Organic Frameworks for Detection and Water Treatment, *Nanomaterials*, 11 (2021), 1651.
- [2] M.S. Humoud, S. Roy, S. Mitra, Enhanced performance of carbon nanotube immobilized membrane for the treatment of high salinity produced water via direct contact membrane distillation, *Membranes*, 10 (2020), 325.
- [3] G. Folaranmi, M. Bechelany, P. Sistat, M. Cretin, F. Zaviska, Towards electrochemical water desalination techniques: a review on capacitive deionization, membrane capacitive deionization and flow capacitive deionization, *Membranes*, 10 (2020), 96.
- [4] R. Borsani, S. Rebagliati, Fundamentals and costing of MSF desalination plants and comparison with other technologies, *Desalination*, 182 (2005), 29-37.
- [5] E. Jones, M. Qadir, M.T. van Vliet, V. Smakhtin, S.-m. Kang, The state of desalination and brine production: A global outlook, *Sci. Total Environ.*, 657 (2019), 1343-1356.
- [6] M. Stolov, V. Freger, Degradation of polyamide membranes exposed to chlorine: an impedance spectroscopy study, *Environ. Sci. Technol. Lett.*, 53 (2019), 2618-2625.
- [7] R. Wang, Z.-X. Low, S. Liu, Y. Wang, S. Murthy, W. Shen, H. Wang, Thin-film composite polyamide membrane modified by embedding functionalized boron nitride nanosheets for reverse osmosis, *J. Membr. Sci.*, 611 (2020), 118389.
- [8] J. Xu, Z. Wang, X. Wei, S. Yang, J. Wang, S. Wang, The chlorination process of crosslinked aromatic polyamide reverse osmosis membrane: New insights from the study of self-made membrane, *Desalination*, 313 (2013), 145-155.
- [9] G.-D. Kang, C.-J. Gao, W.-D. Chen, X.-M. Jie, Y.-M. Cao, Q. Yuan, Study on hypochlorite degradation of aromatic polyamide reverse osmosis membrane, *J. Membr. Sci.*, 300 (2007), 165-171.



- [10] M. Ge, X. Wang, S. Wu, Y. Long, Y. Yang, J. Zhang, Highly antifouling and chlorine resistance polyamide reverse osmosis membranes with g-C<sub>3</sub>N<sub>4</sub> nanosheets as nanofiller, *Sep. Purif. Technol.*, 258 (2021), 117980.
- [11] X. Zhang, H. Huang, Q. Li, H. Yu, X. Tian, M. Zhao, H. Zhang, Facile dual-functionalization of polyamide reverse osmosis membrane by a natural polypeptide to improve the antifouling and chlorine-resistant properties, *J. Membr. Sci.*, 604 (2020), 118044.
- [12] S. Tsukada, Y. Nakanishi, T. Hamada, K. Okada, S. Mineoi, J. Ohshita, Ethylene-bridged polysilsesquioxane/hollow silica particle hybrid film for thermal insulation material, *RSC Advances*, 11 (2021), 24968-24975.
- [13] N. Ahmed, H. Fan, P. Dubois, X. Zhang, S. Fahad, T. Aziz, J. Wan, Nano-engineering and micromolecular science of polysilsesquioxane materials and their emerging applications, *Journal of Materials Chemistry A*, 7 (2019), 21577-21604.
- [14] K. Yamamoto, J. Ohshita, Bridged polysilsesquioxane membranes for water desalination, *Polym. J.*, 51 (2019), 1103-1116.
- [15] T. Maeda, T. Hamada, S. Tsukada, D. Katsura, K. Okada, J. Ohshita, Antifogging Hybrid Materials Based on Amino-Functionalized Polysilsesquioxanes, *ACS Applied Polymer Materials*, 3 (2021), 2568-2575.
- [16] T. Niimi, H. Nagasawa, M. Kanezashi, T. Yoshioka, K. Ito, T. Tsuru, Preparation of BTESE-derived organosilica membranes for catalytic membrane reactors of methylcyclohexane dehydrogenation, *J. Membr. Sci.*, 455 (2014), 375-383.
- [17] M. Takenaka, H. Nagasawa, T. Tsuru, M. Kanezashi, Hydrocarbon permeation properties through microporous fluorine-doped organosilica membranes with controlled pore sizes, *J. Membr. Sci.*, 619 (2021), 118787.
- [18] T. Mizumo, H. Muragishi, K. Yamamoto, J. Ohshita, M. Kanezashi, T. Tsuru, Preparation and separation properties of oxalylurea-bridged silica membranes, *Appl. Organomet. Chem.*, 29 (2015), 433-438.

- [19] L. Brigo, M. Faustini, A. Pistore, H.K. Kang, C. Ferraris, S. Schutzmann, G. Brusatin, Porous inorganic thin films from bridged silsesquioxane sol–gel precursors, *J. Non-Cryst. Solids*, 432 (2016), 399-405.
- [20] S. Yun, H. Luo, Y. Gao, Low-density, hydrophobic, highly flexible ambient-pressure-dried monolithic bridged silsesquioxane aerogels, *Journal of Materials Chemistry A*, 3 (2015), 3390-3398.
- [21] F. Zou, P. Yue, X. Zheng, D. Tang, W. Fu, Z. Li, Robust and superhydrophobic thiourethane bridged polysilsesquioxane aerogels as potential thermal insulation materials, *Journal of Materials Chemistry A*, 4 (2016), 10801-10805.
- [22] O. Esam, G. Zhou, A. Vasiliev, Bridged mesoporous silsesquioxanes as potential CO<sub>2</sub> adsorbents, *J. Sol-Gel Sci. Technol.*, 74 (2015), 740-747.
- [23] S. Inagaki, S. Guan, Y. Fukushima, T. Ohsuna, O. Terasaki, Novel mesoporous materials with a uniform distribution of organic groups and inorganic oxide in their frameworks, *Journal of the American Chemical Society*, 121 (1999), 9611-9614.
- [24] R. Xu, J. Wang, M. Kanezashi, T. Yoshioka, T. Tsuru, Development of robust organosilica membranes for reverse osmosis, *Langmuir*, 27 (2011), 13996-13999.
- [25] K. Yamamoto, S. Koge, K. Sasahara, T. Mizumo, Y. Kaneko, M. Kanezashi, T. Tsuru, J. Ohshita, Preparation of bridged polysilsesquioxane membranes from bis[3-(triethoxysilyl)propyl]amine for water desalination, *Bull. Chem. Soc. Jpn.*, 90 (2017), 1035-1040.
- [26] K. Yamamoto, M. Kanezashi, T. Tsuru, J. Ohshita, Preparation of bridged polysilsesquioxane-based membranes containing 1,2,3-triazole moieties for water desalination, *Polym. J.*, 49 (2017), 401.
- [27] R. Xu, S.M. Ibrahim, M. Kanezashi, T. Yoshioka, K. Ito, J. Ohshita, T. Tsuru, New insights into the microstructure-separation properties of organosilica membranes with ethane, ethylene, and acetylene bridges, *ACS Appl. Mater. Interfaces*, 6 (2014), 9357-9364.

- [28] K. Yamamoto, J. Ohshita, T. Mizumo, M. Kanezashi, T. Tsuru, Synthesis of organically bridged trialkoxysilanes bearing acetoxymethyl groups and applications to reverse osmosis membranes, *Appl. Organomet. Chem.*, 31 (2017), e3580.
- [29] K. Yamamoto, H. Muragishi, T. Mizumo, T. Gunji, M. Kanezashi, T. Tsuru, J. Ohshita, Diethylenedioxane-bridged microporous organosilica membrane for gas and water separation, *Sep. Purif. Technol.*, 207 (2018), 370-376.
- [30] K. Yamamoto, J. Ohshita, T. Mizumo, M. Kanezashi, T. Tsuru, Preparation of hydroxyl group containing bridged organosilica membranes for water desalination, *Sep. Purif. Technol.*, 156 (2015), 396-402.
- [31] F.-T. Zheng, K. Yamamoto, M. Kanezashi, T. Tsuru, J. Ohshita, Preparation of bridged silica RO membranes from copolymerization of bis(triethoxysilyl)ethene/(hydroxymethyl)triethoxysilane. Effects of ethenylene-bridge enhancing water permeability, *J. Membr. Sci.*, 546 (2018), 173-178.
- [32] D. Zhang, J. Ohshita, Preparation of robust RO membranes for water desalination by interfacial copolymerization of bis[(triethoxysilyl)propyl]amine and bis(triethoxysilyl)ethane, *Polym. J.*, 51 (2019), 1231-1234.

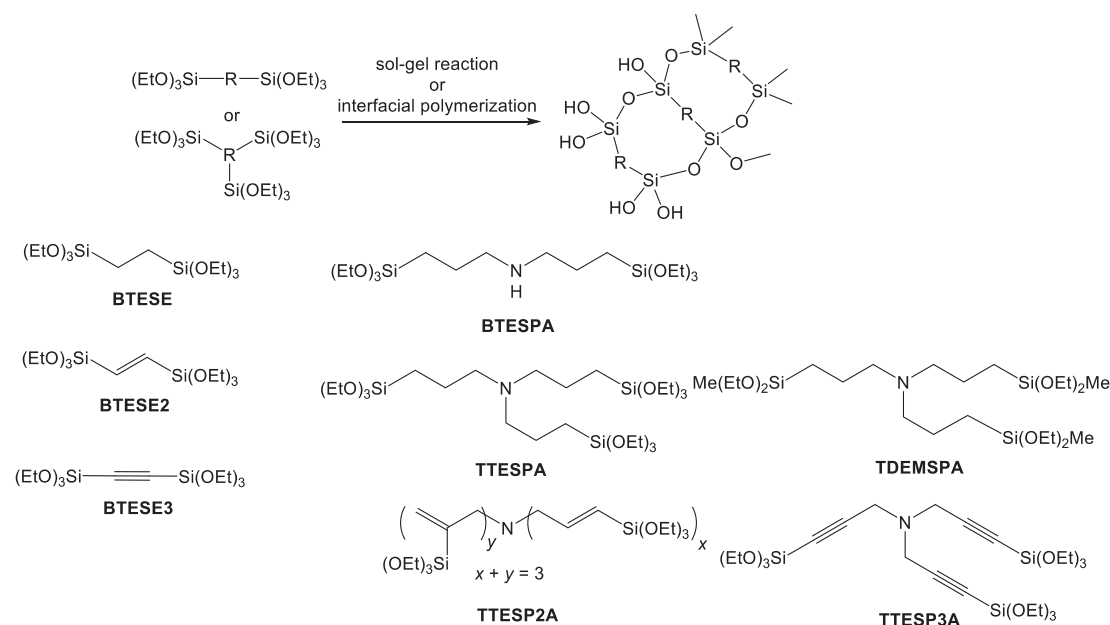
## Chapter 2 Development of PSQ-RO membranes for water desalination from tris[(ethoxysilyl) alkyl]amines by SG process and IP process

### Introduction

The sol-gel (SG) process has been the focus of continuous development for the synthesis of porous materials in the last two decades [1-3]. In the previous research, the SG process has been used for the preparation of PSQ-RO membranes. The SG process is a multistep process that includes sol solution preparation, coating of the sol particles on a support membrane substrate, and calcination of the coated substrate to convert the sol film into the gel. These procedures require exactly controlled sol particle size suitable for membrane preparation and optimization of the sol coating conditions and the calcination conditions. Recently, the interfacial polymerization process (IP) has been reported for the preparation of PSQ-RO membranes [4]. Compared with the SG process, IP is simple and efficient. PSQ-RO membranes prepared by the IP process exhibit RO performance close to that of membranes prepared by the SG process. For example, bis[3-(triethoxysilyl)propyl]amine (BTESPA)-based membranes prepared by the SG process and the IP exhibited the water permeability of  $1.1 \times 10^{-13}$  and  $1.4 \times 10^{-13}$  m<sup>3</sup>/m<sup>2</sup>sPa and NaCl rejection of 96 % and 93.6 %, respectively. However, only precursors containing a self-catalyzing amino group can be used in IP process. For example, bis(triethoxysilyl)ethane (BTESE)-based membranes prepared by the IP process in the presence of an acid catalyst showed only 57.3% NaCl rejection.

To further improve the RO performance of PSQ-RO membranes, the author designed and synthesized precursors with three reactive ethoxysilyl units, namely, tris[(triethoxysilyl)propyl]amine (TTESPA), tris[(diethoxymethylsilyl)propyl] amine (TDEMSPA), and tris[(triethoxysilyl)methyl]amine (TTESMA), and prepared RO membranes on polysulfone support membranes by the SG process and the IP process to obtain information of structure-performance relationship. It is also expected that these precursors with three reactive ethoxysilyl units would form dense RO membranes, thereby improving RO performance. The RO results exhibited that TTESPA-based membranes prepared by the SG process and the IP process exhibited favorable RO

performance. In addition, the author prepared tris[(triethoxysilyl)propenyl]amine (TTESP2A) and tris [3-(triethoxysilyl)prop-2-ynyl]amine (TTESP3A) as the precursors, in which rigid and polar ethenylene and ethynylene linkages were expected to improve RO performance of the resultant membranes, as observed for the BTESE2- and BTESE3-derived membranes [5].



Scheme 2.1. Structures of precursors in this chapter.

## Results and discussion

### Preparation of membranes

As the five precursors TTESPA, TDEMSPA, TTESMA, TTESP2A, and TTESP3A used for membrane preparation had different reactivities with water in the SG process, the author carefully optimized the molar ratio of water for the formation of sols with 1.6-2.0 nm particle size, which would be suitable to prepare RO membranes on the polysulfone support membrane (Nitto Denko NTR-7450) [6]. Figure 2.1 presents DLS particle size distribution for the sols obtained from 2 h treatment of TTESPA with 23 eq of water, TTESMA with 1.5 eq of water, TDEMSPA with 60 eq of water, TTESP2A with 10 eq of water, and TTESP3A with 10 eq of water, respectively, revealing the formation of sols with ideal particle sizes.

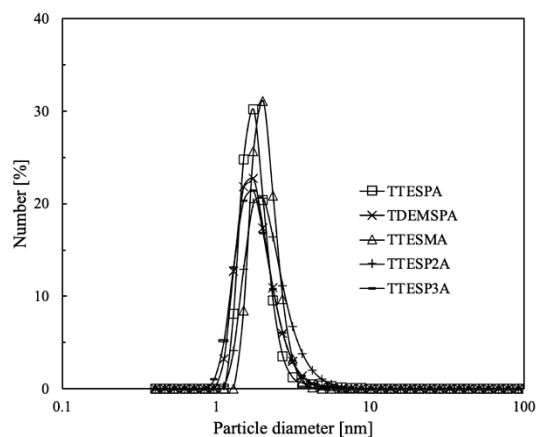


Figure 2.1. Particle size distribution of sols determined by DLS measurement.

For the PSQ-RO membranes preparation by the SG process, calcination temperatures should be as high as possible to promote the gelation leading to dense membranes without decomposing the organic bridges. Decomposition of the organic bridges may lead to significant membrane shrinkage, thereby resulting in crack and pinhole formation in the membranes and hydrophilicity suppression. To determine the calcination temperature, the author conducted a thermogravimetric (TG) analysis of TTESPA, TDEMSPA, TTESMA, TTESP2A, and TTESP3A gels obtained by drying their sol solutions at 60 °C in air for 2 days. The TG analysis was performed under a nitrogen flow at the heating rate of 10 °C/min. Figure 2.2 shows the TG curves of the gels. The first weight loss at temperatures lower than 250 °C is likely to be ascribed to the desorption of adsorbed water in the gel in nitrogen flow, and water liberation by the condensation reaction between Si-OH groups to form Si-O-Si linkages. The second weight loss is probably due to the decomposition of organic bridges in the gels, occurring at temperatures higher than 300 °C. The lesser weight loss at 1,000 °C for TTESMA than the other membranes would be due to its shorter organic bridges. Based on these results and the thermal stability of the polysulfone support membrane (NTR7450), the author set the optimum calcination temperature at 150 °C for the membrane preparation.

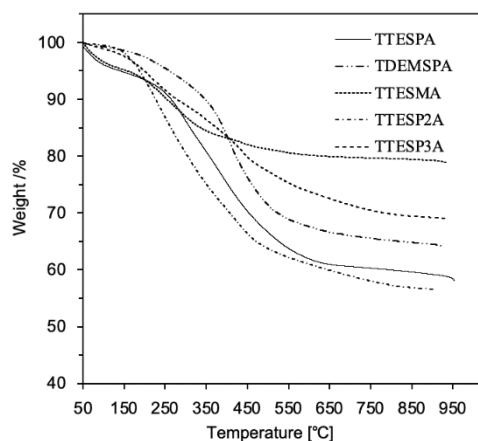


Figure 2.2. TG curves of gel powders in a nitrogen atmosphere.

FT-IR spectra provided information of the progress of polymerization of these precursors. Figure 2.3 shows the FT-IR spectra of the gel films prepared by coating the sol solutions on silicon wafer, followed by heating the films at 150 °C for 10 min. The broad and strong absorption bands centered at 1065  $\text{cm}^{-1}$  are attributed to the stretching frequencies of Si–O–Si linkages in the PSQ networks. Although the Si-O bands of Si-OH groups are also seen at 956  $\text{cm}^{-1}$ , their intensities are low, indicating that the Si-OH groups still remain after calcination at 150 °C, but only to a small extent. Peaks that appear at 2800–2970  $\text{cm}^{-1}$  are attributed to C-H stretching. That the siloxane bands appear sharper in the IR spectra of TTESP2A and TTESP3A-based films than others is likely due to higher rigidity of the gel network, as observed for a BTESE3-based film. An acetylene stretching band is also seen at 2189  $\text{cm}^{-1}$  for the TTESP2A-based film.

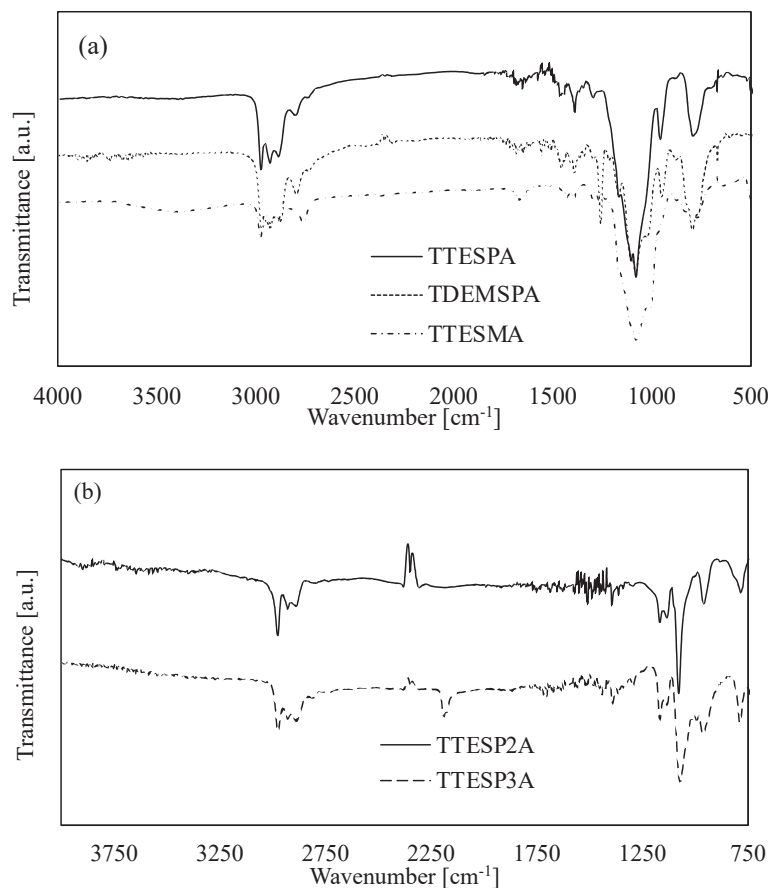


Figure 2.3. FT-IR spectra of (a) TTESPA, TDEMSPA and TTESMA (b) TTESP2A and TTESP3A gel films prepared by heating three precursor sols coated on silicon wafer at 150 °C.

### *Cross-section topography*

The cross-section topography of these membranes obtained by the SG process and the IP process was examined by SEM (Figure 2.4). The SEM images demonstrate that dense PSQ separation layers are formed on the polysulfone support membranes by both the SG process and the IP process. Membranes prepared by the SG process of TTESPA, TDEMSPA, TTESMA, TTESP2A, and TTESP3A exhibit the formation of fine homogeneous separation layers with thicknesses ranging from 60 to 150 nm (Figure 2.4 (a) to (e)). This is attributed to the successful control of the sol particle size and the calcination temperature. In contrast, membranes prepared from TTESPA, TDEMSPA, and TTESMA via IP process exhibit thicknesses ranging from 900 to 1,000 nm (Figure



2.4 (f) to (h)). Membrane thickness could be tuned by controlling precursor concentration during IP process. To investigate the thickness dependence of RO performance for membranes prepared by the IP process, the author carried out TTESPA interfacial polymerization at a lower concentration to obtain a membrane with a similar thickness to that prepared by the SG method (Figure 2.4 (i)). This thinner IP membrane showed a slight increase in water permeability and a decrease in NaCl rejection (see below). In contrast to TTESPA- and TDEMSPA-based membranes, the TTESMA-based membrane shows cracks in and peeling of the separation layer. This deformation may be one reason for its inferior performance compared with the other membranes.

In addition, the cross-sectional SEM images of the TTESP2A- and TTESP3A-based membranes showed ambiguous interfaces between the support membrane and the PSQ layer when prepared via the IP process (Figure 2.4 (j) and (k)), in contrast to those of TTESPA, TTESMA, and TDEMSPA. It is likely that the introduction of polar ethylene and acetylene bonds increased the hydrophilicity of the precursors and their PSQ oligomers to permit their permeation to the aqueous layer in the IP process. This seems to affect the RO performance of the membranes (*vide infra*).

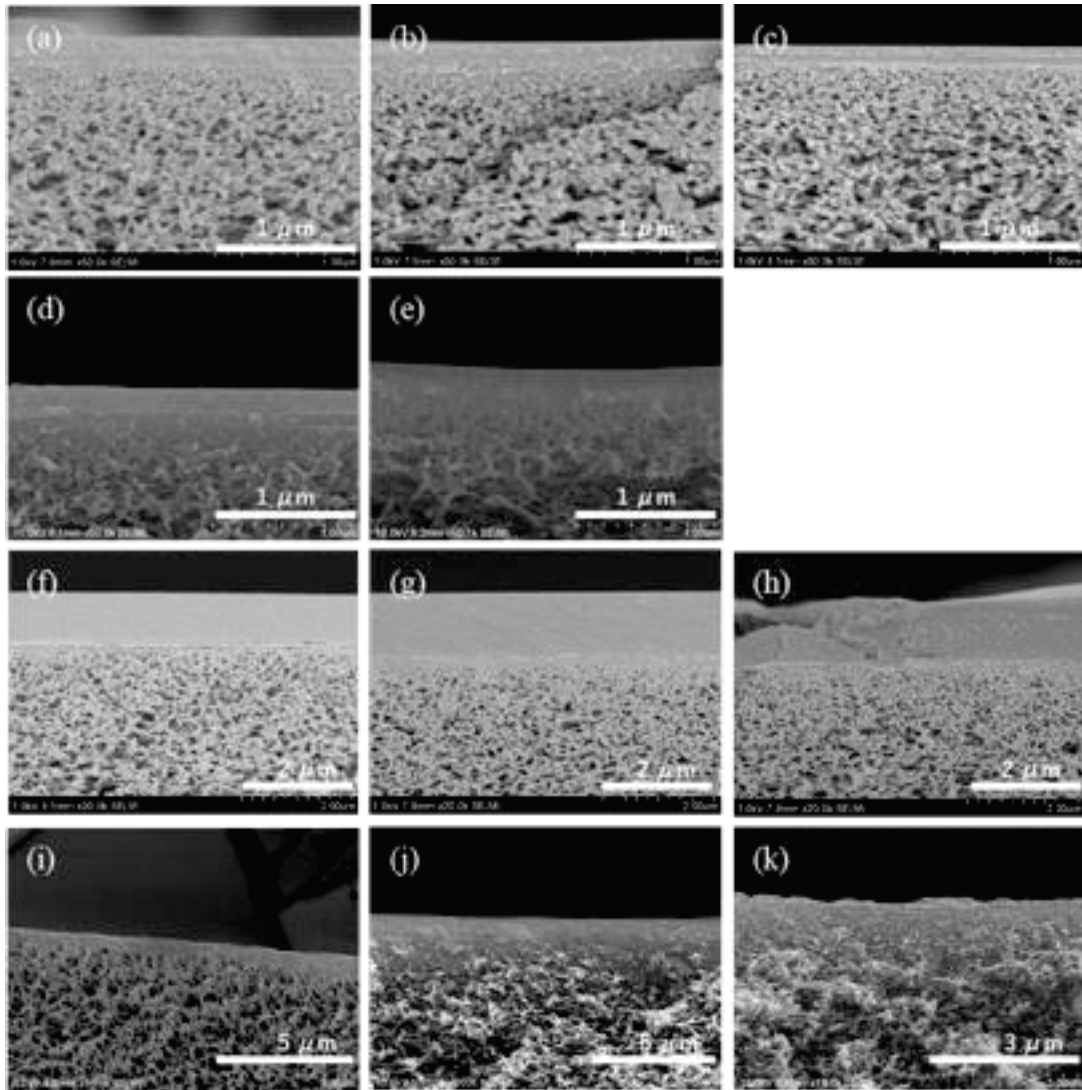


Figure 2.4. Cross-sectional SEM images of membranes prepared by SG process using (a) TTESPA, (b) TDEMSPA, (c) TTESMA, (d) TTESP2A, and (e) TTSEP3A, and those prepared by IP process of (f) TTESPA, (g) TDEMSPA, and (h) TTESMA, (i) TTESPA (1 wt%), (j) TTESP2A, and (k) TTSEP3A.

#### *Mechanical strength and porous properties*

To further study the process dependence of membrane RO properties, the author investigated the pencil hardness test to know the mechanical strength of the membrane surface. TTESPA-based membranes prepared by the IP process of 1 wt% solution and the SG process and having similar thicknesses exhibited pencil hardness indexes of 5B and 3H, respectively. This seems to indicate that the SG process can form a denser film than the IP process. This is consistent with the results obtained from RO experiments,

that is, the membrane prepared by the IP process is thicker than that by the SG process, but has higher water permeability.

Membrane porosity significantly affects water permeability. To investigate the porosity of TTESPA-, TTESMA, TTESP2A, and TTESP3A-based gels, nitrogen adsorption and desorption measurements were performed. Their gel powders were prepared by drying the sols at 60 °C in the air for 2 days followed by calcination at 150 °C in nitrogen for 12 h. The results are presented in Figure 2.5, indicating the non-porous properties of these gel powders, although they exhibit favorable water permeability in RO experiments. This suggests that the water separation properties of the present membranes are likely based on the diffusion-controlled mechanism rather than molecular sieving effects [7]. It seems likely that polymers still had many reactive sites and the structures were fluxional and mobile in the sol states, thus providing non-porous films upon calcination.

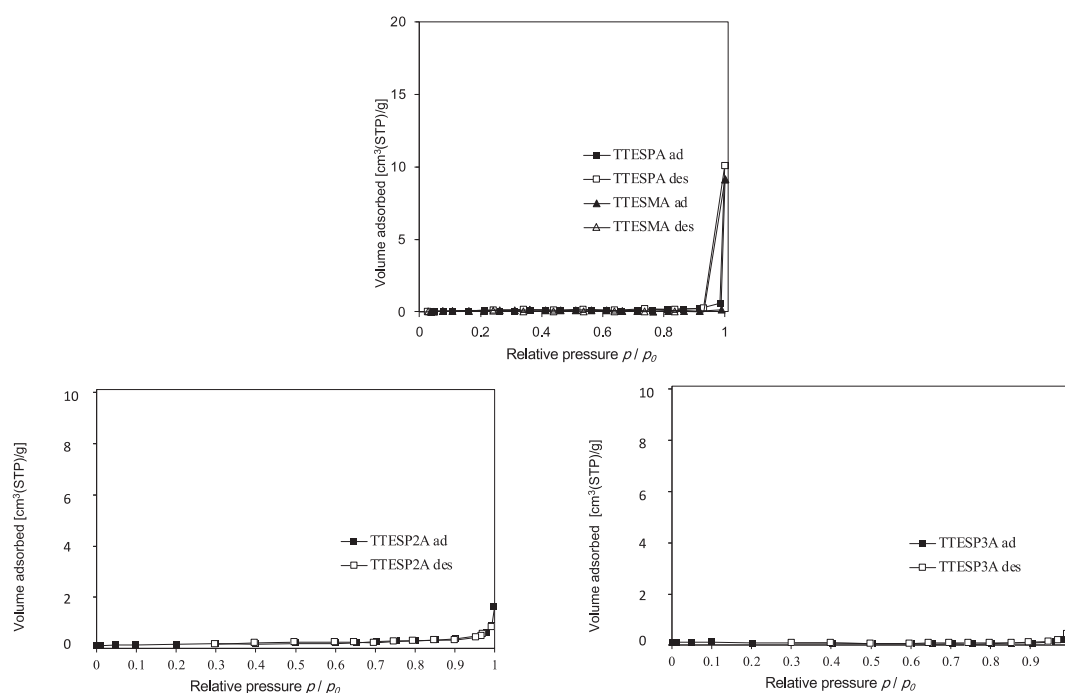


Figure 2.5. N<sub>2</sub> adsorption (solid plot)/desorption (open plot) isotherms of TTESPA and TTESMA (top) and TTESP2A and TTESP3A (bottom) gel powders.

### *RO performance*

RO measurements of these membranes prepared by the SG process and the IP process were performed with 2,000 ppm NaCl aqueous solution under the feed pressure of 1.5 MPa at room temperature. The RO performance is presented in Table 2.1 and Figure 2.6 exhibits the trade-off plots of water permeability and salt rejection. TTESPA-based membranes prepared by the SG process and the IP process exhibit favorable salt rejection of 96.6% and 95.6%, respectively. In contrast to the SG process, the membrane prepared by the IP process has approximately five times higher water permeability ( $7.3 \times 10^{-13} \text{ m}^3/\text{m}^2\text{sPa}$ ) than that prepared by the SG process ( $1.7 \times 10^{-13} \text{ m}^3/\text{m}^2\text{sPa}$ ), although the membrane prepared by the IP process is thicker than that prepared by the SG process (Figure 2.4 (a) and (f)). This is likely due to the growth pattern difference of the membranes during the SG process and the IP process. Although no obviously evident differences in membrane morphologies depending on the process in the FE-SEM images, the fact that the TTESPA-based membrane prepared by the SG process has higher mechanical strength than that prepared by the IP process seems to reflect the difference in membrane denseness. The membrane prepared by the IP process using a lower concentration of TTESPA solution shows lower salt rejection and higher water permeability than the membrane prepared by the SG process, which has almost the same separation layer thickness. In addition, the RO performance of membranes prepared by the copolymerization of TTESPA and BTESE is also shown in Table 2.1 (TT-BT1 and TT-BT3). Compared with the BTESPA and BTESE copolymer-based membrane (BT-BT3 in Table 2.1), TT-BT1 and TT-BT3 do not demonstrate the same degree of increase in water permeability, probably because TTESPA has three reactive ethoxysilyl units that can form a denser film than BTESPA.

The TDEMSPA-based membranes prepared by the SG process and the IP process exhibit water permeability of  $5.3 \times 10^{-14} \text{ m}^3/\text{m}^2\text{sPa}$  and  $6.0 \times 10^{-14} \text{ m}^3/\text{m}^2\text{sPa}$  and salt rejection of 94.3% and 92.5%, respectively. The TDEMSPA- and TTESPA-based membranes exhibit similar salt rejection values. However, the TDEMSPA-based membranes show lower water permeability values than the TTESPA-based membranes,

which is probably due to the methyl groups in the TDEMSPA-based membranes hindering the passage of water molecules through the membrane. In addition, the hydrophobicity of the methyl groups decreased water permeability, as evidenced by the high water contact angles of the TDEMSPA-based membrane surface (Figure 2.6).

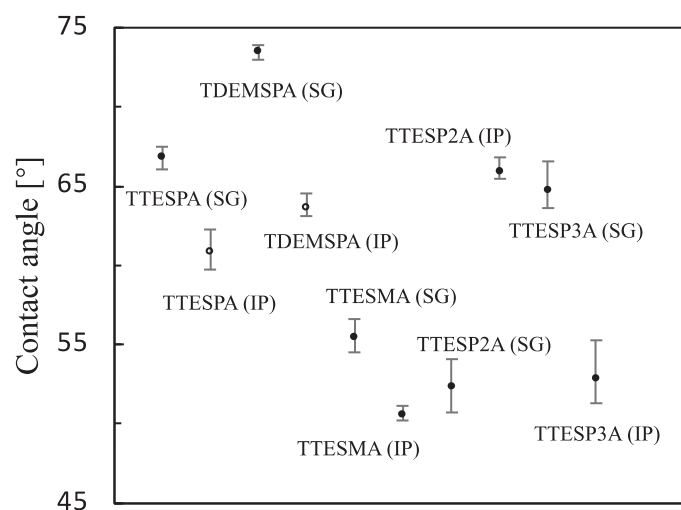


Figure 2.6. Water contact angles of membrane surfaces (SG: SG process; IP: IP process).

The TTESMA-based membrane prepared by the SG process exhibits high water permeability of  $2.6 \times 10^{-12} \text{ m}^3/\text{m}^2\text{sPa}$  but low salt rejection of 70.2%. In contrast, the TTESMA-based membrane prepared by the IP process only exhibits approximately 30% salt rejection. This result is consistent with the result obtained by SEM analysis of the membrane that shows cracks in the separation layer (Figure 2.4(h)). This may be due to the short methylene chains that have little flexibility. It seems that the membrane prepared by the SG process also has some deformations, including small cracks and/or pinholes, which cannot be observed from its cross-sectional SEM image (Figure 2.4(c)).

Comparing the RO performance with our previous work for organically bridged PSQ-RO membranes, which was reported in the literature, (Figure 2.7), the water permeability of the TTESPA-based membrane prepared by the SG process is higher than those of BTESE- and BTESPA-based membranes, and slightly lower than those of BTESE2- (bis(triethoxysilyl)ethane) and BTESE3-(bis(triethoxysilyl)ethyne) based membranes, and the TTESPA-based membrane prepared by the IP process exhibits

favorable water permeability even though a slight decrease of salt rejection is observed. The favorable water permeability and high NaCl rejection of the TTESPA-based membrane would be ascribed to the three propylene chains of TTESPA, which can form a dense separation layer with moderate flexibility.

It was reported that membranes prepared from BTESE2 and BTESE3, which with rigid and polar ethylene and acetylene units showed higher RO performance than the BTESE-derived membranes. For further improve the RO performance of TTESPA-derived membranes, the author introduced ethylene and acetylene units in precursors TTESP2A and TTESP3A. As expected, the RO performance of the SG membranes of TTESP2A and TTESP3A showed higher water permeability than and similar NaCl rejection to those of the TTESPA-membrane (Table 2.1). However, the water permeability and NaCl rejection of the membranes prepared by IP process of TTESP2A and TTESP3A are lower than those of TTESPA. Permeation of the precursors to the aqueous layers forming the gels in the support membrane suggested by the cross-sectional SEM images would be a reason for the lower permeability (Figure 2.4 (j) and (k)).

Table 2.1. Summary of RO performance of TTESPA-, TTESMA-, TDEMSPA-, TTESP2A-, and TTESP3A-based membranes.

Membrane	Process <sup>a</sup>	Liquid permeability/(m <sup>3</sup> /m <sup>2</sup> ·sPa)	NaCl rejection/%
TTESPA	SG	$1.7 \times 10^{-13}$	96.6
TTESPA	IP	$7.3 \times 10^{-13}$	95.6
TTESPA	IP (1 wt%)	$7.9 \times 10^{-13}$	87.2
TDEMSPA	SG	$5.3 \times 10^{-14}$	94.3
TDEMSPA	IP	$6.0 \times 10^{-14}$	92.5
TTESMA	SG	$2.6 \times 10^{-12}$	70.2
TTESMA	IP	$9.7 \times 10^{-12}$	33.0
TT-BT1 <sup>b</sup>	IP	$2.1 \times 10^{-13}$	91.2
TT-BT3 <sup>b</sup>	IP	$2.9 \times 10^{-13}$	92.0
BT-BT3 <sup>c</sup>	IP	$1.3 \times 10^{-12}$	92.0
TTESP2A	SG	$3.3 \times 10^{-13}$	96.5
TTESP2A	IP	$4.4 \times 10^{-14}$	94.2
TTESP3A	SG	$5.5 \times 10^{-13}$	94.1
TTESP3A	IP	$2.1 \times 10^{-13}$	92.5
NTR7450 <sup>d</sup>		$2.4 \times 10^{-11}$	13.1

<sup>a</sup> IP: IP process; SG: SG process.

<sup>b</sup>TT-BT1: TTESPA copolymerized with BTESE in 1:1 ratio; TT-BT3: TTESPA copolymerized with BTESE in 1:3 ratio.

<sup>c</sup>BT-BT3: BTESPA copolymerized with BTESE in 1:3 ratio; data from literature [8].

<sup>d</sup>Polysulfone support membrane.

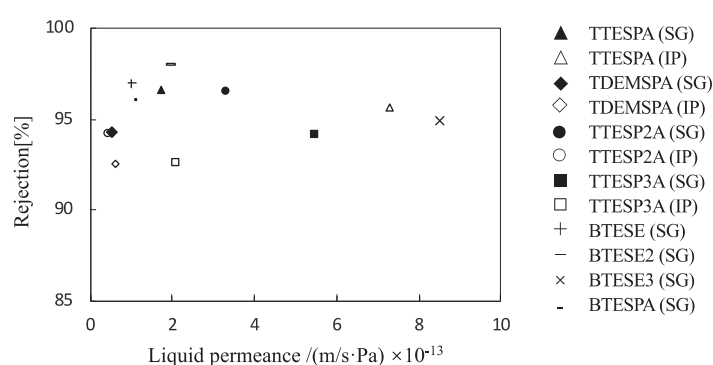


Figure 2.7. Summary of RO performance of membranes, together with those of + BTESE (SG), - BTESE2 (SG), × BTESE3 (SG), and - BTESPA (SG) from the literature.

Stability towards chlorine exposure was examined for the TTESPA-based membrane. As shown in Figure 2.8, when the membrane was immersed in a 1,000 ppm NaOCl aqueous solution, liquid permeability and NaCl rejection were almost unchanged up to the exposure time of 10 h, indicating high stability of the membrane.

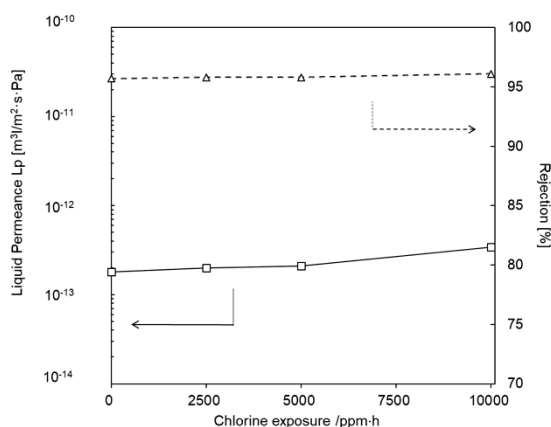


Figure 2.8. Effects of chlorine exposure on liquid permeability and NaCl rejection of TTESPA-based membrane, using 1,000 ppm NaOCl solution.

### Summary

In conclusion, the author examined TTESPA, TTESMA, TDEMSPA, TTESP2A, and TTESP3A as new precursors for PSQ-RO membrane preparation by both IP process and the SG process. The TTESPA-based membrane exhibited good RO performance of  $7.3 \times 10^{-13} \text{ m}^3/\text{m}^2\text{sPa}$  water permeability and 95.6% NaCl rejection (IP process) and  $1.7 \times 10^{-13} \text{ m}^3/\text{m}^2\text{sPa}$  and 96.6% NaCl rejection (sol- gel process). These data are much higher than those of the membrane prepared by homopolymerization of BTESA, suggesting the potential of TTESPA. They are comparable to those of the membrane prepared by SG process of BTESE3, which are the best data so far obtained for PSQ membranes. As high performance BTESE3 membranes can be obtained only by SG process, the use of TTESPA that can form good membranes by simpler IP process seems to be advantageous.

The nonporous structure of the membrane was revealed by nitrogen adsorption and desorption measurements, suggesting that the diffusion-controlled mechanism is operative for water separation. The TDEMSPA-based membranes also demonstrated favorable NaCl rejection, although water permeability was slightly low. Evidence



suggests that the IP process can form a spacer but thicker membrane than the SG process, and as a result, water permeability is improved but salt rejection is slightly lowered. Although the RO performance of the TTESPA-based membrane still has room for improvement, these results offer important information for PSQ precursor design for improving water permeability in future work. Studies on other applications of the membranes such as for gas separation and liquid separation are also in progress.

## Experimental

### *General*

All reactions were carried out in a dry argon atmosphere. TTESMA was purchased from Gelest Inc. and used as obtained. Toluene and diethyl ether used as the reaction solvents were distilled from P<sub>2</sub>O<sub>5</sub> and CaH<sub>2</sub>, respectively, and stored over activated molecular sieves in dark until use. NMR spectra were recorded on Varian 400-MR and 500 spectrometers. MS spectra were measured on a Shimadzu QP2021SE spectrometer. In the NMR spectra of TTESPA, TDEMSPA, TTESP2A, and TTESP3A, small unidentified signals are seen (Figure 2.10-2.13), but they were used for the following experiments without further purification, because further attempted purification by silica gel chromatography lowered their purity.

### *Preparation of TTESPA and TDEMSPA*

A solution of 1.00 g (7.28 mmol) of triallylamine in 30 mL of toluene was placed in a 200 mL two-necked flask equipped with a magnetic stirrer and a reflux condenser. To this were added 3.59 g (21.8 mmol) of triethoxysilane and two drops of Karstedt's catalyst (19.0–21.5% as Pt in THF). The reaction mixture was heated to reflux for 20 h. Trace amounts of reactants remaining in the reaction mixture and the solvent were removed under vacuum to give a yellow liquid, which was then purified by preparative gel permeation chromatography (GPC) using toluene as the eluent to yield TTESPA as a colorless liquid (4.10 g, 89% yield). <sup>1</sup>H NMR (500 MHz, chloroform-d) δ 3.81 (q, *J* = 7.0 Hz, 18H), 2.45–2.33 (m, 6H), 1.52 (dtd, *J* = 9.9, 8.0, 5.7 Hz, 6H), 1.22 (t, *J* = 7.0

Hz, 27H), 0.62–0.51 (m, 6H).  $^{13}\text{C}$  NMR (126 MHz, chloroform-d)  $\delta$  58.28, 57.15, 20.27, 18.28, 8.02. MS  $m/z$  627 ( $\text{M}^+$ ).

Tris[3-(diethoxymethylsilyl)propyl]amine was prepared in a fashion similar to TTESPA. Into a 200 mL two-necked flask equipped with a magnetic stirrer and a reflux condenser were added 1.00 g (7.28 mmol) of triallylamine and 2.94 g (21.8 mmol) of diethoxymethylsilane in 30 mL of toluene. To this was added two drops of Karstedt's catalyst (19.0-21.5 % as Pt in THF), and the reaction mixture was heated to reflux for 20 h. Excess reactants and the solvent were removed under vacuum to give a yellow liquid that mainly contained TDEMSPA. After purification by GPC, TDEMSPA was obtained as a colorless oil (4.10 g, 85% yield).  $^1\text{H}$  NMR (500 MHz, chloroform-d)  $\delta$  3.75 (q,  $J = 7.0, 0.8$  Hz, 12H), 2.48–2.36 (m, 6H), 1.53–1.43 (m, 6H), 1.20 (td,  $J = 7.0, 0.8$  Hz, 18H), 0.59–0.50 (m, 6H), 0.11 (s, 9H).  $^{13}\text{C}$  NMR (125 MHz, chloroform-d)  $\delta$  58.04, 57.54, 20.56, 18.38, 11.48, -4.91. MS  $m/z$  538 ( $\text{M}^+$ ).

#### *Preparation of TTESP2A*

A mixture of 1.00 g (7.62 mmol) of tripropargylamine and 3.76 g (23.0 mmol) of triethoxysilane in 30 mL of toluene was placed in a 200 mL two-necked flask equipped with a magnetic stirrer and a reflux condenser. To this was added two drops of Karstedt's catalyst (19.0-21.5 % as Pt in THF), and the reaction mixture was heated to 85 °C for 6 h. Excess reactants and the solvent were removed under vacuum to give a yellow liquid. Kugelrohr distillation of the residue (1 Torr, 200 °C) gave a mixture of tris[3-(triethoxysilyl)prop-2-enyl]amine and its isomers as a colorless oil (2.1 g, 44 % yield) (unit ratio of trans- and gem-(triethoxysilyl)prop-2-enyl was calculated to be 5 : 3 based on  $^1\text{H}$  NMR integrations).  $^1\text{H}$  NMR (400 MHz, chloroform-d)  $\delta$  6.48-6.37 (m, 1.88H), 6.21 (dt,  $J = 3.7, 2.1$  Hz, 0.29H), 6.14 (dt,  $J = 3.7, 1.8$  Hz, 0.41H), 5.97 (dt,  $J = 3.5, 1.7$  Hz, 0.42H), 5.77-5.73 (m, 1.12H), 5.64, 5.63, 5.61 (3 br d,  $J = 18.8$  Hz, 1.88H), 3.83-3.77 (m, 18H), 3.16-3.06 (m, 6H), 1.26-1.18 (m, 27H).  $^{13}\text{C}$  NMR (126 MHz, chloroform-d)  $\delta$  150.47, 149.80, 128.99, 128.19, 122.26, 121.51, 58.71, 58.40, 18.18. MS  $m/z$  623 ( $\text{M}^+$ ).

### *Preparation of TTESP3A*

A solution of 8.51 mL of 2.69 M *n*-BuLi in hexane (22.9 mmol) and 80 mL of diethyl ether was placed in a 500 mL three-necked flask and a magnetic stirrer and the flask was cooled at  $-78\text{ }^{\circ}\text{C}$ . To this was slowly added 1.00 g (7.63 mmol) of tripropargylamine in 30 mL of diethyl ether within 1 h. The mixture was then stirred for 1 h at this temperature and further stirred for 12 h at room temperature. The mixture was again cooled to  $-78\text{ }^{\circ}\text{C}$  and added to a mixture of chlorotriethoxysilane (5.44 g, 27.5 mmol) in 30 mL of diethyl ether cooled at  $-78\text{ }^{\circ}\text{C}$  within 1 h. The mixture was further stirred for 1 h at  $-78\text{ }^{\circ}\text{C}$  and for 12 hours at room temperature. The resultant precipitates were filtered, and solvents were removed under vacuum. The residue was subjected to Kugelrohr distillation (1 Torr,  $225\text{ }^{\circ}\text{C}$ ) to give 2.00 g (43 %) of tris[(triethoxysilyl)propynyl]amine as a colorless oil.  $^1\text{H}$  NMR (500 MHz, Chloroform-*d*)  $\delta$  3.84 (q,  $J = 7.0\text{ Hz}$ , 18H), 3.51 (s, 6H), 1.22 (t,  $J = 7.0\text{ Hz}$ , 27H).  $^{13}\text{C}$  NMR (126 MHz, chloroform-*d*)  $\delta$  99.27, 82.25, 59.01, 42.72, 17.96. MS  $m/z$  616 ( $\text{M}^+$ )

### *SG process for membrane preparation*

The SG process was carried out as reported in the literature [9]. A solution of 5 wt% of precursor in EtOH containing different ratios of distilled water (the ratio depends on the reactivity of precursor) was stirred at room temperature until the sol particle sizes determined by dynamic light scattering (DLS) measurement reached 1.6 to 2 nm (2–12 h). The reaction mixture was then diluted with ethanol to 1 wt% and preserved in a refrigerator at  $4\text{ }^{\circ}\text{C}$  until use.

A polysulfone support membrane (Nitto Denko Corporation NTR-7450 pore size: 1 nm) was washed with ethanol and air-dried in a drying oven at  $60\text{ }^{\circ}\text{C}$  for 10 min. After that, the prepared sol solution was poured onto the support membrane surface at room temperature. After 30 sec, excess sol solution was removed by decantation and the membrane was air-dried at room temperature for 10 min. After repeating this process twice, the membrane was calcined at  $150\text{ }^{\circ}\text{C}$  for 10 min to facilitate gelation. After

cooling to room temperature, the membrane was washed with distilled water and used in the following RO experiments.

#### *IP process for membrane preparation*

The IP process for the preparation of PSQ membranes was performed as reported previously [4]. A polysulfone support membrane (Nitto Denko NTR-7450 pore size: 1 nm) was washed with ethanol and dried in a drying oven at 60 °C for 10 min. Sodium dodecyl sulfate (SDS) aqueous solution was then poured onto the support membrane surface at room temperature to allow permeation of the SDS aqueous solution. After 5 min, excess SDS aqueous solution was removed by decantation and a solution of 5 wt% of precursor in hexane was poured onto the wet support membrane surface at room temperature. After 5 min, the hexane solution was removed by decantation and the membrane was calcined at 150 °C for 10 min, to complete the polymerization. After cooling to room temperature, the membrane was washed with distilled water and used in the following RO experiments.

#### *Evaluation of RO performance*

RO experiments were performed using 2,000 ppm NaCl aqueous solution on a device shown in Figure 2.9. The feed pressure of 1.5 MPa was applied to the solution to promote permeation through the membrane at room temperature. RO performance parameters, water permeability ( $L_p$ ) and NaCl rejection ( $R$ ), were determined by equations (1) and (2) [10], respectively, in which  $\Delta P$  and  $\Delta\pi$  are differences in applied and osmotic pressures and  $J_v$  is the permeate water flux.  $C_f$  and  $C_p$  are NaCl concentrations of feed and permeate determined by their conductivities, which were obtained using a conductivity meter (HORIBA, ES-51).

$$L_p = J_v / (\Delta P - \Delta\pi) \quad (1)$$

$$R = \left(1 - \frac{C_p}{C_f}\right) \times 100\% \quad (2)$$

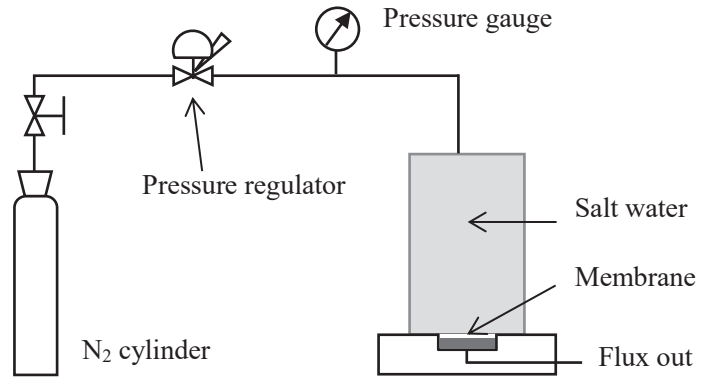


Figure 2.9. Apparatus for RO experiment.

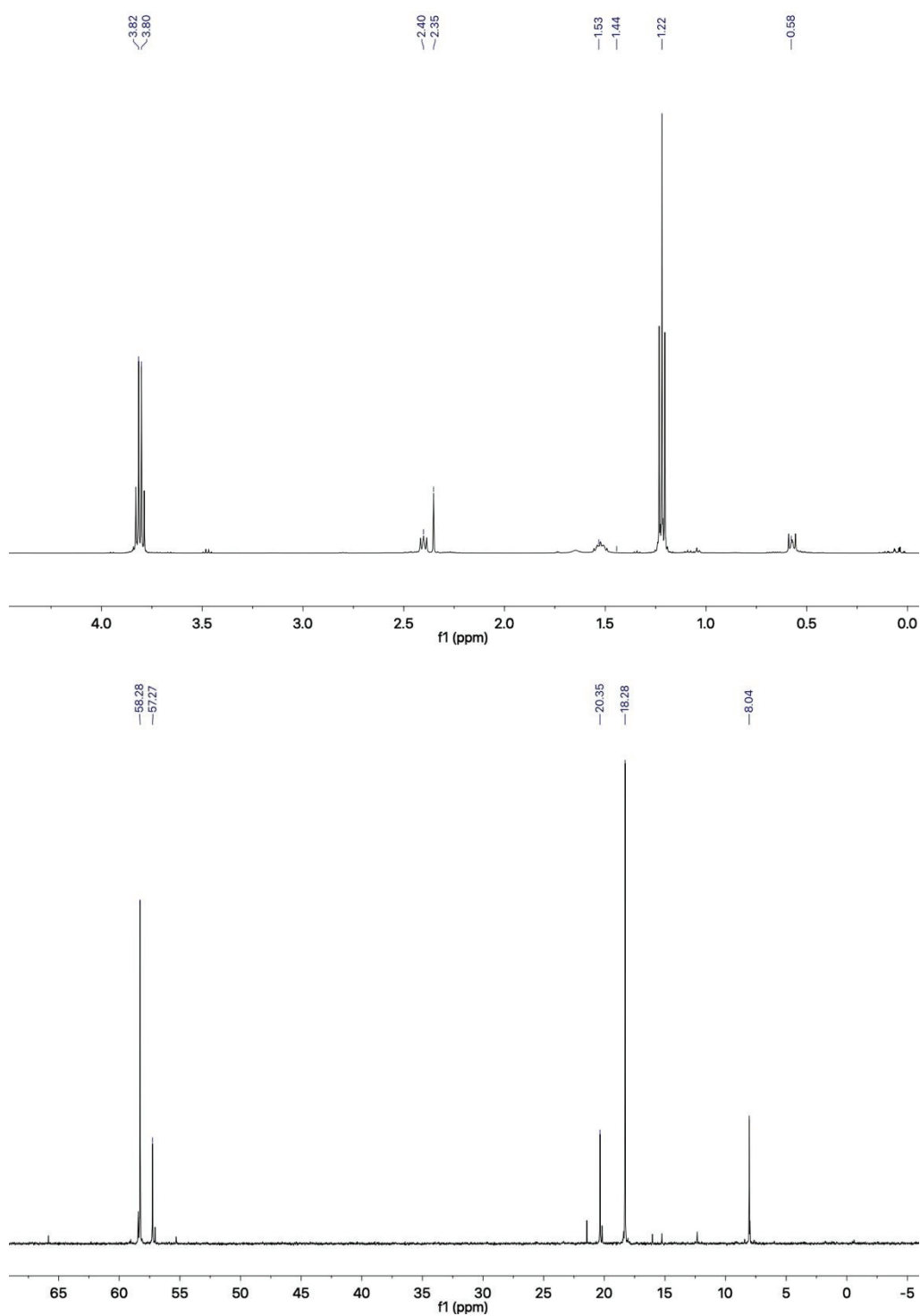


Figure 2.10.  $^1\text{H}$  NMR (top) and  $^{13}\text{C}$  NMR (bottom) spectra of TTESPA.

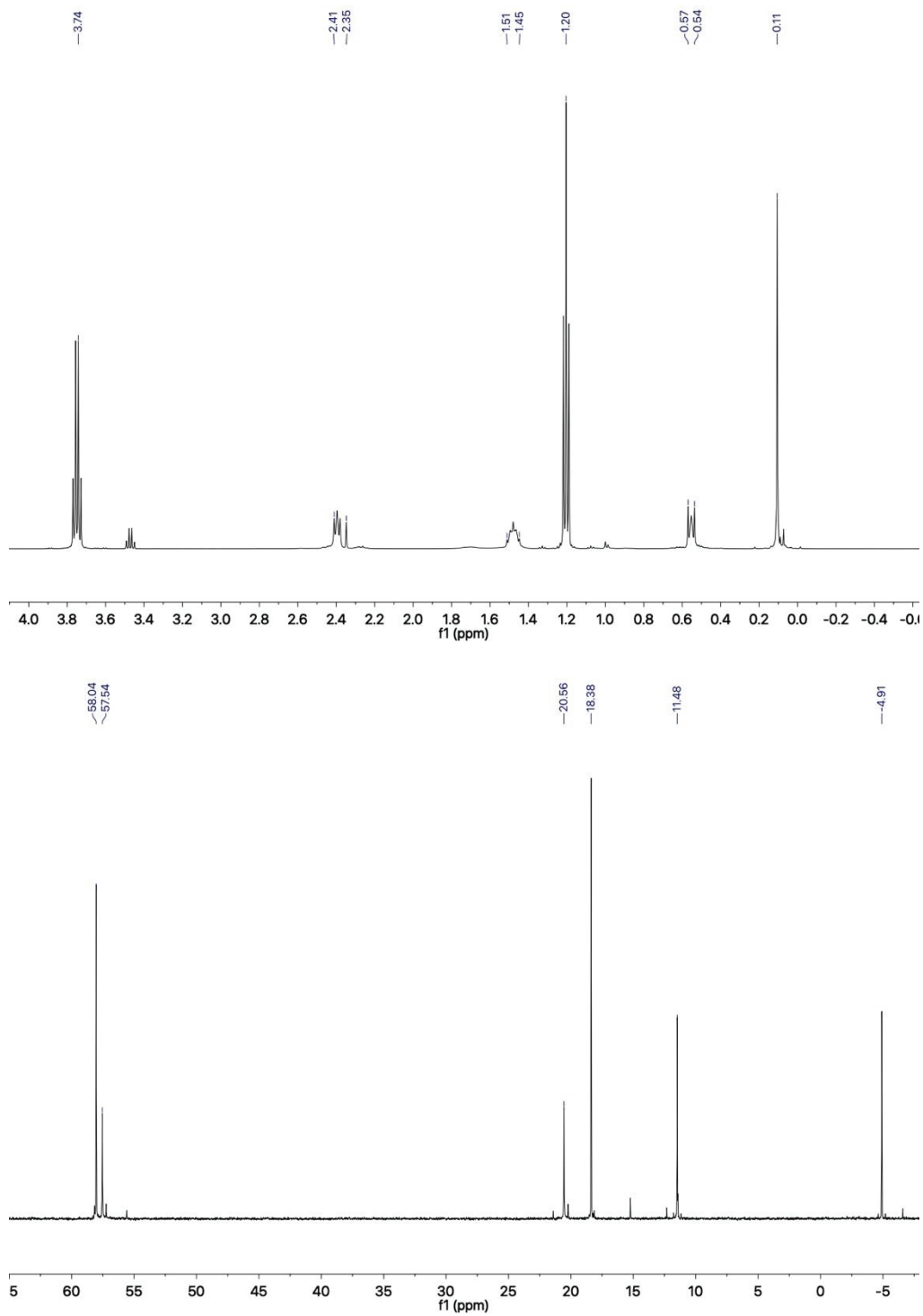


Figure 2.11.  $^1\text{H}$  NMR (tip) and  $^{13}\text{C}$  NMR (bottom) spectra of TDEMSPA.

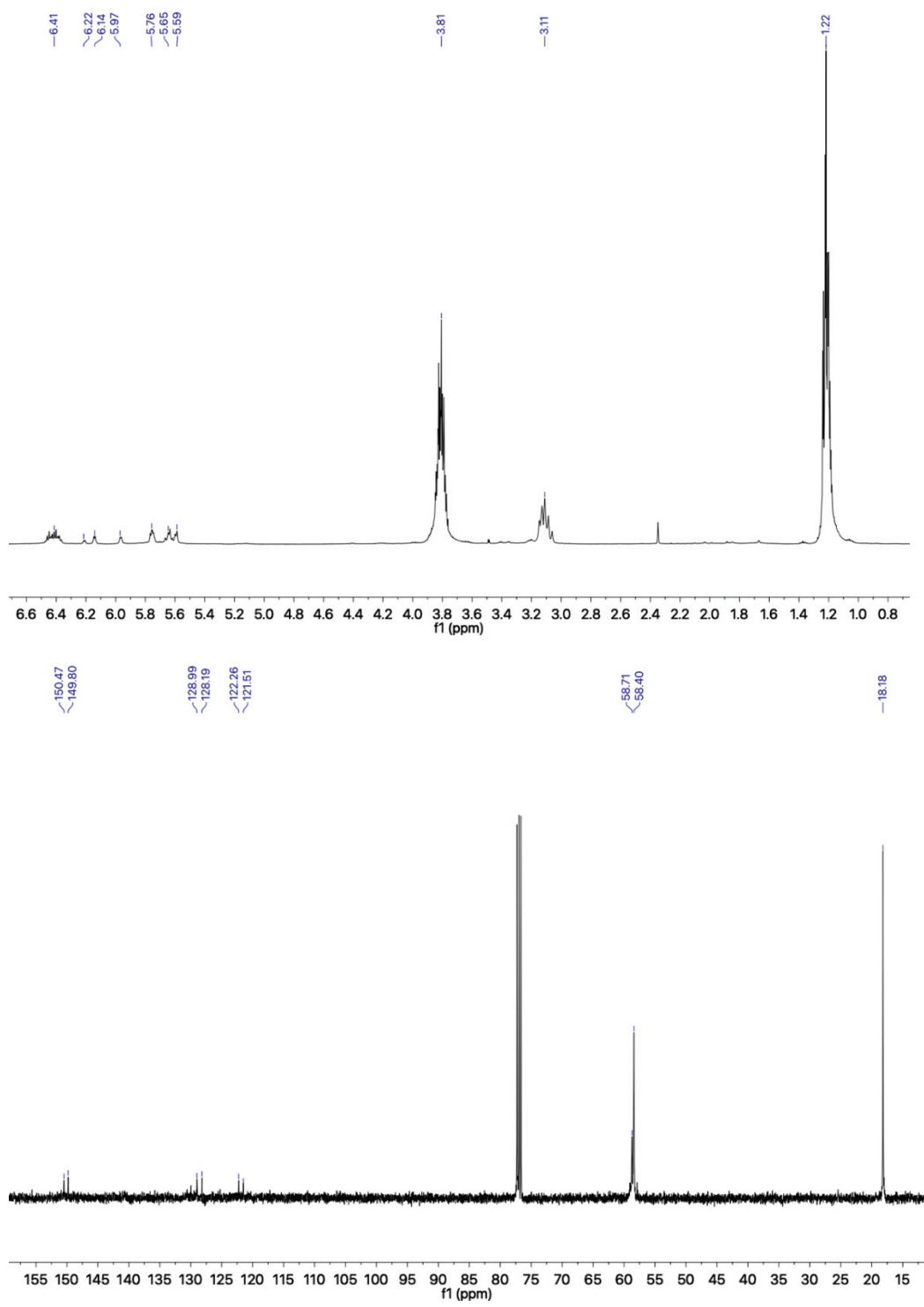


Figure 2.12.  $^1\text{H}$  NMR (top) and  $^{13}\text{C}$  NMR (bottom) spectra of TTESP2A.



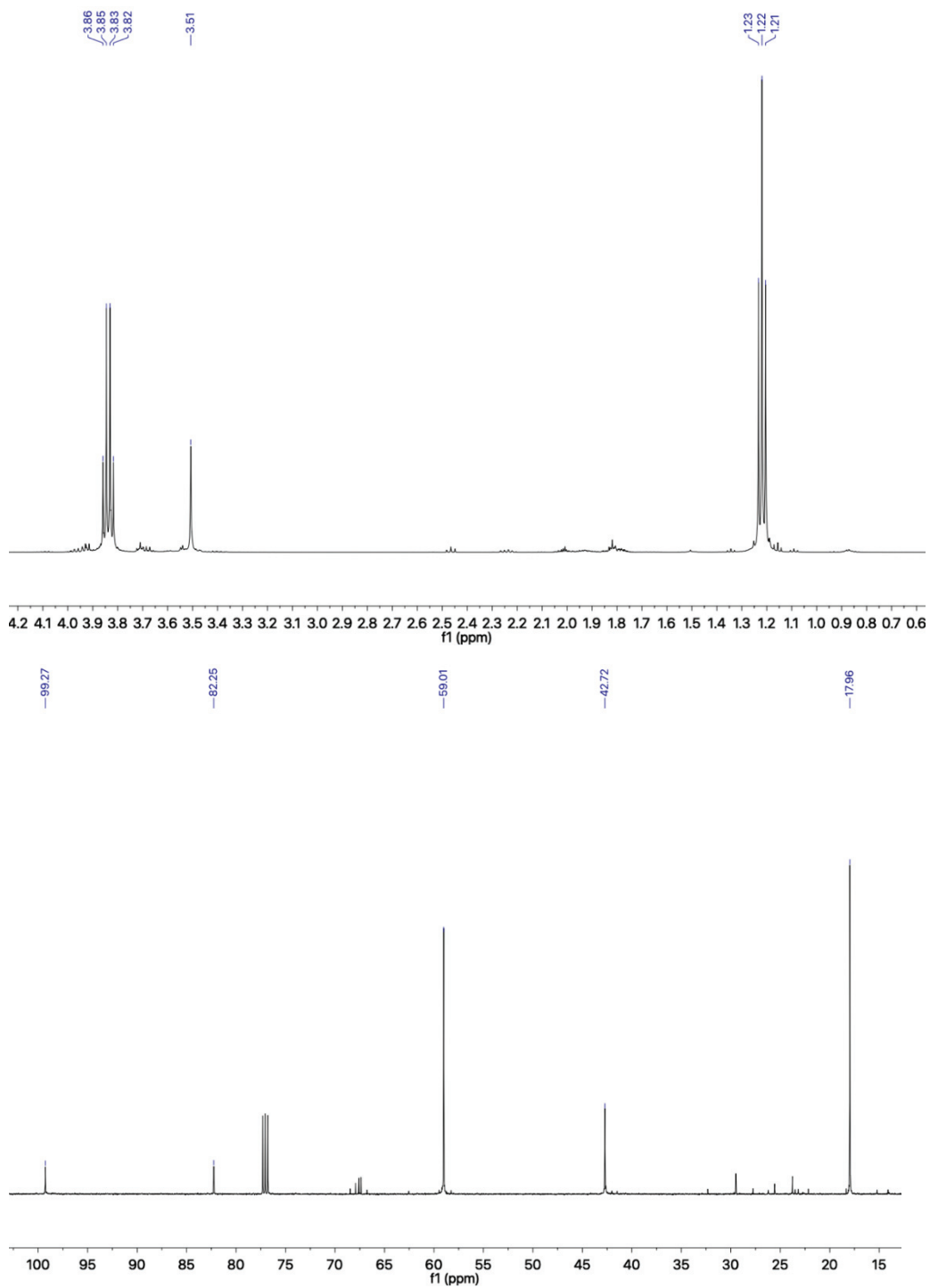


Figure 2.13.  $^1\text{H}$  NMR (top) and  $^{13}\text{C}$  NMR (bottom) spectra of TTESP3A.

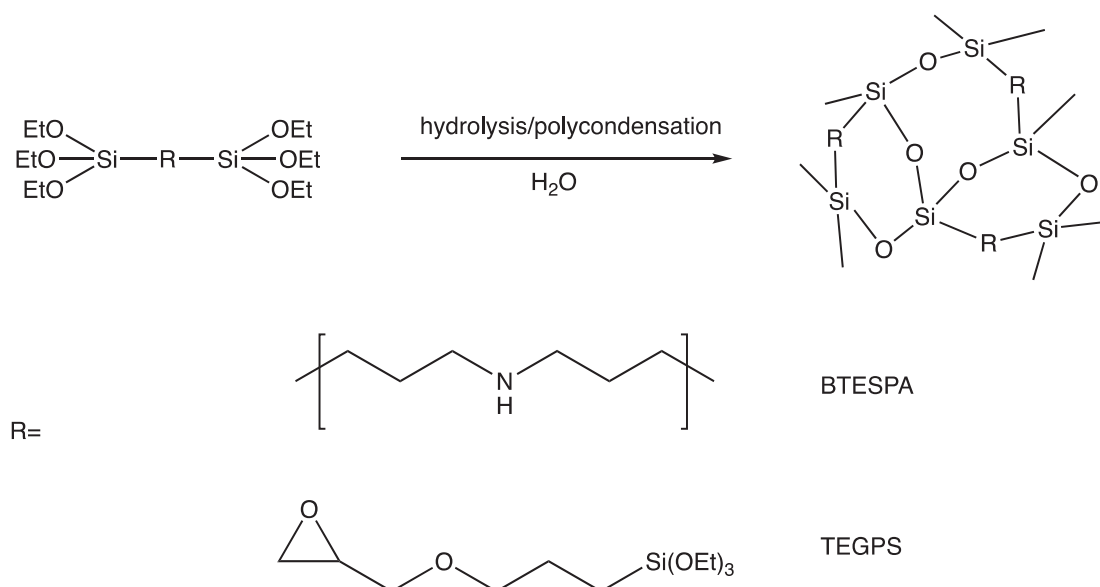
## References

- [1] M.R.N. Monton, E.M. Forsberg, J.D. Brennan, Tailoring sol–gel-derived silica materials for optical biosensing, *Chem. Mater.*, 24 (2012), 796-811.
- [2] L.L. Hench, J.K. West, The SG process, *Chem. Rev.*, 90 (1990), 33-72.
- [3] A. Larbot, A. Julbe, C. Guizard, L. Cot, Silica membranes by the SG process, *J. Membr. Sci.*, 44 (1989), 289-303.
- [4] F.-T. Zheng, K. Yamamoto, M. Kanezashi, T. Gunji, T. Tsuru, J.J.C.L. Ohshita, Preparation of Hybrid Organosilica Reverse Osmosis Membranes by IP process of Bis[(trialkoxysilyl) propyl] amine, *Chem. Lett.*, 47 (2018), 1210-1212.
- [5] R. Xu, S.M. Ibrahim, M. Kanezashi, T. Yoshioka, K. Ito, J. Ohshita, T. Tsuru, New insights into the microstructure-separation properties of organosilica membranes with ethane, ethylene, and acetylene bridges, *ACS Appl. Mater. Interfaces*, 6 (2014), 9357-9364.
- [6] K. Yamamoto, H. Muragishi, T. Mizumo, T. Gunji, M. Kanezashi, T. Tsuru, J. Ohshita, Diethylenedioxane-bridged microporous organosilica membrane for gas and water separation, *Sep. Purif. Technol.*, 207 (2018), 370-376.
- [7] K. Yamamoto, J. Ohshita, Bridged polysilsesquioxane membranes for water desalination, *Polym. J.*, 51 (2019), 1103-1116.
- [8] D. Zhang, J. Ohshita, Preparation of robust RO membranes for water desalination by interfacial copolymerization of bis[(triethoxysilyl)propyl]amine and bis(triethoxysilyl)ethane, *Polym. J.*, 51 (2019), 1231-1234.
- [9] T. Niimi, H. Nagasawa, M. Kanezashi, T. Yoshioka, K. Ito, T. Tsuru, Preparation of BTESE-derived organosilica membranes for catalytic membrane reactors of methylcyclohexane dehydrogenation, *J. Membr. Sci.*, 455 (2014), 375-383.
- [10] M.L. Lind, D. Eumine Suk, T.-V. Nguyen, E.M. Hoek, Tailoring the structure of thin film nanocomposite membranes to achieve seawater RO membrane performance, *Environ. Sci. Technol. Lett.*, 44 (2010), 8230-8235.

### Chapter 3 Preparation of PSQ-RO membranes with hydroxyl groups by copolymerization of bis[3-(triethoxysilyl)propyl]amine and triethoxy(3-glycidyloxypropyl)silane

#### Introduction

In this chapter, the author demonstrates a strategy for controlling the permeability of PSQ-RO membranes by using the ring-opening reaction of epoxy-containing precursor. In general, the introduction of hydrophilic groups, such as alcohol, ethylene glycol, and chitosan, is a simple and common method to enhance membrane hydrophilicity [1-3]. In PSQ-based materials, these hydrophilic groups can be introduced easily by modification of the bridging units, or more simply by copolymerization with trialkoxysilanes that have a hydrophilic group [4, 5]. In this chapter, to improve water permeability, bis[3-(triethoxysilyl)propyl]amine (BTESPA)-based membranes were copolymerized with triethoxy(3-glycidyloxypropyl)silane (TEGPS) (Scheme 3.1), expecting that the epoxy groups would improve the hydrophilicity of RO membranes. The author also anticipated that the epoxy groups would undergo ring opening with an amine unit of BTESPA and form hydroxy (C-OH) groups, further improving membrane hydrophilicity.



Scheme 3.1. Precursors for organically bridged RO membranes in present studies.

## Results and discussion

### *Preparation of membranes by the SG process*

Stirring the mixtures of BTESPA/TEGPS (structures are shown in Scheme 3.1) in 2:1 and 5:1 weight ratios with 20 eq water and BTESPA/TEGPS in 10:1 weight ratio with 40 eq water in ethanol for 2 h at room temperature yielded PA-TEG2, PA-TEG5 and PA-TEG10 sols, respectively. Figure 3.1 shows the particle size distribution of PA-TEG2 and PA-TEG5 sols determined by dynamic light scattering (DLS). Particle size should be as small as possible to improve water permeability, as large particles tend to increase membrane thickness and induce membrane cracking and peeling [6], but should be larger than the pore size of the support membrane to avoid penetration of the sols into the support membrane as already mentioned in Chapter 1. The particle sizes of PA-TEG2, PA-TEG5 and PA-TEG10 are around 1.5 nm, 2.3 nm and 2.0 nm, as shown in Figure 3.1, which are suitable to prepare RO membranes on the polysulfone support (Nitto Denko NTR-7450 with 1 nm pore size ).

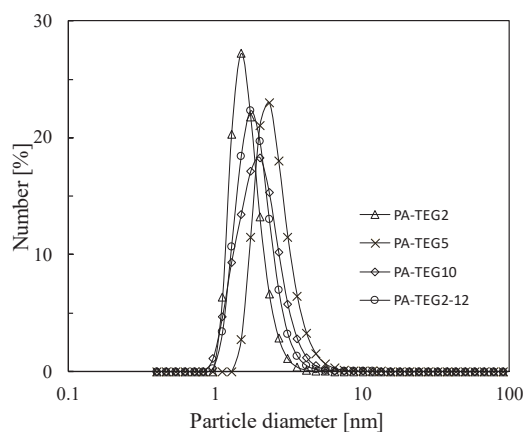


Figure 3.1. Particle size distribution of sols determined by DLS.

Thermogravimetric (TG) analysis provides information on the thermal stability of PSQ gels. For PSQ membranes prepared by the SG process, an exceedingly high calcination temperature leads to the thermal decomposition of organic units, but the temperature must be sufficiently high to facilitate gelation for the formation of a dense membrane. Overall, the calcination temperature should be as high as possible but lower than the decomposition temperature of the organic units. TG analysis was performed at

the heating rate of 10 °C/min under a nitrogen atmosphere for PA-TEG2, PA-TEG5, and PA-TEG10 gel powders obtained by drying their sol solutions in a dry oven at 60 °C for 2 days, and the results are shown in Figure 3.2. The gel powder that had a higher TEGPS ratio tended to exhibit higher weight loss. Specifically, the first slight weight loss observed at temperatures up to 250 °C was due to the desorption of adsorbed water and water liberation by the condensation reaction between Si-OH groups, forming Si-O-Si linkages. The greater weight loss at higher temperatures could be ascribed to the decomposition of organic units. Based on these results, the calcination temperature was set to 150 °C, which is the upper limit of the operation temperature of the support membrane.

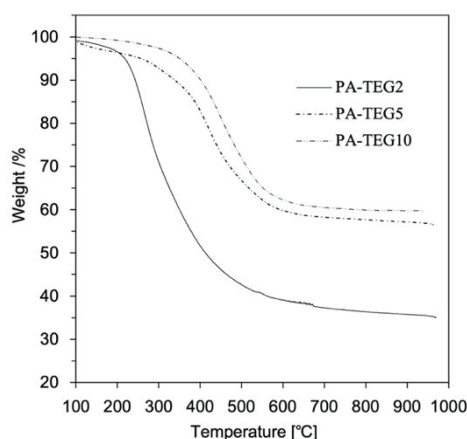


Figure 3.2. TG curves of gel powders in a nitrogen atmosphere at the heating rate of 10 °C/min.

The FT-IR spectra of films were prepared by coating these sol solutions on the silicon wafer, and calcination the coated wafer at 150 °C in a dry oven in air, as shown in Figure 3.3 and Figure 3.4. The absorption bands centered at 1065  $\text{cm}^{-1}$  were attributed to the stretching frequencies of Si-O-Si. In addition, Si-O stretching bands of Si-OH were observed from 920  $\text{cm}^{-1}$  to 980  $\text{cm}^{-1}$ . However, their intensities were low, and only a weak absorption around 3200  $\text{cm}^{-1}$  was observed for O-H vibration, indicating the low contents of Si-OH groups even though they were present.

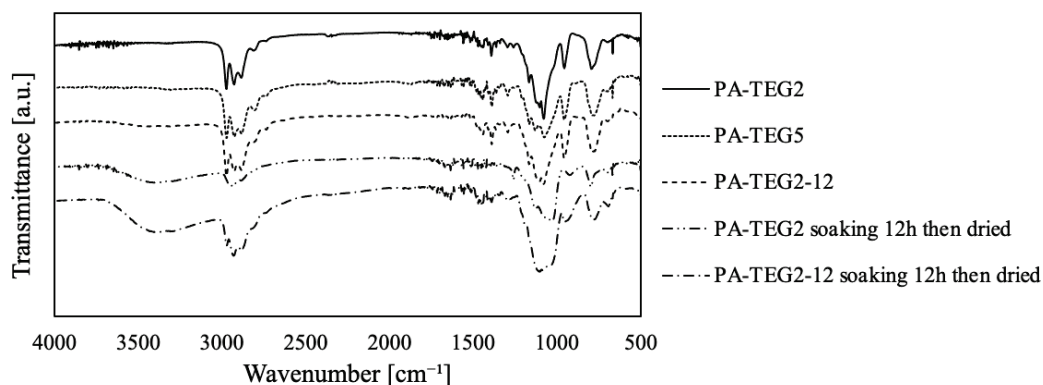


Figure 3.3. FT-IR spectra of PA-TEG2, PA-TEG5, and PA-TEG2-12 films prepared by heating precursor sols coated on silicon wafer at 150 °C, and those of PA-TEG2 and PA-TEG2-12 films after soaking in water and drying at 100 °C.

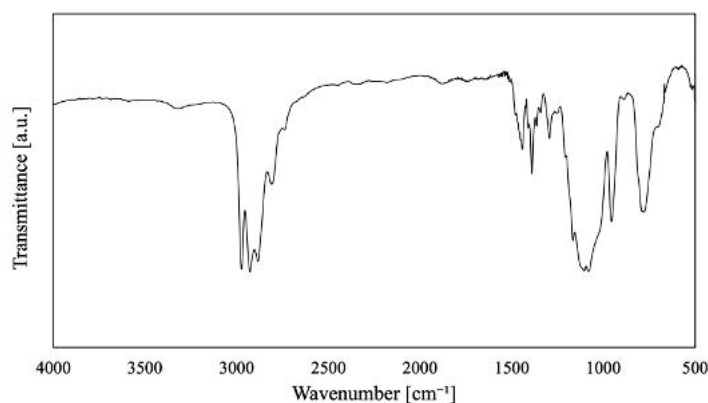


Figure 3.4. FT-IR spectra of PA-TEG10 film prepared by heating precursor sols coated on silicon.

A nitrogen adsorption/desorption isotherm is used to evaluate membrane porosity due to membrane porosity considerably affects its permeability. Figure 3.5 shows the isotherms of PA-TEG2 and PA-TEG5 gels that were prepared by drying their sol solutions at 60 °C in the air for two days, followed by calcination at 150 °C in a nitrogen atmosphere for 12 h, similar to the conditions used to prepare the gel films for IR spectrometry. The adsorption/desorption isotherms of BTESPA are also presented in Figure 3.5 for comparison [7]. In contrast to the BTESPA-based gel powder, the PA-TEG2- and PA-TEG5-based gel powder exhibited no volume adsorption, suggesting that the gel powder was non-porous. In the water separation process of the PA-TEG2-

and PA-TEG5-based membranes, therefore, the solution-diffusion mechanism is operative rather than the molecular sieving effects for water separation.

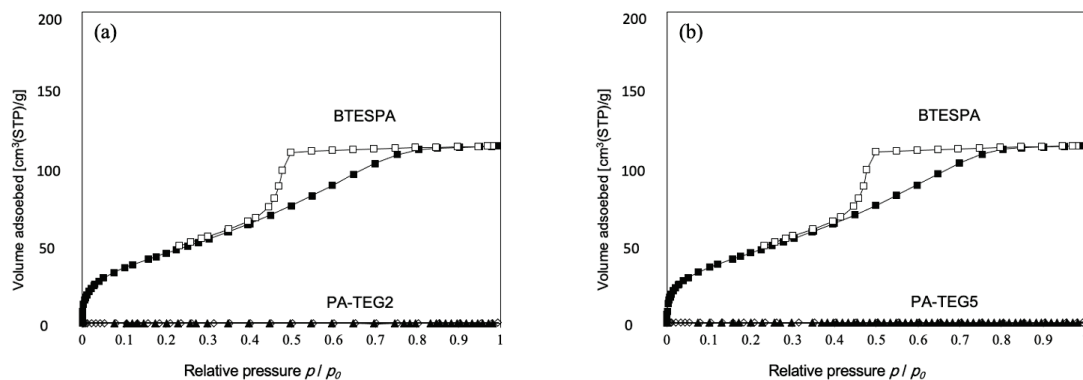


Figure 3.5.  $N_2$  adsorption/desorption isotherms of PA-TEG2, PA-TEG5, and BTESPA gel powder.

The surface and cross-sectional morphologies of membranes of PA-TEG2 and PA-TEG5 were examined by SEM. Generally, water permeability of RO membranes is inversely proportional to its thickness, that is, the thicker the PSQ layer tends to exhibit lower water permeability. However, too thin PSQ layer will lead to decreases in salt rejection. Figures 3.6a and 3.6b show the cross-sectional morphologic SEM images of the PA-TEG2- and PA-TEG5-based membranes, respectively. The PSQ separation layer could be clearly seen as the top layer whose thickness ranged from 100 to 120 nm. In addition, surface topography was also characterized by SEM (Figure 3.6c). The smooth and defect-free surface can be observed, indicating the formation of a homogeneous separation layer.

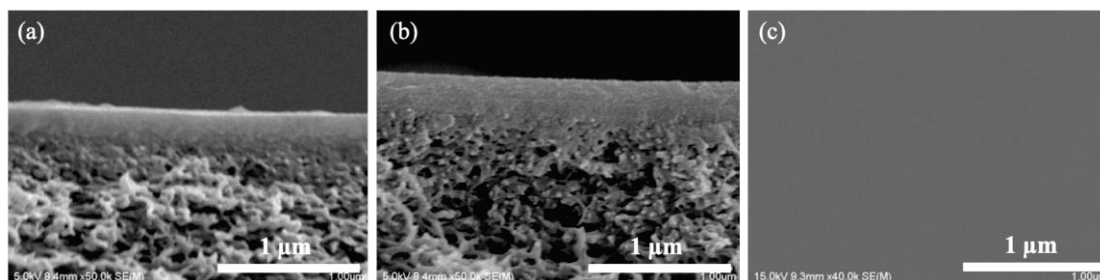
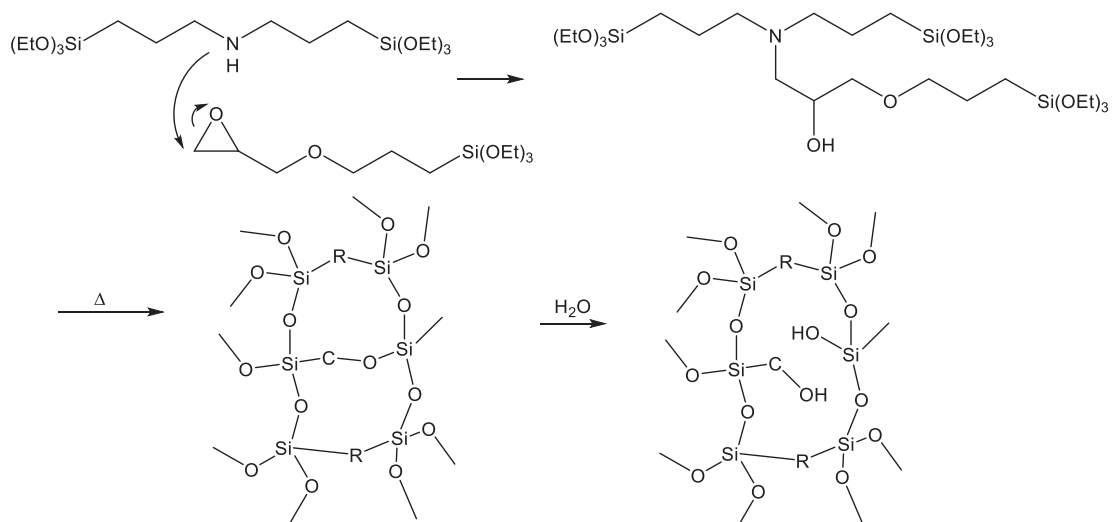


Figure 3.6. Cross-sectional SEM images of (a) PA-TEG2- and (b) PA-TEG5-based membranes. (c) SEM image of PA-TEG2-based membrane surface.

### *Reversible hydrolytic C-O-Si bond cleavage*

To obtain the molecular structure information of these gels, the author prepared TEGPS homo-based gel powder by homopolymerization of TEGPS as the control sample under the same conditions as those for the preparation of PA-TEG2 and PA-TEG5-based membranes. The  $^{13}\text{C}$  solid-state NMR spectra of the gel powders prepared from TEGPS homopolymer and PA-TEG2 copolymer are shown in Figure 3.7(a) and 3.7(b), respectively. These gel powders were obtained by the same process as that for TG analysis. For the PA-TEG2-based gel powder, broad peaks centered at approximately 9, 20, and 55 ppm were clearly observed, and these were attributed to the propyl group carbons from BTESPA and TEGPS. Peaks (1) to (3) attributed to the carbons of glycidyoxy group in Figure 3.7(a) disappeared in Figure 3.7(b), indicating that the ring opening reaction occurred by interaction with BTESPA (Scheme 3.2). The broad peak centered at 50 ppm observed in Figure 3.7(b) is likely due to a small amount of glycidyoxy group remaining. To further promote the ring-opening reaction, the author prepared PA-TEG2-12-based gel powder by reacting PA-TEG2 sol with 20 eq of water for an additional 12 h and drying the resultant gel by the same process. The particle size distribution of PA-TEG2-12 sol determined by DLS is shown in Figure 3.1. The PA-TEG2-12-based gel powder showed no clear signal around 50 ppm in Figure 3.7(c). As expected, the longer reaction time resulted in the smaller amount of glycidyoxy group remaining in PA-TEG2-12-based gel. When the PA-TEG2-12-based gel powder was soaked in water for 12 h and then dried, the peak observed at 15 ppm in Figure 3.7(b) and 3.7(c) disappeared, as shown in Figure 3.7(d). This peak is likely due to the C-O-Si group undergoing hydrolysis to form C-OH and Si-OH groups upon immersion of the gel powder in water. It is known that the C-O-Si bond is less stable towards hydrolysis than the Si-O-Si bond. In the gelation process, the C-OH groups produced by the ring opening of epoxy units condense with Si-OH in PA-TEG2 and PA-TEG2-12 sols to form C-O-Si bonds. However, the C-OH groups in much less mobile gel cannot undergo condensation under the same conditions (Scheme 3.3).





Scheme 3.2. Schematic diagram of generation of C-OH bonds by hydrolyzing C-O-Si bonds in the membranes.

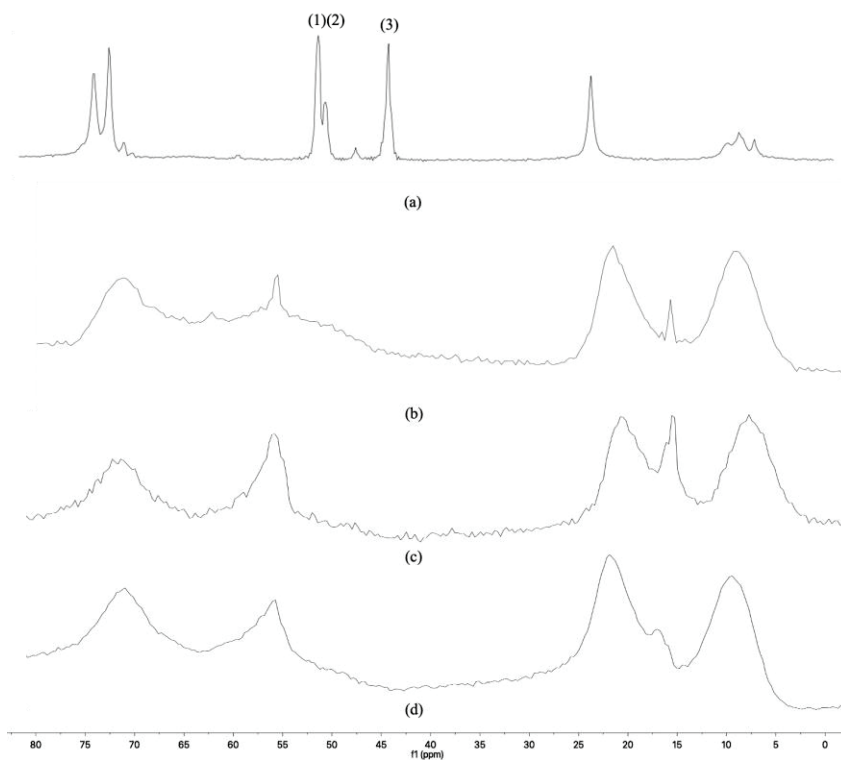
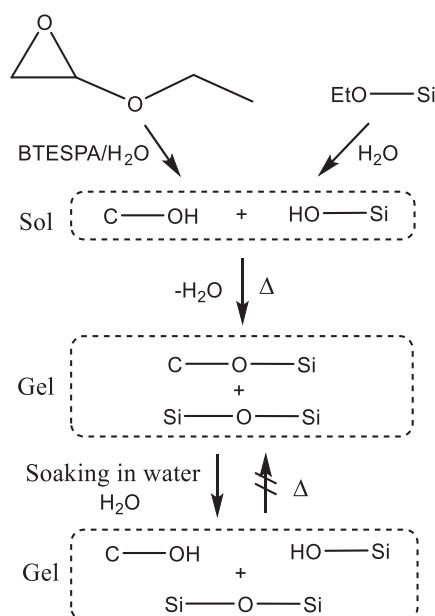


Figure 3.7.  $^{13}\text{C}$  DD/MAS NMR spectra of (a) TEGPS homopolymer-based gel powder, (b) PA-TEG2-based gel powder, (c) PA-TEG2-12-based gel powder before soaking, and (d) PA-TEG2-12-based gel powder after soaking/drying.



Scheme 3.3. Hydrolysis and condensation of copolymers of TEGPS and BTESPA.

To further characterize the structures of the PA-TEG2- and PA-TEG2-12-based membranes, the author carried out FT-IR analysis of their gel films, which were prepared by drop casting the sol solutions on a silicon wafer, followed by the calcination at 150 °C in air. The PA-TEG2 and PA-TEG2-12 gel films were subjected to an additional immersion experiment. These gel films were soaked in water at room temperature for 12 h and then dried at 100 °C in air for 1 h. Figure 3.3 exhibits the FT-IR spectra of PA-TEG2 and PA-TEG2-12 before and after soaking experiments in water. A broad peak from 3100  $\text{cm}^{-1}$  to 3600  $\text{cm}^{-1}$  was observed in the spectra of both gel films after soaking, which was due to the presence of OH groups. In contrast, the IR spectrum of the PA-TEG2 gel film before soaking showed no clear peak in this wavelength range. This may be explained by assuming that the C-OH groups arising from the hydrolysis of the epoxy units underwent condensation to form C-O-Si bonds in PA-TEG2, as shown in Scheme 3.2. Additional treatment with water resulted in the hydrolysis of epoxy or C-O-Si bonds to form C-OH groups. The water contact angles of the gel film surface also provided evidence of increased hydrophilicity, that is, after soaking/drying, the contact angles of PA-TEG2 and PA-TEG2-12 gel films prepared on glass plates were decreased from 55.8° to 41.1° and from 60.5° to 43.8°, respectively (Table 3.1 and

Figure 3.8). Increasing hydrophilicity improved the water permeability of the membranes (*vide infra*).

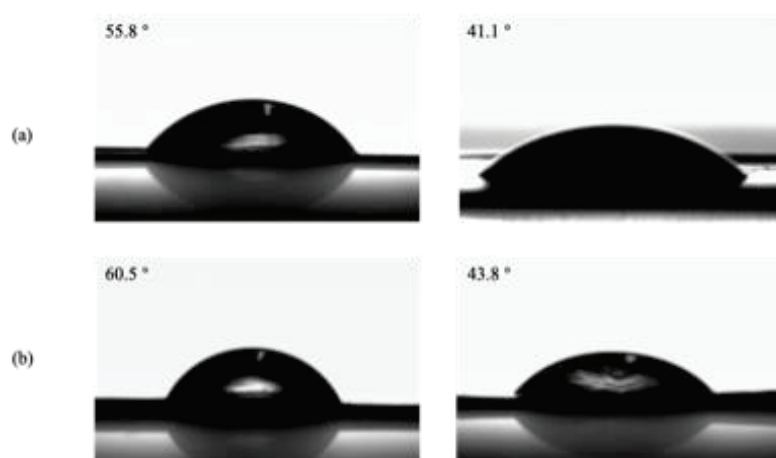


Figure 3.8. Water contact angles of the membranes of (a)PA-TEG2, (b) PA-TEG2-12 based membrane before and after soaking in water.

Table 3.1. Contact angles of PA-TEG2-, PA-TEG5-, PA-TEG10 and PA-TEG2-12-based membranes.

Membrane	PA-TEG2	PA-TEG5	PA-TEG10	PA-TEG2 soaking 12 h then dried	BTESPAa
CA	55.8	47.4	56.6	41.1	61.4

### *RO performance*

RO experiments of PA-TEG2-, PA-TEG5-, PA-TEG10- and PA-TEG2-12-based membranes were performed by using a 2000 ppm NaCl aqueous solution under the feed pressure of 1.5 MPa at room temperature. A summary of RO performance is presented in Figure 3.9(a). For the PA-TEG2-based membranes, the author examined their preparation five times and the data of the membrane that showed the highest salt rejection are presented in Table 3.2. The membrane exhibited excellent water permeability of  $9.6 \times 10^{-13} \text{ m}^3/\text{m}^2\text{sPa}$ , which is approximately nine times higher than that of the BTESPA homopolymer-based membrane which was reported in the literature ( $1.1 \times 10^{-13} \text{ m}^3/\text{m}^2\text{sPa}$ ) [8]. In addition, compared to the BTESPA homo-based membranes which exhibited salt rejection of 96 %, the PA-TEG2-based membrane

exhibited a slightly higher salt rejection of 97.5%. RO performance of the PA-TEG2-based membrane was a little lower than but close to that of commercially available organic RO membrane SW30HR (water permeability of  $1.1 \times 10^{-12} \text{ m}^3/\text{m}^2\text{sPa}$  and salt rejection of 98.5%). In addition, the PA-TEG5- and PA-TEG-10 based membranes also exhibited high water permeability of  $1.1 \times 10^{-12}$  and  $7.4 \times 10^{-13} \text{ m}^3/\text{m}^2\text{sPa}$  and good salt rejection of 94.4 and 94.1 %, respectively. A summary of the RO performance of the membranes examined herein is presented in Figure 3.9(c), together with those previously reported for BTESE-, BTESE2-, BTESE3-, and BTESPA-based PSQ membranes [9, 10]. The PA-TEG2-based membrane exhibited higher water permeability and salt rejection than the membranes prepared in the previous studies. The introduction of the epoxy-containing comonomer significantly improved water permeability, which is likely attributed to the ring opening of the epoxy units that resulted in the formation of C-OH groups during sol formation, which was supported by small water contact angles of the PA-TEG-based membrane surface (Table 3.1). In agreement with the observation that C-O-Si bonds were cleaved by soaking in water, the PA-TEG2-based membrane showed a slight increase in water permeability from  $8.9 \times 10^{-13} \text{ m}^3/\text{m}^2\text{sPa}$  to  $1.0 \times 10^{-12} \text{ m}^3/\text{m}^2\text{sPa}$  during the first two h of the RO experiment, (Figure 3.9(b)), which stabilized with time. The long-term stability of this membrane was also investigated. As described in Figure 3.10, although the salt rejection is lowered and the water permeability was increased after the 100 h RO experiment, the changes were slight showing good durability.

More pronounced changes in water permeability were seen in the PA-TEG2-12-based membrane. The PA-TEG2-12-based membrane exhibited water permeability of  $5.5 \times 10^{-13} \text{ m}^3/\text{m}^2\text{sPa}$  and salt rejection of 93.3% at the early stage of the RO experiment and then reached a stable state after 10 h to give the water permeability of  $9.3 \times 10^{-13} \text{ m}^3/\text{m}^2\text{sPa}$  and a slight decrease of salt rejection from 93.3% to 93.0% (Figure 3.9(b)). Although the water permeability is lower than that of the PA-TEG2-based membrane, it is higher than that of the BTESPA-based membrane.

Table 3.2. Summary of RO performance of PA-TEG2, PA-TEG5 and PA-TEG2-12-based membranes.

Membrane	Liquid permeability [(m <sup>3</sup> /m <sup>2</sup> s·Pa)]	NaCl rejection [%]
PA-TEG2	$9.6 \times 10^{-13}$	97.5
PA-TEG5	$1.1 \times 10^{-12}$	94.4
PA-TEG10	$7.4 \times 10^{-13}$	94.1
PA-TEG2-12	$9.3 \times 10^{-13}$	93.0
TEGPS	$1.3 \times 10^{-12}$	78.0
BTESPA <sup>[a]</sup>	$1.2 \times 10^{-13}$	97.0
BTESE <sup>[b]</sup>	$1.0 \times 10^{-13}$	98.0
BTESE2 <sup>[b]</sup>	$2.0 \times 10^{-13}$	98.0
BTESE3 <sup>[b]</sup>	$8.5 \times 10^{-13}$	92.0

<sup>a</sup> Data from literature

<sup>b</sup> Data from literature

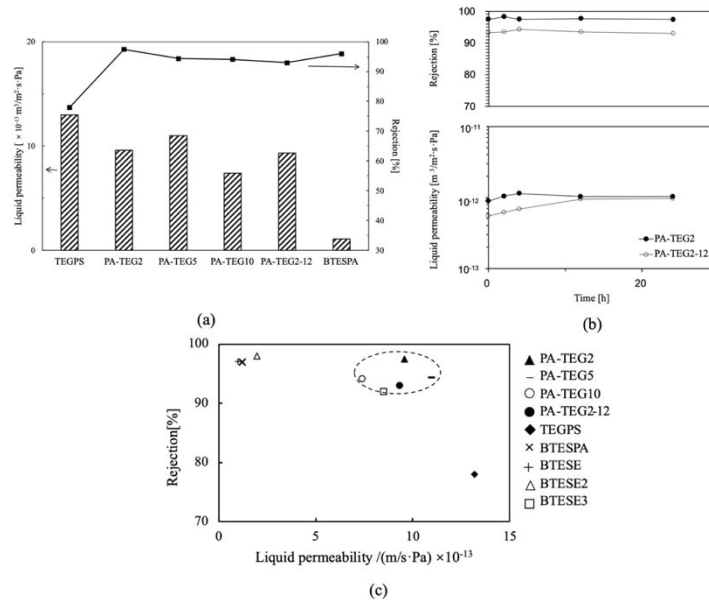


Figure 3.9. (a) Summary of RO performance in this work. (b) RO measurement of PA-TEG2- and PA-TEG2-12-based membranes by using 2000 ppm NaCl aqueous solution. (c) Summary of RO performance of the present membranes, together with those of × BTESPA (SG), + BTESE (SG), Δ BTESE2 (SG), and □ BTESE3 (SG) from the literature [10].

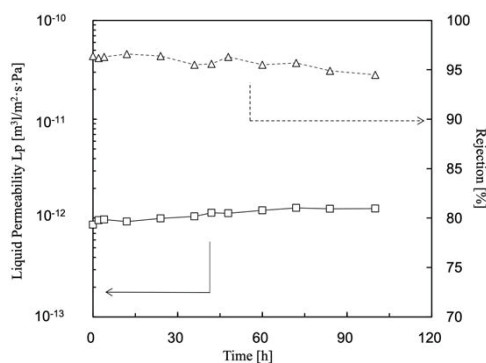


Figure 3.10. Long-term stability experiment of PA-TEG2-based membrane.

### *Resistance to chlorine and thermal stability*

For practical RO applications, RO membranes are expected to exhibit thermal stability and resistance to chlorine. The PA-TEG2-based membrane demonstrated excellent resistance to chlorine: the membrane exposed to 1000 ppm NaClO aqueous solution at room temperature exhibited no obvious changes in water permeability and salt rejection up to 10 h exposure (10000 ppm·h), as illustrated in Figure 3.11(a). To investigate the thermal stability of the membrane, RO measurement was carried out at elevated temperatures. The PA-TEG2-based membrane showed high thermal stability up to 60 °C. At this temperature, water permeability increased from  $9.6 \times 10^{-13} \text{ m}^3/\text{m}^2\text{sPa}$  to  $1.82 \times 10^{-12} \text{ m}^3/\text{m}^2\text{sPa}$ , and salt rejection decreased from 97.5% to 95.5%. Moreover, when the temperature was lowered to room temperature, the original water permeability and salt rejection were recovered (water permeability of  $9.6 \times 10^{-13} \text{ m}^3/\text{m}^2\text{sPa}$  and salt rejection of 97.5 %), as shown in Figure 3.11(b). On the other hand, when water temperature exceeded 80 °C, salt rejection decreased dramatically and did not return to its original value (Figure 3.12). Exceedingly high temperatures seemed to cause serious damage to the membrane. Indeed, when the coated film of PA-TEG2 on a silicon wafer was treated with hot water at 90 °C for 2 h, C-H vibration bands around  $2900 \text{ cm}^{-1}$  were weakened, suggesting that organic units were liberated from the film to an extent (Figure 3.13). However, thermal stability of the present membrane was

superior to that of commercial polyamide-based membranes for which the operating temperature limit is 45 °C [11].

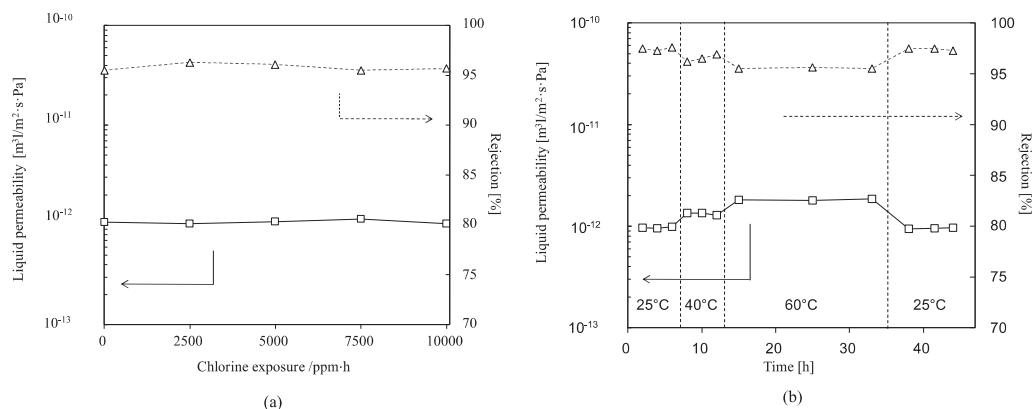


Figure 3.11. (a) Chlorine exposure test by using 1000 ppm NaClO aqueous solution. (b) Thermal stability test by using 2000 ppm NaCl aqueous solution.

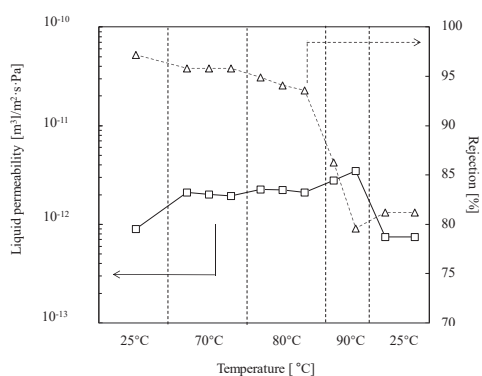


Figure 3.12. Thermal stability test for PA-TEG2-based membrane using 2000 ppm NaCl aqueous solution.

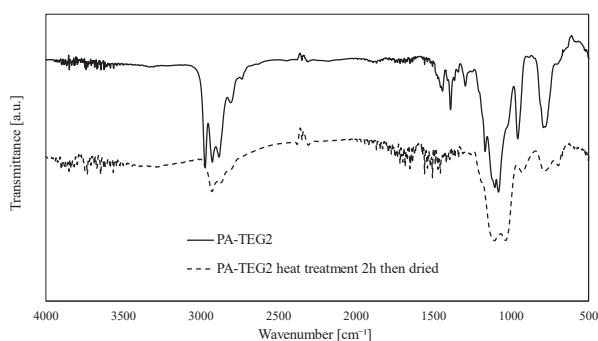


Figure 3.13. FT-IR spectra of PA-TEG2 film prepared by heating precursor sols coated on silicon wafer at 150 °C, before and after heat treatment in water at 90 °C for 2 h and drying at 100 °C.

## Summary

In conclusion, the author successfully introduced epoxy groups into PSQ-RO membranes. The epoxy groups significantly improved membrane hydrophilicity through the ring opening reaction, thereby increasing membrane permeability. Although the PA-TEG2-based gel powder exhibited non-porous properties, its membrane exhibited high water permeability of  $9.6 \times 10^{-13} \text{ m}^3/\text{m}^2\text{sPa}$  and excellent salt rejection of 97.5%, which were close to those of commercially available organic RO membrane SW30HR. In addition, this membrane showed high resistance to chlorine and excellent thermal stability up to 60 °C, indicating potential application as a robust membrane. The author also conducted studies on the condensation/hydrolysis of the C-O-Si group. The surface C-OH group content increased as the immersion time in water increased, resulting in the improvement of membrane permeability.

## Experimental

### *General*

Bis[3-(triethoxysilyl)propyl]amine with 95% purity was purchased from Gelest Inc. Triethoxy(3-glycidyloxypropyl)silane with 96% purity was purchased from TCI Co., Ltd. All chemicals were used without further purification. Ethanol used as the reaction solvent during the SG process was distilled from Mg and stored over activated molecular sieves in the dark until use. DLS measurements were carried out on a Malvern Zetasizer Nano (Malvern, ZEN3600) analyzer. TGA was conducted using an SII EXSTAR TG-DTA6200 thermal analyzer in the temperature range of 25 °C to 1000 °C in a nitrogen atmosphere. Contact angle measurements were performed with a Kyowa DM300 contact angle meter.



### *Sol-gel process for membrane preparation and Evaluation of RO performance*

The SG process, membrane preparation process was conducted as chapter 1 membrane preparation section.

The evaluation of RO performance method was conducted as reported in chapter 1. Two RO performance parameters, water permeability ( $L_p$ ) and salt rejection ( $R$ ), were determined by using equations (1) and (2) [12], respectively, in which  $\Delta P$  and  $\Delta\pi$  are differences in applied and osmotic pressures, and  $J_v$  is the permeate water flux.  $C_f$  and  $C_p$  are NaCl concentrations of feed and permeate, which were determined from their conductivities obtained using a conductivity meter (HORIBA, ES-51).

$$L_p = J_v / (\Delta P - \Delta\pi) \quad (1)$$

$$R = \left(1 - \frac{C_p}{C_f}\right) \times 100\% \quad (2)$$

### **References**

- [1] S. Krishnan, C.J. Weinman, C.K. Ober, Advances in polymers for anti-biofouling surfaces, *J. Mater. Chem.*, 18 (2008), 3405-3413.
- [2] A.C. Sagle, E.M. Van Wagner, H. Ju, B.D. McCloskey, B.D. Freeman, M.M. Sharma, PEG-coated reverse osmosis membranes: desalination properties and fouling resistance, *J. Membr. Sci.*, 340 (2009), 92-108.
- [3] L.-Y. Chen, X.-H. Lin, J.-G. Gai, Polyethylenimine linked glycidol surface antifouling reverse osmosis membrane, *Industrial & Engineering Chemistry Research*, 57 (2018), 2322-2328.
- [4] F.-T. Zheng, K. Yamamoto, M. Kanezashi, T. Tsuru, J. Ohshita, Preparation of bridged silica RO membranes from copolymerization of bis(triethoxysilyl)ethene/(hydroxymethyl)triethoxysilane. Effects of ethenylene-bridge enhancing water permeability, *J. Membr. Sci.*, 546 (2018), 173-178.
- [5] K. Yamamoto, J. Ohshita, T. Mizumo, M. Kanezashi, T. Tsuru, Preparation of hydroxyl group containing bridged organosilica membranes for water desalination, *Sep. Purif. Technol.*, 156 (2015), 396-402.

- [6] G. Li, M. Kanezashi, T. Tsuru, Preparation of organic–inorganic hybrid silica membranes using organoalkoxysilanes: the effect of pendant groups, *J. Membr. Sci.*, 379 (2011), 287-295.
- [7] K. Yamamoto, S. Koge, K. Sasahara, T. Mizumo, Y. Kaneko, M. Kanezashi, T. Tsuru, J. Ohshita, Preparation of bridged polysilsesquioxane membranes from bis[3-(triethoxysilyl)propyl]amine for water desalination, *Bull. Chem. Soc. Jpn.*, 90 (2017), 1035-1040.
- [8] E.S. Hatakeyama, C.J. Gabriel, B.R. Wiesenauer, J.L. Lohr, M. Zhou, R.D. Noble, D.L. Gin, Water filtration performance of a lyotropic liquid crystal polymer membrane with uniform, sub-1-nm pores, *J. Membr. Sci.*, 366 (2011), 62-72.
- [9] R. Xu, J. Wang, M. Kanezashi, T. Yoshioka, T. Tsuru, Development of robust organosilica membranes for reverse osmosis, *Langmuir*, 27 (2011), 13996-13999.
- [10] R. Xu, S.M. Ibrahim, M. Kanezashi, T. Yoshioka, K. Ito, J. Ohshita, T. Tsuru, New insights into the microstructure-separation properties of organosilica membranes with ethane, ethylene, and acetylene bridges, *ACS Appl. Mater. Interfaces*, 6 (2014), 9357-9364.
- [11] M. Mänttari, A. Pihlajamäki, E. Kaipainen, M. Nyström, Effect of temperature and membrane pre-treatment by pressure on the filtration properties of nanofiltration membranes, *Desalination*, 145 (2002), 81-86.
- [12] M.L. Lind, D. Eumine Suk, T.-V. Nguyen, E.M. Hoek, Tailoring the structure of thin film nanocomposite membranes to achieve seawater RO membrane performance, *Environ. Sci. Technol. Lett.*, 44 (2010), 8230-8235.

## **Chapter 4** Preparation of high water permeable PSQ-RO membranes by introducing hydroxyethylurea-based hydrophilic water channels

### **Introduction**

In the previous works, several strategies have been reported to increase the permeability of water of PSQ-RO membranes by introducing hydroxyl groups. For example, membranes prepared by the copolymerization of bis(triethoxysilyl)ethane (BTESE) with hydroxymethyl(triethoxy)silane (HMTES) exhibited about three times higher permeability of water than BTESE homopolymer membranes [1]. Similarly, the copolymerization of bis(triethoxysilyl)ethene (BTESE2) with HMTES resulted in approximately seven times higher permeability of water than BTESE2 homopolymer-based membranes [2]. In addition, in chapter 2, we proposed a strategy to improve water permeability by the introduction of epoxy groups via the copolymerization of bis[3-(triethoxysilyl)propyl]amine (BTESPA) and triethoxy(3-glycidyloxypropyl)silane. Although we have obtained similar water permeability to those of commercial polyamide RO membranes, higher water permeability PSQ-RO membrane should be explored

In this chapter, to realize the even higher water permeability of PSQ-based RO membranes, the author copolymerized BTESPA with N-(2-hydroxyethyl)-N'-[3-(triethoxysilyl)propyl]urea (HETESPU). Two other hydroxyurea derivatives were also examined as the comonomers. It has been reported that ureidosiloxane precursors tended to self-organize by hydrogen bonding during the sol-gel (SG) process [3], and the hydroxyl groups in the HETESPU units enhanced the water affinity of the channel and the membrane surface [4]. The author found that during the preparation of the membranes, aggregation through hydrogen bonding occurred in the PSQ-based membrane (see Figure 4.1 for schematic illustration), which can be regarded as a hydrophilic water channel, thereby dramatically increasing the permeability. In addition, the tight packing of urea units through the hydrogen bonding enhanced the robustness of the resultant membranes.

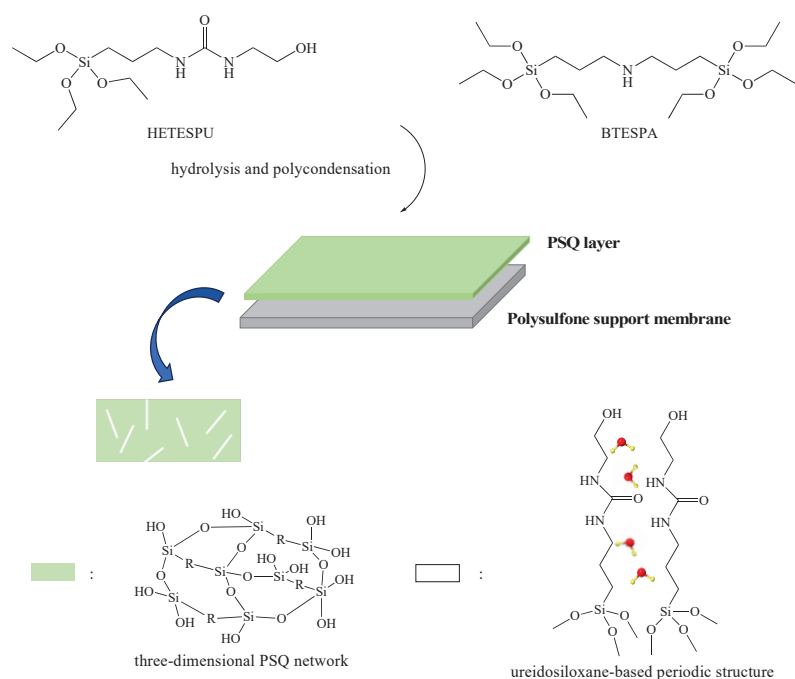


Figure 4.1. Schematic explanation of the structure of HETESPU-BTESPA copolymer membrane.

## Results and discussion

### Membrane preparation

Mixtures of BTESPA: HETESPU = 90:10, 75:25, and 50:50 were subjected to hydrolysis/copolymerization via sol-gel process to yield sols PAHE10, PAHE25, and PAHE50, respectively. The particle size distribution of these sols is presented in Figure 4.2(a). The sol sizes were well controlled into the range of 1.5 to 2 nm, which are suitable for coating on a polysulfone support membrane as described in Chapter 1.

Thermogravimetric analysis (TGA) was performed to determine the calcination temperature for membrane formation on the support membrane. The TGA curves of these gel powders are presented in Figure 4.2(b). The gradual weight loss below 200 °C would be ascribed to the liberation of water adsorbed and generated by the dehydration of Si-OH groups giving Si-O-C and Si-O-Si bonds. At higher temperatures, the decomposition of organic units would take place, resulting in the larger weight loss. Based on these results, the calcination temperature of the membranes was set at 150 °C.

FT-IR spectral analyses were performed to obtain information on polymer gel formation. Coating the sol solutions on a silicon wafer and heating the sol films at 150 °C in nitrogen gave the gel films. The FT-IR spectra are presented in Figure 4.2(c). The broad Si-O-Si stretching bands were seen at 1065  $\text{cm}^{-1}$ . With regard to the urea units, peaks attributed to C-N and C=O stretching appeared at 1265  $\text{cm}^{-1}$  and 1645 to 1635  $\text{cm}^{-1}$ , respectively [5]. The band assignable to N-H bending was apparent at 1570  $\text{cm}^{-1}$ . Compared with the standard absorption values of the C=O peak (1760 to 1670  $\text{cm}^{-1}$ ) and the N-H peak (1650 to 1580  $\text{cm}^{-1}$ ), these peaks appeared at lower wavenumbers, most likely because of the hydrogen bonding of the N-H---O=C and/or OH---O=C units [6].

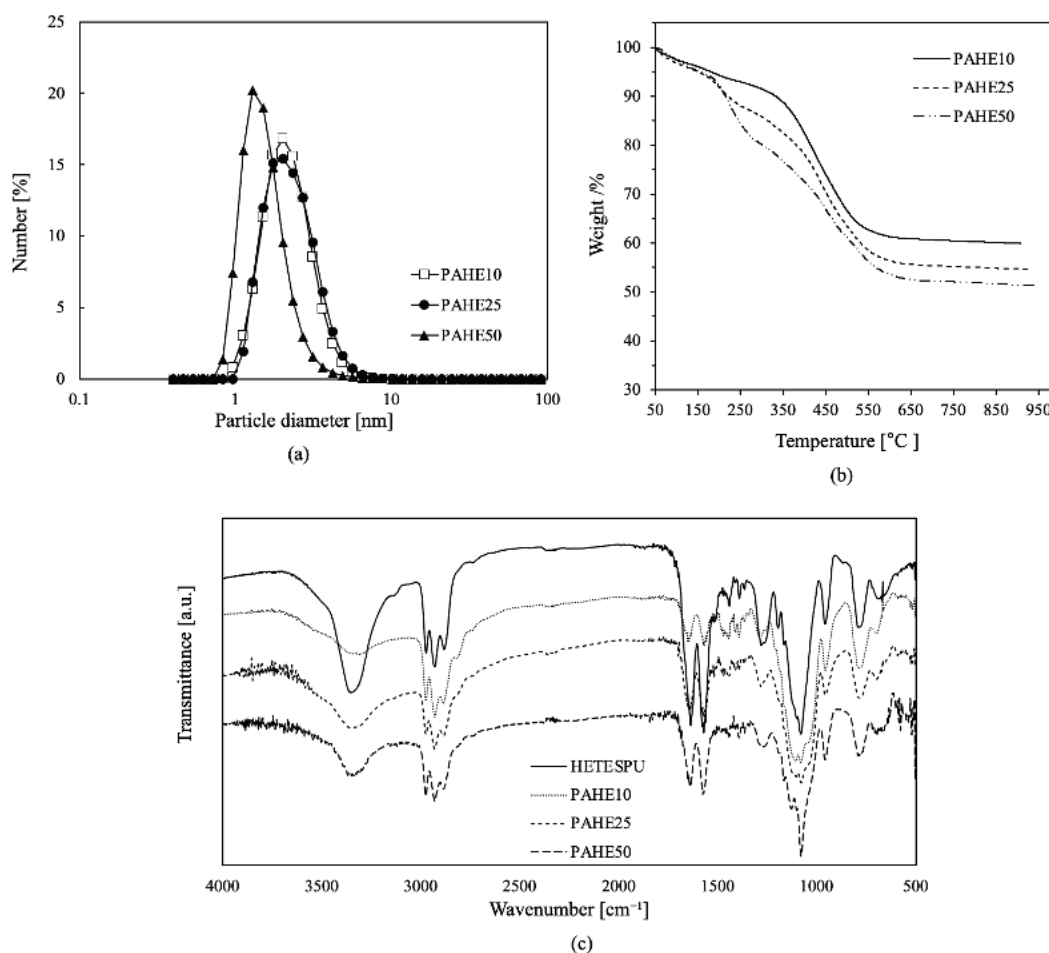


Figure 4.2. (a) Dynamic light scattering (DLS) plots for particle size distribution. (b) TGA traces of gel powders in nitrogen. (c) FT-IR spectra of gel films on silicon wafer.

### *SEM surface morphologies and cross-sectional topographies*

The cross-sectional topographies of membranes of PAHE10, PAHE25, PAHE50, and HETESPU and BTESPA homopolymers were examined by SEM, and the images are shown in Figures 4.3(a) to (e). The PSQ-based membrane layer could be observed at the top with around 50 nm thickness, although the boundary of the support membrane and the PSQ-based membrane could not be clearly seen. Typically, the membrane thickness is inversely related to the water permeability, a thin PSQ layer tends to increase the permeability. However, when a PSQ-based membrane layer is too thin, a drastic decrease in NaCl rejection may occur, due to insufficient diffusion control and sieving effect. The SEM surface images of the membranes are shown in Figures 4.3 (f) to (j). The membranes prepared from PAHE10 and PAHE25 exhibited a smooth surface, indicating the formation of fine, homogeneous, and defect-free PSQ-based separation layers, similar to that exhibited by the BTESPA homopolymer membrane (Figure 4.3(j)), although particulates were noticeable on the surface, likely due to the aggregation of HETESPU units during gelation. The excess content of HETESPU led to the formation of pinholes (Figures 4.3(h) and 3(i)). The pinhole depth curve of the PAHE50-based membrane was examined by AFM and shown in Figure 4.4. Pinhole depth was approximately 10 to 12 nm, and pinhole diameter was approximately 500 nm, consistent with those observed in the SEM images. It seemed that these pinholes contributed to inferior water separation performance (*vide infra*).

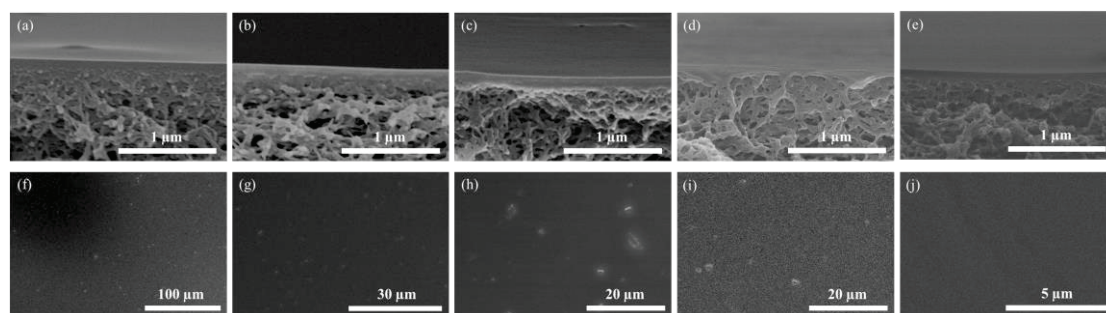


Figure 4.3. Cross-sectional topographies of membranes of (a) PAHE10, (b) PAHE25 (c) PAHE50, and (d) HETESPU and (e) BTESPA homopolymers, and surface morphologies of membranes of (f) PAHE10, (g) PAHE25, and (h) PAHE50, and (i) HETESPU and (j) BTESPA homopolymers, determined by SEM

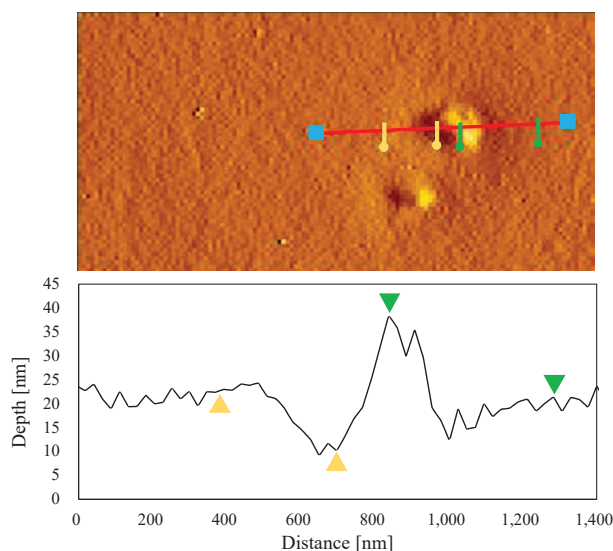


Figure 4.4. Pinhole depth curve of PAHE50-based membrane analyzed by AFM.

AFM topographical and phase images of these membranes' surfaces based on BTESPA, PAHE10, PAHE25, and PAHE50 are shown in Figure 4.5. The BTESPA-based membrane exhibited a smooth surface in both topographical and phase images. In the phase images, as HETESPU content increased, brightly colored aggregates gradually appeared (Figures 4.5(e) to (h)), suggesting that HETESPU tended to aggregate during the membrane formation. AFM hardness images also provided evidence of the aggregate formation on these membrane surfaces (Figure 4.6). As HETESPU content increased, more bright spots could be seen on the AFM hardness images which are likely due to aggregates. The average roughness ( $R_a$ ) of the copolymer membranes was larger than that of the membrane based on BTESPA homopolymer, in agreement with the formation of aggregates.



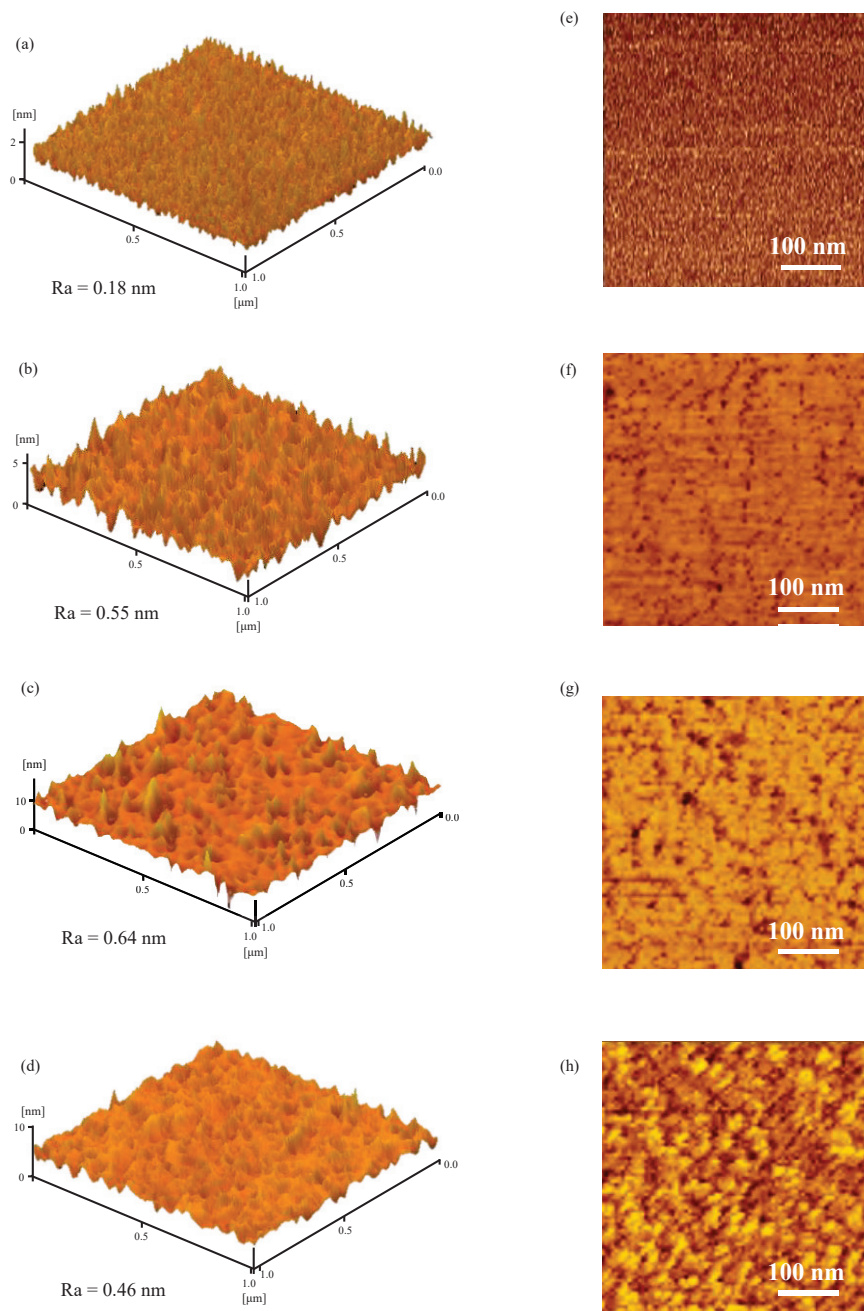


Figure 4.5. AFM topographical images of membranes of (a) BTESPA, (b) PAHE10, (c) PAHE25, and (d) PAHE50, and phase images of membranes of (e) BTESPA, (f) PAHE10, (g) PAHE25, and (h) PAHE50.

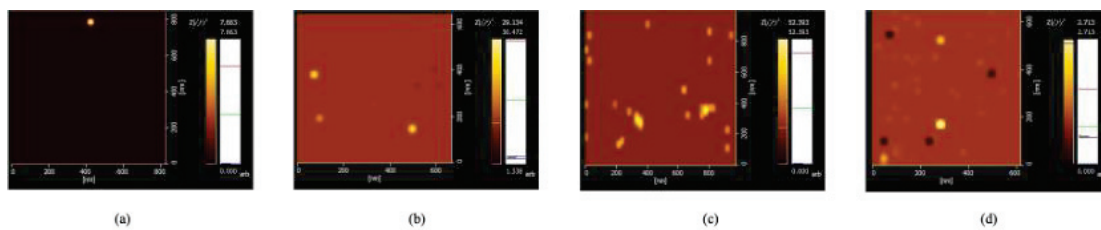


Figure 4.6. AFM hardness images of membranes (a) BTESPA, (b) PAHE10, (c) PAHE25, and (d) PAHE50.



### *Porous properties*

Nitrogen adsorption/desorption measurements of PAHE10, PAHE25, and PAHE50 copolymer and BTESPA homopolymer gels were performed to reveal their porous properties. In general, the increased porosity is proportional to water permeability. The nitrogen adsorption/desorption isotherms of these gel powders are shown in Figure 4.7. Compared with the surface area of 176 m<sup>2</sup>/g for the reference sample of BTESPA homopolymer gel, the surface area was 237 m<sup>2</sup>/g for PAHE10 and 15.0 m<sup>2</sup>/g for PAHE25, whereas the PAHE50-derived gel was non-porous. Suggesting that a small amount of HETESPU increased the porosity, However, an excess amount of HETESPU made the porosity decrease. Although the reason for porosity changes depending on the HETESPU content is still unclear, probably due to enhanced aggregation by hydrogen bonding of HETESPU units would increase the porosity, but excessive aggregation would lead to shrinkage of the gel decreasing the porosity. A similar tendency was observed for surface roughness determined by AFM measurements (Figure 4.5), which increased with increasing the HETESPU content from BTESPA homopolymer to PAHE25-derived membrane but decreased for PAHE50-derived membrane. These results contrasted the results for the PAHE25- and PAHE50-derived membranes, which exhibited extremely high water permeability (see next section). The author presumed that the enhancement of hydrophilicity by increasing HETESPU content was responsible for the improvement of water permeability, as described below.

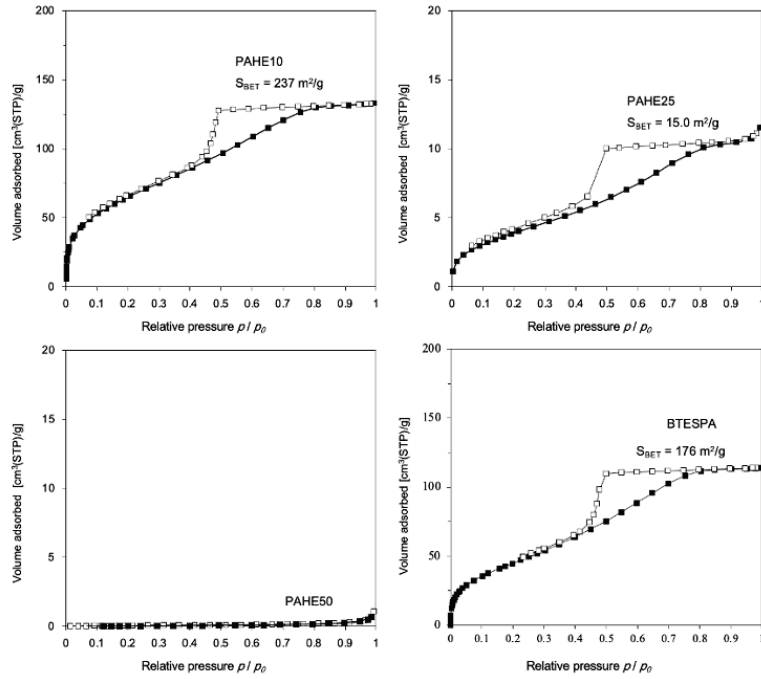


Figure 4.7. N<sub>2</sub> adsorption/desorption isotherms of PAHE10, PAHE25, PAHE50, and BTESPA gel powder.

Table 4.1. Surface areas and micropore volumes.

Sample	BET surface area $S_{\text{BET}}$ (m <sup>2</sup> /g)	Micropore volume VP (cm <sup>3</sup> /g)
BTESPA	176	0.1762
PAHE10	237	0.2053
PAHE25	15	0.0180
PAHE50	non-porous	non-porous

### RO performance

RO performance of PAHE10-, PAHE25-, PAHE50-, and HETESPU homopolymer-based membranes were summarized in Figure 4.8(a). The RO measurement was carried out under the feed pressure of 1.5 MPa at room temperature with a NaCl aqueous solution (2000 ppm). The HETESPU homopolymer membrane exhibited the highest water permeability ( $2.6 \times 10^{-12}$  m<sup>3</sup>/m<sup>2</sup>sPa) among the membranes, with a NaCl rejection of 91.1%. However, the HETESPU-homo-based membrane was unstable. After an 8-h RO experiment, water permeability was increased to  $4.7 \times 10^{-12}$  m<sup>3</sup>/m<sup>2</sup>sPa and NaCl rejection was drastically decreased from 91.1% to 75.8%. The high water permeability was probably attributed to the high hydrophilicity by the introduction of urea and

hydroxy groups, as shown in the FT-IR spectrum in Figure 4.2(c). In addition, it was hypothesized that the aggregation of HETESPU units formed a hydrophilic channel for water permeation as presented in Figure 4.1. However, the HETESPU homopolymer-based membrane possessed pinholes on the surface (Figure 4.3(h)), which was likely due to excessive aggregation of HETESPU. This seemed to be also responsible for the relatively high permeability of water and low NaCl rejection, in comparison with the BTESPA homopolymer membrane (water permeability =  $1.1 \times 10^{-13} \text{ m}^3/\text{m}^2\text{sPa}$ , NaCl rejection = 96%) [7]. For membranes that were prepared from the copolymerization, the PAHE25-based membrane exhibited the best RO performance with high water permeability of  $1.86 \times 10^{-12} \text{ m}^3/\text{m}^2\text{sPa}$  and the NaCl rejection of 95.9%, exceeding the RO performance of PSQ-based RO membranes, so far reported previously, as summarized in Figure 4.8(c). Indeed, the PAHE25-based membrane exhibited approximately 19-fold higher water permeability than the BTESPA homopolymer membrane, whereas their NaCl rejection values were nearly the same. Further increase of HETESPU content to 50% resulted in a slight increase in water permeability, although NaCl rejection was decreased to 82.2%. The aggregation of HETESPU units was expected to increase water permeability through the formation of hydrophilic water channels, as described above. However, excessive aggregation resulted in the formation of pinholes, which decreased NaCl rejection, as in the case of the HETESPU homopolymer membrane. Increased porosity by the copolymerization with HETESPU may be also a reason for improved permeability compared to the BTESPA homopolymer membrane. However, PAHE50 is non-porous, thereby being difficult to discuss the porosity-permeability relationship of the present HETESPU-containing membranes.

Improved water permeability can be achieved by increasing the surface hydrophilicity of RO membranes. Figure 4.8(b) demonstrates that the surface water contact angles of these membranes gradually decreased from  $61.4^\circ$  to  $53.9^\circ$  as the HETESPU content increased from 0 to 50 %, which is consistent with the increase of membrane permeability in the same order, due to the higher hydrophilicity of

HETESPU with urea and hydroxy units than BTESPA with an amine unit. Membrane porosity, surface hydrophilicity, and aggregation forming hydrophilic channels always played important roles in affecting the water permeability of the present membranes. The porosity of the PAHE10-based membrane seemed to be increased compared to BTESPA homopolymer membrane, judging from the higher BET surface area of the PAHE10-based gel powder than that of the BTESPA homopolymer (Table 4.1). In addition, the smaller water contact angle indicated enhanced surface hydrophilicity. For the PAHE25-based membranes, their porosity seemed to be suppressed, but hydrophilicity was further enhanced overcoming the suppressed porosity, which lead to an even more enhanced water permeability than that of PAHE10-based membrane. To understand the effects of BTESPA, another precursor BTESE was also used for the copolymerization with HETESPU, and the RO performance is summarized in Table 4.2. As shown in Table 4.3, water permeability was significantly improved as the HETESPU content increased. However, at the same time, NaCl rejection was markedly lowered, due to the pinholes on the surface (Figure 4.9). This might be due to the lack of hydrogen bonding between comonomers BTESE and HETESPU, which leads to poor miscibility between them. Controlling the hydrogen bonding between and within comonomers is essential to obtaining high-performance membranes using HETESPU.

Expecting to obtain the urea-derived membranes with even higher performance, the author prepared *N*-[2,3-bis(trimethylsiloxy)propyl]-*N'*-[3-(triethoxysilyl)propyl]urea and *N*-[1,3-bis(trimethylsiloxy)propyl]-*N'*-[3-(triethoxysilyl)propyl]urea as new monomers. Trimethylsilyl units were used to protect hydroxyl groups to induce synthesis to proceed, and these trimethylsilyl units could be easily removed by hydrolysis of the trimethylsiloxy units during the SG process for the formation of hydroxy units. Membranes were prepared by the copolymerization of these precursors with BTESPA in the weight ratios of 1 to 3 by the same process as that for PAHE-based membranes. The sample names and the RO performance are summarized in Table 4.3. The gel powders prepared from PAHE2-25 and PAHE2'-25 exhibited similar porosity to the PAHE25-based gel powders (Figure 4.10). The addition of one hydroxyl group

Table 4.2. Summary of RO performance.

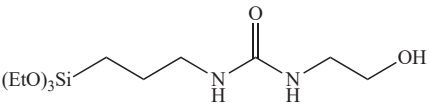
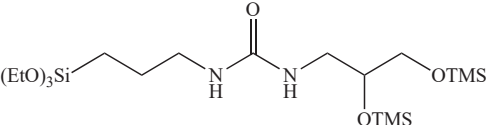
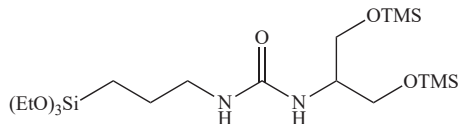
Membrane	Liquid permeance/(m/s·Pa)	NaCl rejection [%]
HETESPU	$2.6 \times 10^{-12}$	91.1
BTESE <sup>[a]</sup>	$1.0 \times 10^{-13}$	98.0
BTHE5 <sup>[b]</sup>	$4.1 \times 10^{-12}$	86.7
BTHE10 <sup>[b]</sup>	$4.8 \times 10^{-12}$	82.2
BTHE25 <sup>[b]</sup>	$3.3 \times 10^{-12}$	82.2

[a] data from a literature [8]

[b] Membranes prepared from copolymerization of BTESE/HETESPU with the ratio of 95:5, 90:10 and 75:25.

did not significantly increase water permeability, namely, the PAHE2-25-based RO membrane exhibited a slight improvement in water permeability to  $1.94 \times 10^{-12}$  m<sup>3</sup>/m<sup>2</sup>sPa compared with the PAHE25-based membrane ( $1.86 \times 10^{-12}$  m<sup>3</sup>/m<sup>2</sup>sPa), with increased NaCl rejection to 96.8% from 95.9%. In contrast, the membrane based on PAHE2'-25- showed lower permeability and lower rejection than the PAHE25-based membrane.

Table 4.3. Summary of RO performance of PAHE25-, PAHE2-25-, and PAHE2'-25-based membranes.

Precursors for copolymerization with BTESPA in the ratio of 1:3	Sample name	Water permeability/(m/s·Pa)	NaCl rejection [%]
	PAHE25	$1.86 \times 10^{-12}$	95.9
	PAHE2-25	$1.94 \times 10^{-12}$	96.8
	PAHE2'-25	$1.04 \times 10^{-12}$	88.9

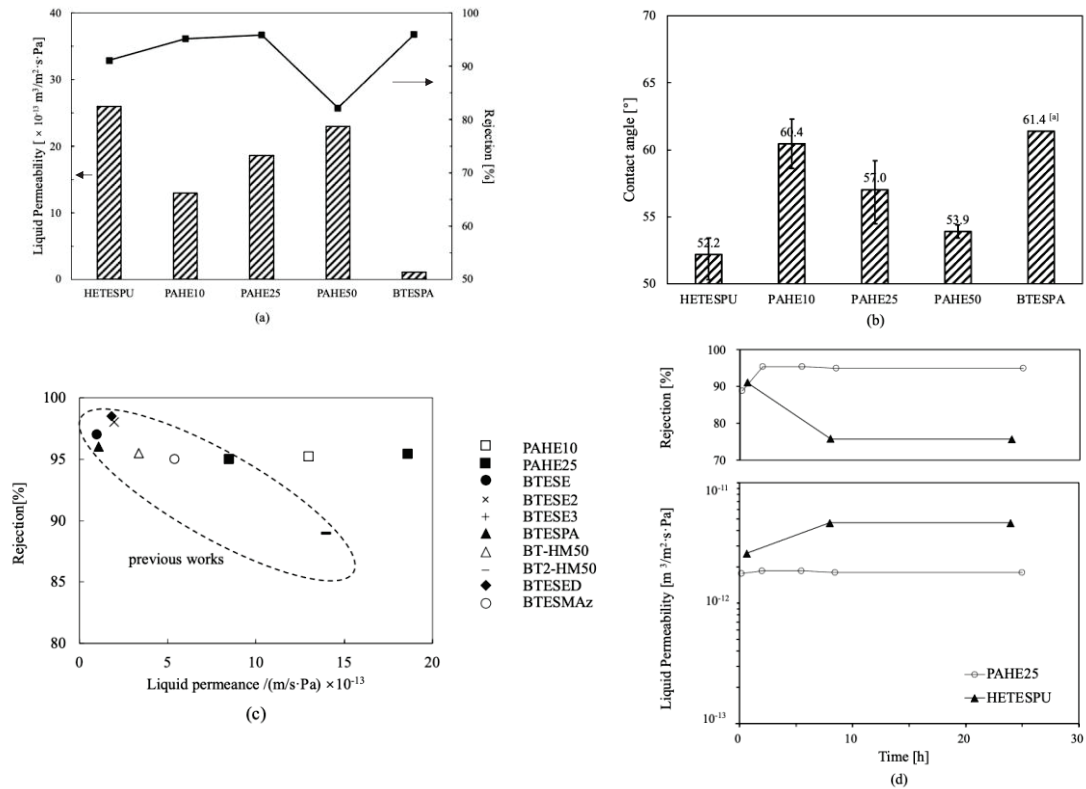


Figure 4.8. (a) RO performance of HETESPU-, PAHE10-, PAHE25-, PAHE50-, and BTESPA-based membranes. (b) Water contact angles of HETESPU-, PAHE10-, PAHE25-, PAHE50-, and BTESPA-based membranes. (c) Plots of RO performance of the present membranes, and those of BTESE, BTESE2, BTESE3, BTESPA, BT-HM50, BT2-HM20, 2,5-bis[2-(triethoxysilyl)ethyl]-1,4-dioxane (BTESED) and 1,4-bis (triethoxysilylmethyl)1,2,3-triazole (BTESMAz) from the literature [1, 2, 7, 9, 10]. (d) RO measurement of PAHE25- and HETESPU-based membranes for 24 h.

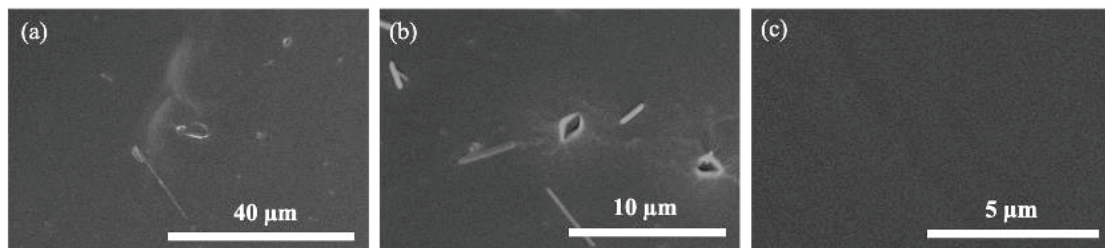


Figure 4.9. Surface morphologies SEM images of membranes (a)HETESPU, (b) BTHE25 and (c) BTESPA

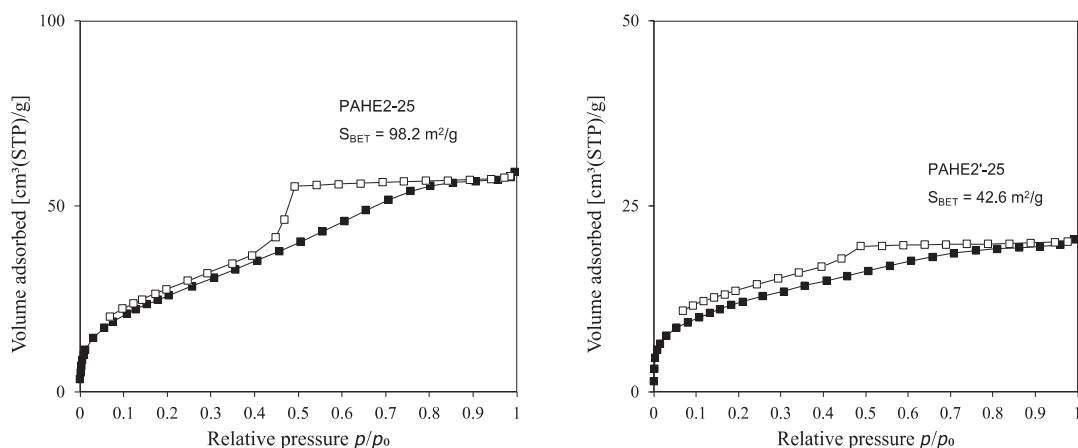
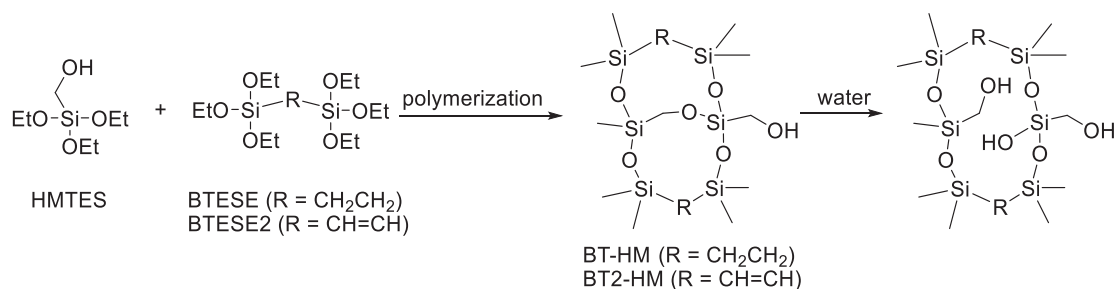


Figure 4.10. N<sub>2</sub> adsorption/desorption isotherms of PAHE2-25 and PAHE2'-25-based gel powder.

Previously, membrane preparation was carried out by the copolymerization of BTESE and BTESE2 with (hydroxymethyl)triethoxysilane (HMTES) to enhance the water permeability of PSQ-based RO membranes (Scheme 4.1) [1, 2]. Figure 4.8(c) shows the RO performance of various membranes with optimum copolymer ratio. The copolymer membranes with the BTESE/BTESE2:HMTES ratio of 50:50 (BT-HM50 and BT2-HM50) had water permeability of  $3.4 \times 10^{-13} \text{ m}^3/\text{m}^2\text{sPa}$  and  $5.0 \times 10^{-13} \text{ m}^3/\text{m}^2\text{sPa}$  and rejection of 95.5% and 92%, respectively. Thus, the introduction of hydroxyl groups into BTESE and BTESE2 through the copolymerization with HMTES improved water permeability by approximately three and seven times, respectively, and slightly decreased NaCl rejection compared with BTESE and BTESE2 homopolymer membranes. Throughout the RO experiments, these membranes showed a gradual increase in water permeability and reached constant values, as shown in Figure 4.8(c). The mechanism is outlined in Scheme 4.1. Dehydration condensation reaction occurred during gelation, Si-OH groups forming Si-O-Si linkages and Si-OH and C-OH groups generating Si-O-C bonds. The hydrolysis of Si-O-C bonds occurs more easily than Si-O-Si linkages, and the hydrolysis of the Si-O-C bonds took place to form C-OH and Si-OH bonds during the RO experiment, which was responsible for the enhancement of permeability and the slight decrease of rejection. However, it was found that the

water permeability of these HETESPU-derived membranes was stable even when the membranes were immersed in water. As shown in Figure 4.8(d), no clear changes were observed in the PAHE25-based membrane in water permeability and NaCl rejection even after RO experiments for 24 h. The IR spectra of the PAHE25-based gel film also exhibited no significant changes upon soaking in water for 12 h and then dried at 100 °C (Figure 4.11). This was likely due to the structural rigidity of the HETESPU-derived gels as a result of hydrogen bonding. The rigid structure hindered the dehydration condensation of the C-OH units with the Si-OH units to form C-O-Si linkages during the gelation. However, the HETESPU homopolymer membrane might be highly hydrophilic and readily underwent hydrolysis changing the membrane performance as presented in Figure 4.8(d). The author speculated that the high water flux in the pinholes would accelerate the hydrolysis and liberation of monomeric and/or oligomeric molecules from the membrane.



Scheme 4.1. Formation and dehydration of C-O-Si units in BT-HM and BT2-HM membranes.

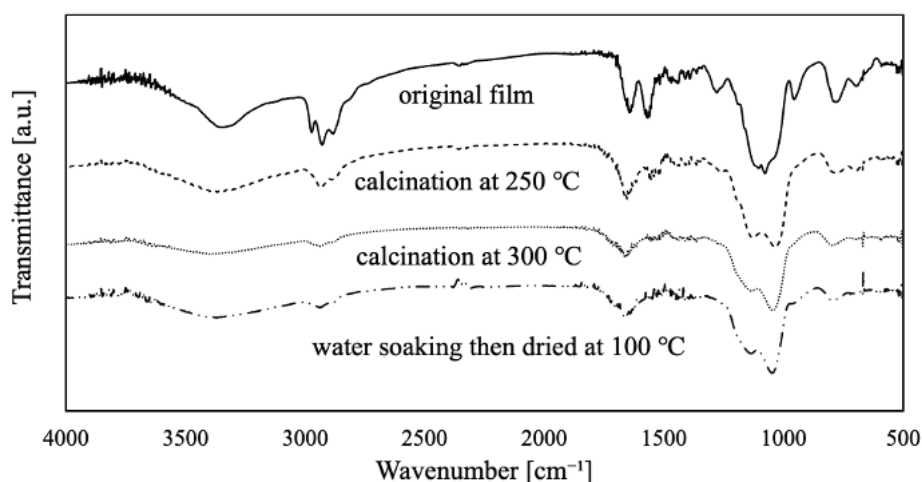


Figure 4.11. FT-IR spectra of PAHE25 based films on repetitive process of calcination at 250 and 300 °C, and soaking in water and drying at 100 °C.



### *Thermal stability*

To study the thermal property of the PAHE25-based membrane, the thermal stability was investigated and presented in Figure 4.12. PAHE25-based membrane exhibited excellent thermostability up to 60 °C. At 60 °C, NaCl rejection slightly decreased from 95.9% to 92.8%, but lowering the temperature to room temperature recovered NaCl rejection to 94.5%. Water permeability was recovered as well. However, when the operating temperature was further raised to 80 °C, the decreased NaCl rejection could not be recovered even on cooling the temperature to room temperature, indicating membrane damage partly (Figure 4.13). PAHE25-based membrane exhibited higher thermal stability than that of commercially available polyamide-based membranes whose upper operating temperature limit is 45 °C [11]. The high thermal stability was attributed to the robust Si-O-Si linkage. In addition, strong hydrogen bonding of HETESPU is also anticipated to stabilize the structure by immobilization. Unfortunately, the PAHE25-based membrane did not show high chlorine resistance even though it contained robust Si-O-Si linkage. The chlorine exposure experiment was performed at room temperature by using a 1000 ppm NaOCl aqueous solution. On exposure up to 5000 ppm·h, NaCl rejection slightly decreased from 95.8% to 90.1% but markedly decreased from 90.1% to 76.0% after further 5000 ppm·h exposure, although water permeability remained stable without significant changes (Figure 4.14).

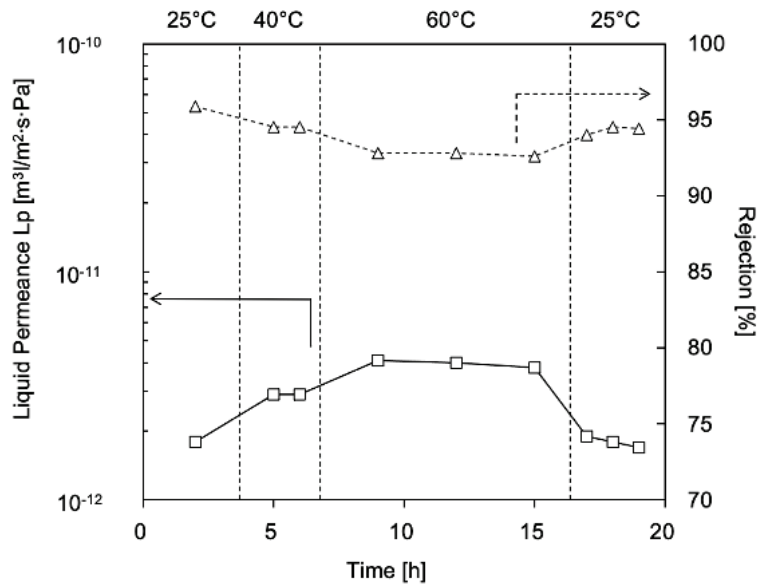


Figure 4.12. Thermal stability test for PAHE25-based membrane by using NaCl aqueous solution (2000 ppm).

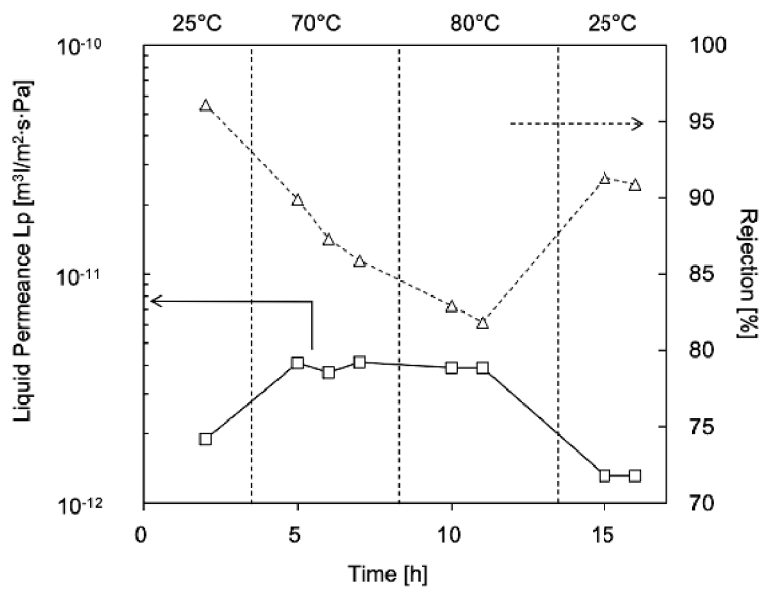


Figure 4.13. Thermal stability measurement by using 2000 ppm NaCl aqueous solution.

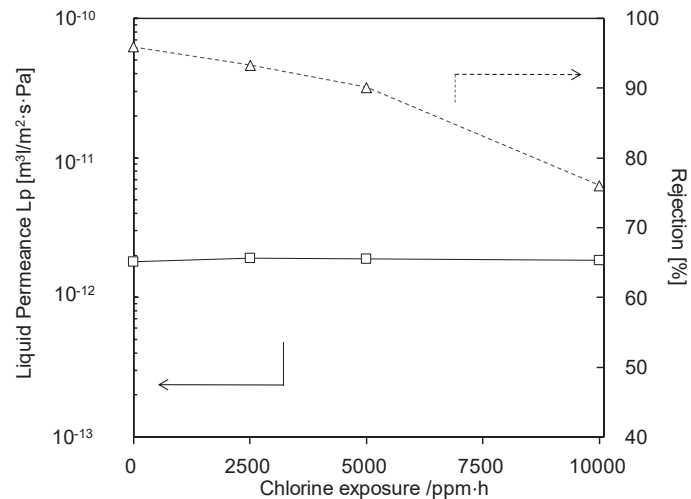


Figure 4.14. Chlorine exposure measurement of PAHE25-based membrane by using 1000 ppm NaClO aqueous solution.

## Summary

In this chapter, the author have discussed a strategy to introduce hydroxyethyl urea groups to PSQ-based RO membranes to increase the permeability of water. The hydroxyethylurea precursor tended to aggregate through hydrogen bonding during the gelation, which can be regarded as a hydrophilic water channel that significantly increased the permeability of the RO membranes. PAHE25- and PAHE2-25-based membranes exhibited excellent permeability of water of  $1.86 \times 10^{-12}$  and  $1.94 \times 10^{-12}$   $\text{m}^3/\text{m}^2\text{sPa}$ , and NaCl rejection of 95.9 and 96.8%, respectively, suggesting that the RO performance was as good as that of commercial organic RO membrane SW30HR ( $1.1 \times 10^{-12}$   $\text{m}^3/\text{m}^2\text{sPa}$  and  $98.5 \pm 0.7\%$ ). It was also demonstrated that the membrane exhibited much higher thermal stability and chlorine resistance than polyamide-based membranes.

## Experimental

### General

Ethanolamine (>99% purity) and (3-isocyanatopropyl)triethoxysilane (95% purity) were obtained from TCI Co., Ltd. BTESPA (95% purity) was obtained from Gelest Inc. These reagents were used as obtained. Dichloromethane employed as the reaction solvent was distilled from  $\text{CaH}_2$  and stored over activated molecular sieves in the dark

until use. Polysulfone support membranes (NTR-7450, pore size: 1 nm) were obtained from Nitto Denko Corporation. NMR spectra were obtained on Varian System 400MR and system500 spectrometers (Figure 4.15 to 20). DLS analysis was performed on a Malvern Zetasizer Nano (ZEN3600) analyzer. TGA was performed on an SII EXSTAR TG-DTA6200 thermal analyzer under a gentle nitrogen flow from 25 °C to 1000 °C. Water contact angles were determined using a Kyowa DM300 contact angle meter. (SEM and AFM images were obtained on an S-4800 HITACHI scanning electron microscope and an AFM-5500 HITACHI atomic force microscope, respectively.

#### *Synthesis of N-(2-hydroxyethyl)-N'-(3-(triethoxysilyl)propyl)urea*

In a two-necked flask fitted with a magnetic stirrer was placed a solution of 0.30 g (4.8 mmol) of ethanolamine in 15 mL of dichloromethane in a dry argon atmosphere. To this was added a solution of 0.80 g (3.2 mmol) of (3-isocyanatopropyl)triethoxysilane in 15 mL of dichloromethane at room temperature, and the resultant mixture was stirred for 0.5 h at this temperature. A colorless liquid (1 g, > 99% yield) was obtained by evaporation of the solvent and excess ethanolamine in vacuo, whose NMR analysis indicated sufficient purity for use in the following reaction without further purification. <sup>1</sup>H NMR (400 MHz in CDCl<sub>3</sub>) δ 5.04 (s, 1H), 4.90 (s, 1H), 3.81 (q, 6H, *J* = 7.0 Hz), 3.58 (t, 2H, *J* = 4.7 Hz), 3.30 (q, *J* = 5.6 Hz, 2H), 3.15 (q, *J* = 7.0 Hz, 2H), 1.61 (m, 2H), 1.22 (t, *J* = 7.0 Hz, 9H), 0.68–0.60 (m, 2H). <sup>13</sup>C NMR (126 MHz in CDCl<sub>3</sub>) δ 159.78, 62.52, 58.34, 43.01, 42.82, 23.55, 18.15, 7.59. MS *m/z* 247 (M<sup>+</sup> -NHCH<sub>2</sub>CH<sub>2</sub>OH).

#### *Synthesis of N-[2,3-bis(trimethylsiloxy)propyl]-N'-[3-(triethoxysilyl)propyl]urea and N-[1,3-bis(trimethylsiloxy)propyl]-N'-[3-(triethoxysilyl)propyl]urea*

In a three-necked flask equipped with a magnetic stirrer 1.00 g (11.0 mmol) of 3-amino-1,2-propandiol was dissolved in 30 mL of nitromethane in a dry argon atmosphere at room temperature. To this was added 0.88 g (5.5 mmol) of bis(trimethylsilyl)amine and the mixture was stirred for 30 min. After that solvent was

removed under vacuum, 2.71 g (11.0 mmol) of (3-isocyanatopropyl)triethoxysilane in 10 mL dry ethanol was subsequently added and stirred for 2 days at room temperature. The solvent was removed under vacuum and the residue was purified by preparative GPC to give a mixture of *N*-[2,3-bis(trimethylsiloxy)propyl]-*N'*-[3-(triethoxysilyl)propyl]urea and its hydrolysis product containing -OTMS groups in 60.3 % yield. <sup>1</sup>H NMR (500 MHz, CD<sub>3</sub>OD) δ 3.81 (q, 6H, *J* = 7.0 Hz), 3.66-3.43 (m, 5H), 3.09 (t, 2H, *J* = 7.3 Hz), 1.59-1.52 (m, 2H), 1.20 (t, 9H, *J* = 7.0 Hz), 0.62-0.59 (m, 2H), 0.14-0.11 (m, 18H). <sup>13</sup>C NMR (100 MHz, CD<sub>3</sub>OD) δ 161.53, 72.70, 65.72, 59.46, 43.98, 43.67, 24.75, 18.67, 8.42, 0.32. MS *m/z* 482 (M<sup>+</sup>).

*N*-[1,3-bis(trimethylsiloxy)propyl]-*N'*-[3-(triethoxysilyl)propyl]urea was synthesized by a similar process using 2-amino-1,3-propanediol. The mixture was purified by preparative GPC with 80.4 % yield. <sup>1</sup>H NMR (400 MHz, CD<sub>3</sub>OD) δ 3.81 (q, 6H, *J* = 7.0 Hz), 3.73-3.53 (m, 5H), 3.09 (t, 2H, *J* = 7.0 Hz), 1.62-1.49 (m, 2H), 1.20 (t, 9H, *J* = 7.0 Hz), 0.60 (t, 2H, *J* = 8.4 Hz), 0.11 (s, 18H). <sup>13</sup>C NMR (100 MHz, CD<sub>3</sub>OD) δ 160.62, 62.00, 59.43, 53.52, 43.51, 24.76, 18.69, 8.44, 0.55. MS *m/z* 482 (M<sup>+</sup>).

#### *SG process for membrane preparation and RO experiments*

The SG process and membrane preparation process was conducted as described in chapter 1, The measurement method of two RO performance parameters, water permeability ( $L_p$ ) and salt rejection ( $R$ ), is the same as described in Chapter 1, which were determined by using equations (1) and (2) [12], respectively.

$$L_p = J_v / (\Delta P - \Delta \pi) \quad (1)$$

$$R = \left(1 - \frac{c_p}{c_f}\right) \times 100\% \quad (2)$$

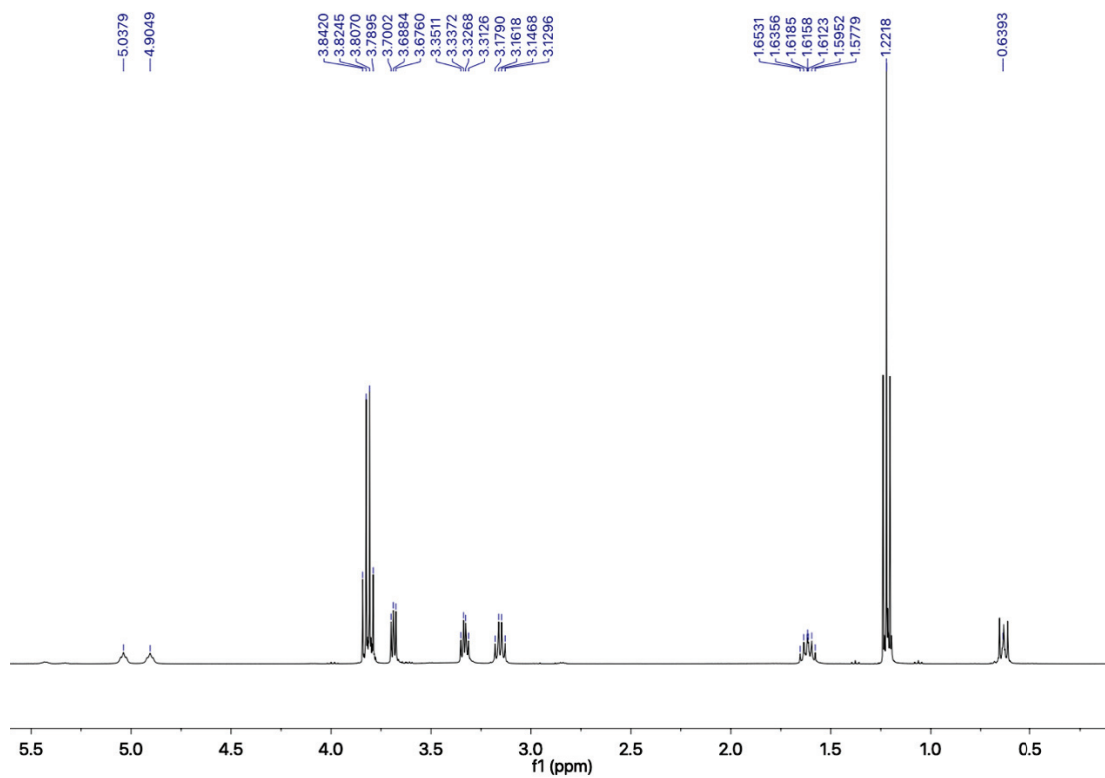


Figure 4.15.  $^1\text{H}$  NMR spectra of HETESPU.

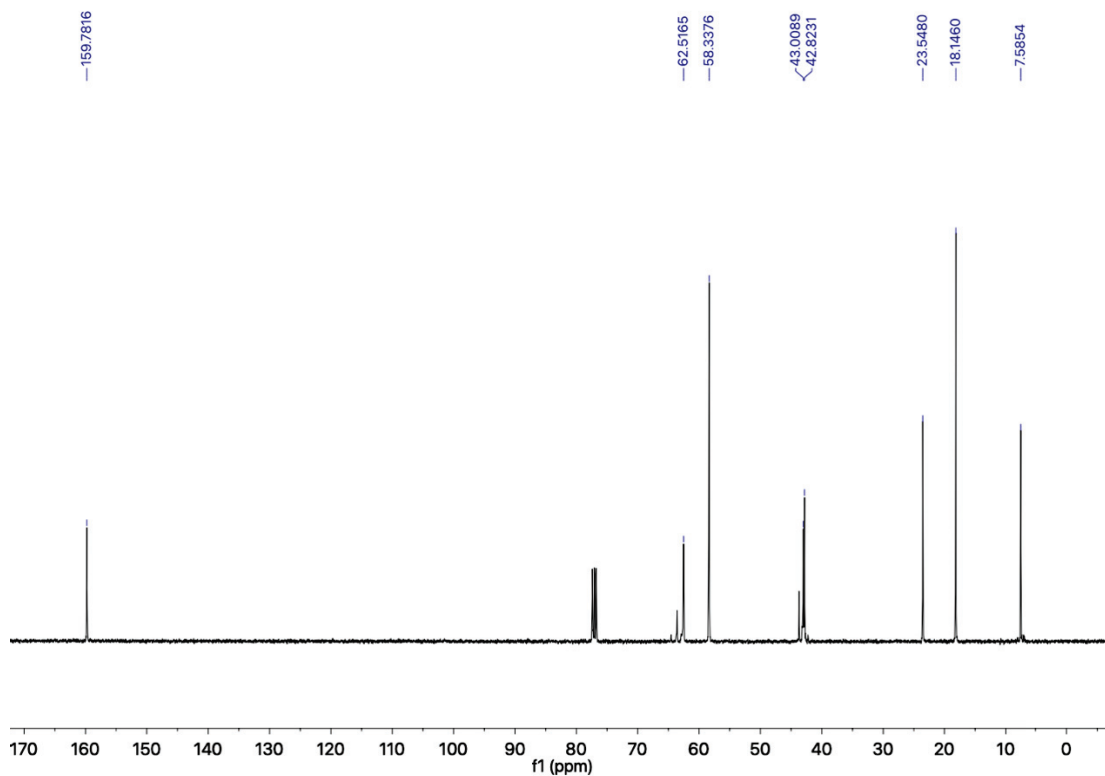


Figure 4.16.  $^{13}\text{C}$  NMR spectra of HETESPU.

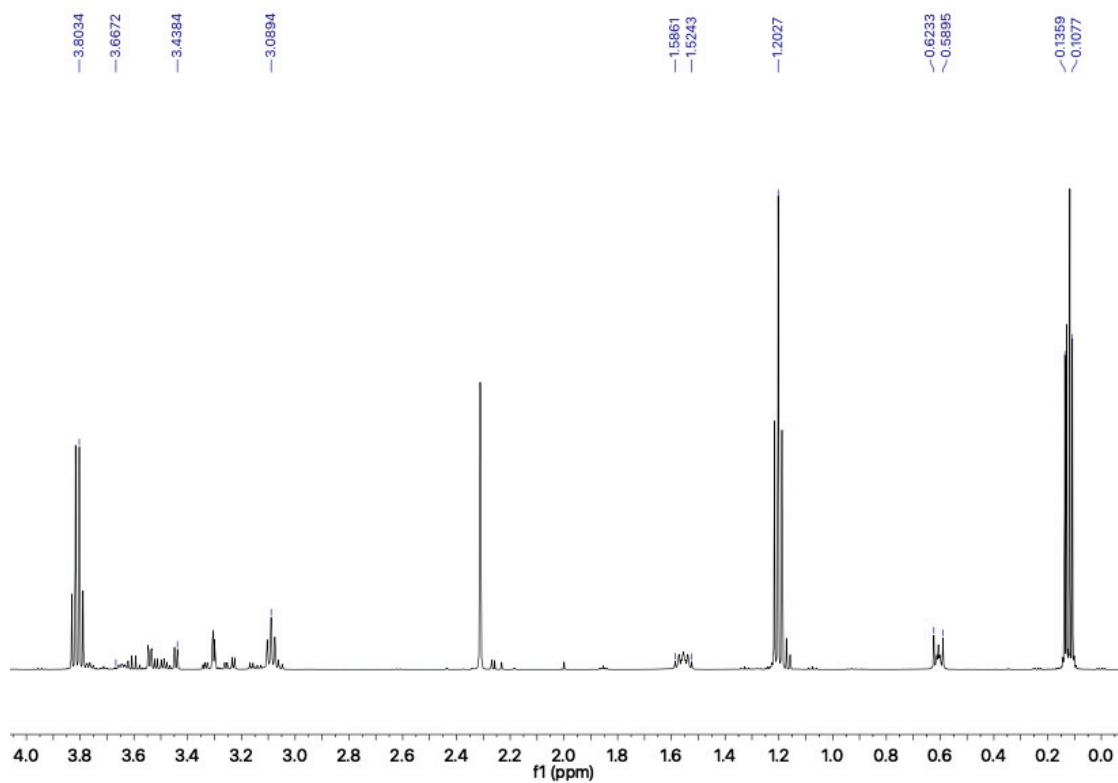


Figure 4.17.  $^1\text{H}$  NMR spectra of *N*-[2,3-bis(trimethylsiloxy)propyl]-*N'*-[3-(triethoxysilyl)propyl]urea.

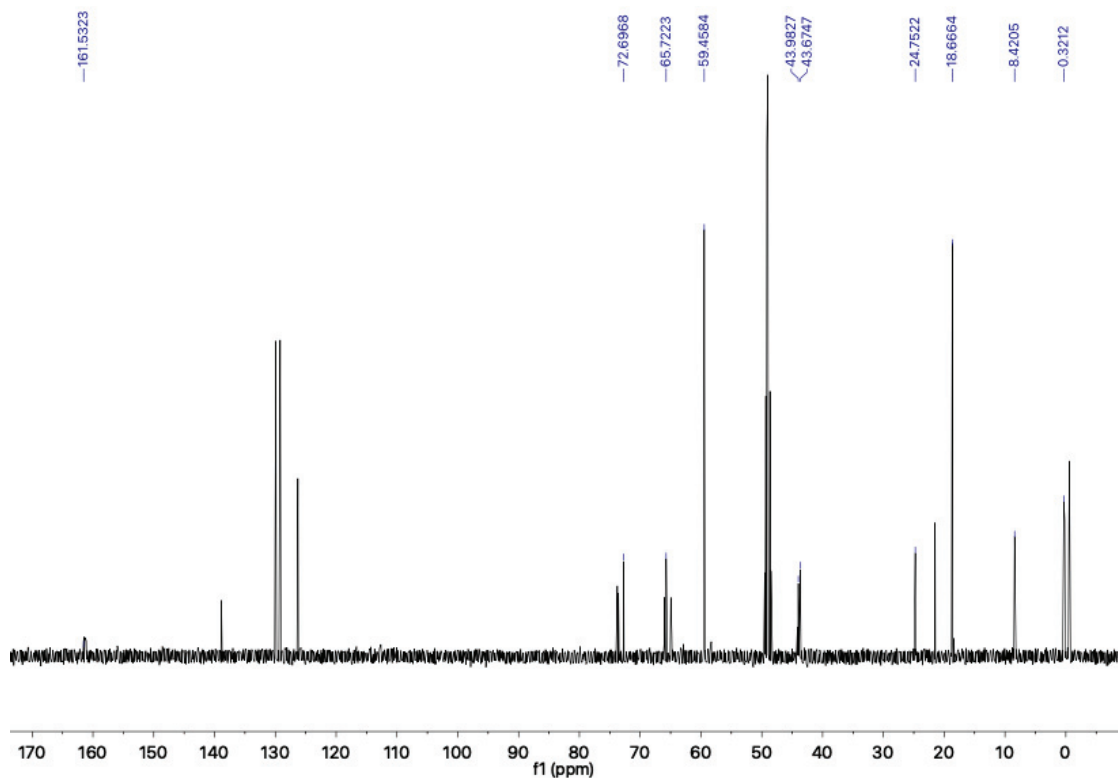


Figure 4.18.  $^{13}\text{C}$  NMR spectra of *N*-[2,3-bis(trimethylsiloxy)propyl]-*N'*-[3-(triethoxysilyl)propyl]urea.

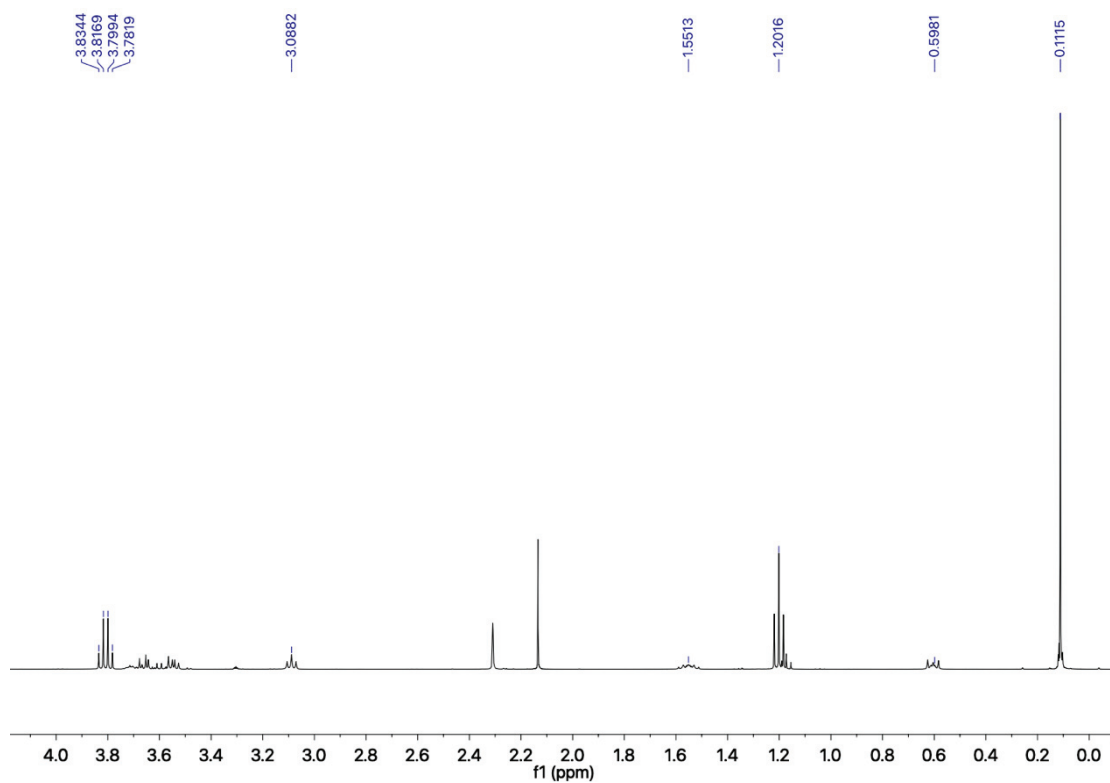


Figure 4.19.  $^1\text{H}$  NMR spectra of *N*-[1,3-bis(trimethylsiloxy)propyl]-*N'*-[3-(triethoxysilyl)propyl]urea.

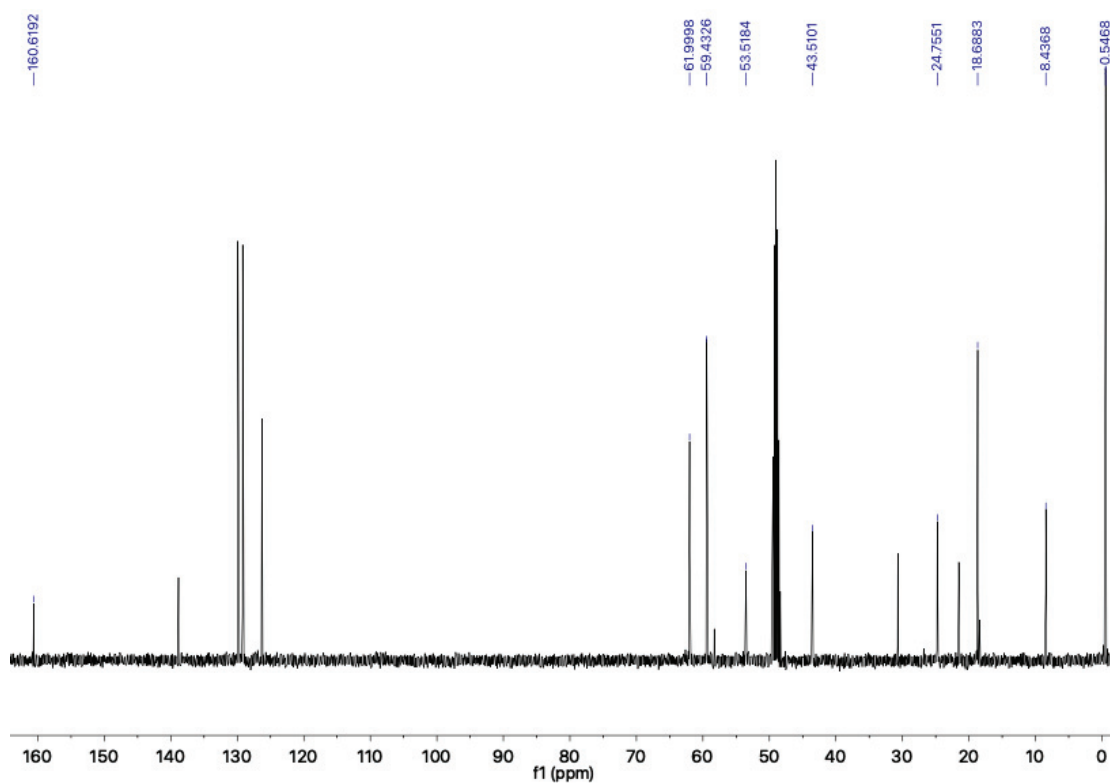


Figure 4.20.  $^{13}\text{C}$  NMR spectra of *N*-[1,3-bis(trimethylsiloxy)propyl]-*N'*-[3-(triethoxysilyl)propyl]urea.



## References

- [1] K. Yamamoto, J. Ohshita, T. Mizumo, M. Kanezashi, T. Tsuru, Preparation of hydroxyl group containing bridged organosilica membranes for water desalination, *Sep. Purif. Technol.*, 156 (2015), 396-402.
- [2] F.-T. Zheng, K. Yamamoto, M. Kanezashi, T. Tsuru, J. Ohshita, Preparation of bridged silica RO membranes from copolymerization of bis(triethoxysilyl)ethene/(hydroxymethyl)triethoxysilane. Effects of ethenylene-bridge enhancing water permeability, *J. Membr. Sci.*, 546 (2018), 173-178.
- [3] E. Licsandru, E. Petit, S. Moldovan, O. Ersen, M. Barboiu, Biomimetic Autocatalytic Synthesis of Organized Silica Hybrids, *Eur. J. Inorg. Chem.*, 2015 (2015), 3637-3641.
- [4] L.-B. Huang, A. Hardiagon, I. Kocsis, C.-A. Jegu, M. Deleanu, A. Gilles, A. van der Lee, F. Sterpone, M. Baaden, M. Barboiu, Hydroxy Channels—Adaptive Pathways for Selective Water Cluster Permeation, *Journal of the American Chemical Society*, 143 (2021), 4224-4233.
- [5] T. Kamitani, A. Ishida, H. Imoto, K. Naka, Supramolecular organogel of polyureas containing POSS units in the main chain: dependence on the POSS and comonomer structures, *Polym. J.*, (2021), 1-7.
- [6] D.S. Bergsman, R.G. Closser, C.J. Tassone, B.M. Clemens, D. Nordlund, S.F. Bent, Effect of backbone chemistry on the structure of polyurea films deposited by molecular layer deposition, *Chem. Mater.*, 29 (2017), 1192-1203.
- [7] K. Yamamoto, S. Koge, K. Sasahara, T. Mizumo, Y. Kaneko, M. Kanezashi, T. Tsuru, J. Ohshita, Preparation of bridged polysilsesquioxane membranes from bis[3-(triethoxysilyl)propyl]amine for water desalination, *Bull. Chem. Soc. Jpn.*, 90 (2017), 1035-1040.
- [8] R. Xu, S.M. Ibrahim, M. Kanezashi, T. Yoshioka, K. Ito, J. Ohshita, T. Tsuru, New insights into the microstructure-separation properties of organosilica membranes with ethane, ethylene, and acetylene bridges, *ACS Appl. Mater. Interfaces*, 6 (2014), 9357-9364.

- [9] K. Yamamoto, H. Muragishi, T. Mizumo, T. Gunji, M. Kanezashi, T. Tsuru, J. Ohshita, Diethylenedioxane-bridged microporous organosilica membrane for gas and water separation, *Sep. Purif. Technol.*, 207 (2018), 370-376.
- [10] K. Yamamoto, M. Kanezashi, T. Tsuru, J. Ohshita, Preparation of bridged polysilsesquioxane-based membranes containing 1,2,3-triazole moieties for water desalination, *Polym. J.*, 49 (2017), 401.
- [11] M. Mänttari, A. Pihlajamäki, E. Kaipainen, M. Nyström, Effect of temperature and membrane pre-treatment by pressure on the filtration properties of nanofiltration membranes, *Desalination*, 145 (2002), 81-86.
- [12] M.L. Lind, D. Eumine Suk, T.-V. Nguyen, E.M. Hoek, Tailoring the structure of thin film nanocomposite membranes to achieve seawater RO membrane performance, *Environ. Sci. Technol. Lett.*, 44 (2010), 8230-8235.

## Chapter 5 Preparation of robust and high RO performance PSQ-RO membranes modified by SiO<sub>2</sub> nanoparticles

### Introduction

In this chapter, as a new strategy to improve the water permeability of PSQ-RO membranes, the author introduced SiO<sub>2</sub> nanoparticles into the bis[3-(triethoxysilyl)propyl]amine (BTESPA)-based RO membrane. The author anticipated that the introduction of SiO<sub>2</sub> nanoparticles will increase not only surface area but also micropore volume in the PSQ separation layer by the filler effect, which will lead to the increase of porosity and thus improve water permeability. In addition, it has been reported that nanoparticle fillers increase the rigidity of the polymer chain through the interaction between the nanoparticles and the polymer, which results in the improvement of thermal stability [1]. The author also anticipated that the introduction of robust and rigid inorganic SiO<sub>2</sub> nanoparticles would stabilize the organically bridged PSQ structure by immobilization, which will increase the thermal stability of the RO membranes.

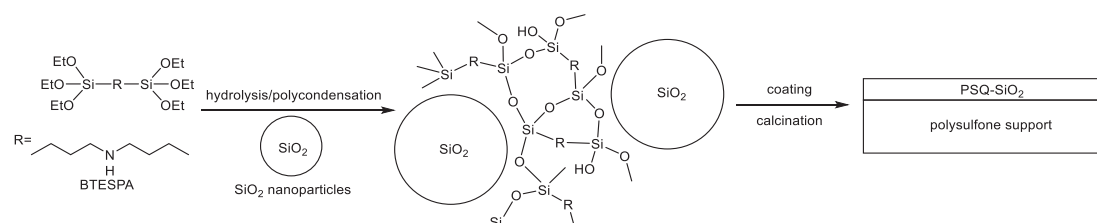


Figure 5.1. Preparation of PSQ-RO membranes modified by SiO<sub>2</sub> nanoparticles.

### Results and discussion

#### *Preparation of membranes by the sol-gel process*

BTESPA-based membranes containing SiO<sub>2</sub> nanoparticles (hereinafter referred to as PASiNP) were prepared by the SG process. Sols were prepared by stirring BTESPA and hydrophobic SiO<sub>2</sub> nanoparticle powders (10 nm, Admatechs Inc) having different weights in 60 eq water of precursor in ethanol for 2 h at room temperature. Membranes obtained after coating and calcination were denoted as PASiNP-X, where X represents the weight percentage of the nanoparticles to the BTESPA precursor. BTESPA

membrane without SiO<sub>2</sub> nanoparticles was also prepared and used as the control membrane (hereinafter, PA membrane).

For PSQ membranes prepared by the SG process, a high calcination temperature tends to promote the gelation, leading to a dense PSQ separation layer for high separation selectivity. However, an excessively high-temperature results in the decomposition of organic bridges, which leads to the loss of separation properties of membranes. To determine the calcination temperature, the author conducted Thermogravimetric analysis (TGA) of these gel powders, as presented in Figure 5.2. The initial mass loss was observed up to 100 °C, which was likely due to the evaporation of adsorbed water in the gels. The second mass loss starting from approximately 300 °C to 320 °C for BTESPA and 350 °C to 400 °C for PASiNP gels can be ascribed to the thermal decomposition of organic units. The second mass loss percentages were calculated based on the mass after the removal of adsorbed water at 100 °C. BTESPA gels exhibited approximately 33 % mass loss, and the mass loss values of PASiNP0.5, PASiNP5, and PASiNP10 gels were 30 %, 29 %, and 25 %, respectively, suggesting smaller second mass loss for the gels with SiO<sub>2</sub> nanoparticles. Compared with BTESPA gels, the PASiNP gels exhibit higher decomposition temperatures, indicating the filler effect of SiO<sub>2</sub> nanoparticles. On the basis of these observations, the author set the calcination temperature at 150 °C for the membrane preparation, which is the upper-temperature limit for the operation of the polysulfone support membrane [2]. RO performance of the supporting membrane before and after calcination at 150 °C for 10 min is summarized in Table 5.1, suggesting indeed that the calcination at this temperature did not affect the supporting membrane properties with respect to water separation. It was reported that calcination of the BTESPA-homopolymer sol at this temperature showed no decomposition of the organic units and the formation of a PSQ network composed of T<sup>2</sup> (-Si(OSi)<sub>2</sub>OH) and T<sup>3</sup> (-Si(OSi)<sub>3</sub>) units.

Table 5.1. RO performance of supporting membrane (NTR-7450), before and after calcination at 150 °C for 10 min.

	Liquid permeance/(m <sup>3</sup> /m <sup>2</sup> ·s·Pa)	NaCl rejection [%]
Before calcination	$2.4 \times 10^{-11}$	13.1
After calcination	$2.5 \times 10^{-11}$	13.1

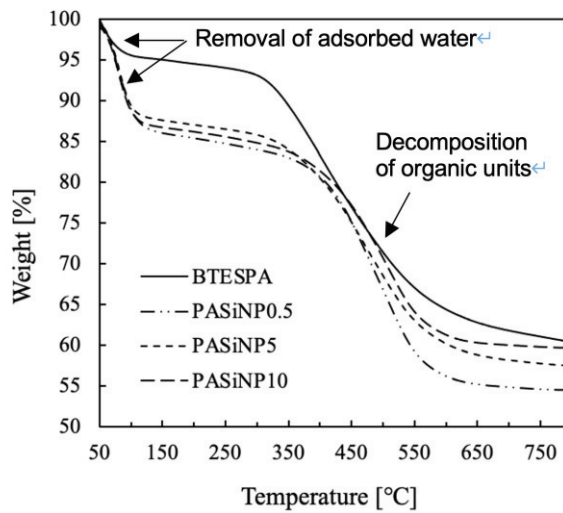


Figure 5.2. TG curves of gel powders in nitrogen atmosphere at the heating rate of 10 °C/min.

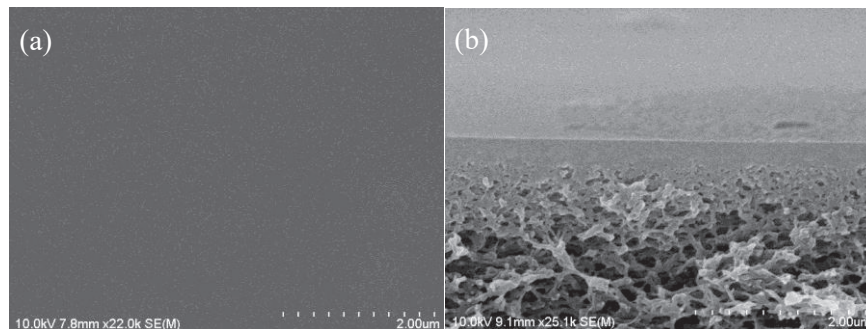


Figure 5.3. (a) Surface image of membrane of PASiNP1. (b) Cross-sectional topographies of membranes of PASiNP1

The surface morphology was examined by SEM, and the image is presented in Figure 5.3(a). A smooth surface on SEM scale was observed without any significant aggregation, although these membranes exhibited roughness in the Atomic force

microscopy (AFM) scale. The cross-sectional morphologies of PASiNP membranes were also examined by SEM, and the image of PASiNP1 membrane is presented in Figure 5.3(b) as a typical example. The border between the PSQ layer and the support layer cannot be clearly seen in the image, indicating good adhesion between them. The AFM structure images and the phase images of the PA and PASiNP membranes are shown in Figure 5.4. Surface roughness ( $S_a$ ) was calculated on the basis of the AFM structure images. The PA membrane showed a smooth surface with  $S_a$  of 0.18 nm. On the other hand, the PASiNP0.5 membrane exhibited  $S_a$  of 0.82 nm. Further increasing the SiO<sub>2</sub> nanoparticle content led to a slight decrease in  $S_a$  and PASiNP10 membrane exhibited  $S_a$  of 0.56 nm. The PA membrane also exhibited a homogeneous surface in the phase image. However, brightly colored areas gradually appeared in the phase images when SiO<sub>2</sub> nanoparticles were introduced, as shown in Figures 5.4(b)–(f), indicating that SiO<sub>2</sub> nanoparticles form hard segments on the surface. As increasing the amount of SiO<sub>2</sub> nanoparticles on the surface, the gaps may be reduced, as illustrated in Figure 5.4(g) through increased coverage of the surface by SiO<sub>2</sub> nanoparticles. However, the roughness was still small with respect to the SiO<sub>2</sub> nanoparticle size (10 nm), thereby indicating no significant aggregation of SiO<sub>2</sub> nanoparticles formed in the membranes probably because of the good miscibility between BTESPA-derived PSQ and SiO<sub>2</sub> nanoparticles. It is presumable that the hydrophobic interaction between the organic units of BTESPA and hydrophobic SiO<sub>2</sub> nanoparticle surface is operative. Hydrophilic interaction and/or bond formation may be also assumed between the BTESPA-derived silanol or amine units and trace silanol groups on the hydrophobic SiO<sub>2</sub> nanoparticle surface. The well dispersed SiO<sub>2</sub> nanoparticles in PSQ matrix were observed by high-resolution Transmission microscope (TEM) images in Figure 5.5.

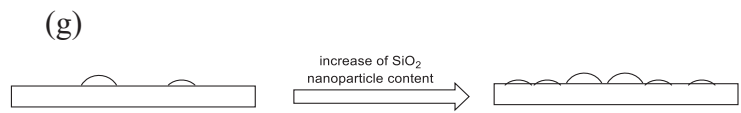
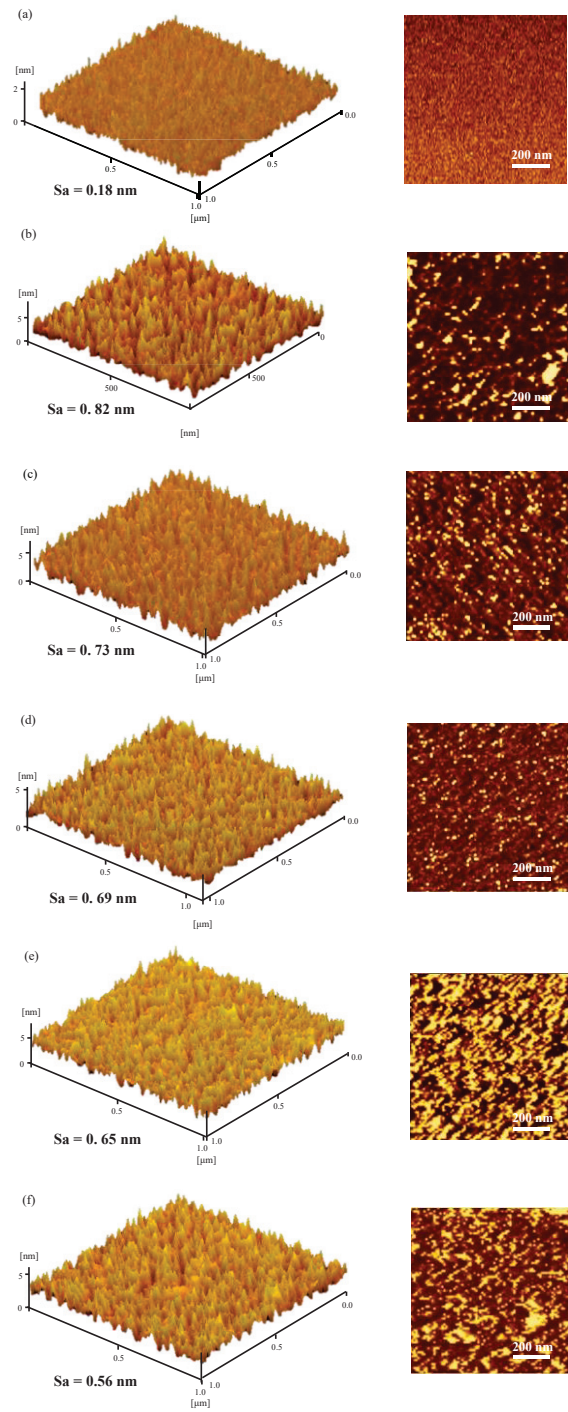


Figure 5.4. AFM structure images (left) and phase images (right) of (a) PA, (b) PASiNP0.5, (c) PASiNP1, (d) PASiNP2.5, (e) PASiNP5, and (f) PASiNP10 membranes, and (g) possible explanation for the decrease of surface roughness as increasing the SiO<sub>2</sub> nanoparticle content. The roughness was calculated for 1 μm × 1 μm area.



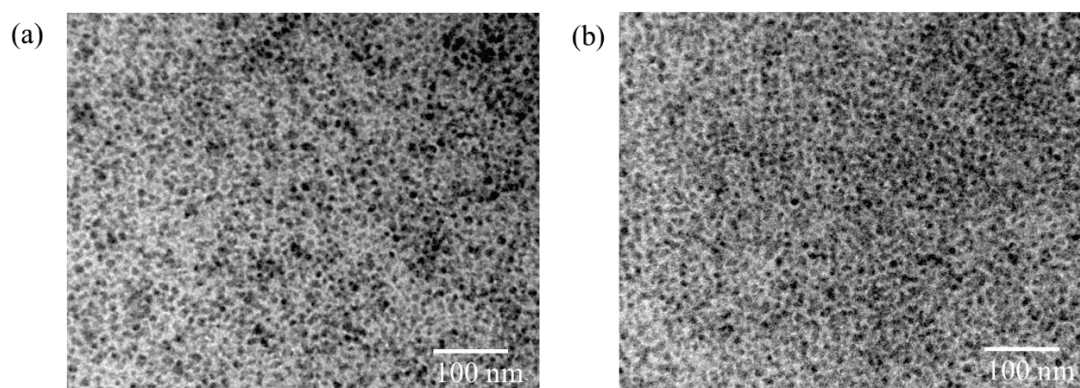


Figure 5.5. TEM images of (a) PASiNP2.5 and (b) PASiNP10 gels.

### *Porous properties*

In general, water permeability of RO membranes was significantly affected by membrane porosity, and porous membranes exhibit high water permeability. To investigate the effect of the introduced SiO<sub>2</sub> nanoparticles on porosity, nitrogen adsorption/desorption isotherm measurements of these gel powders of PA and PASiNP were performed. The respective gel powders were prepared by drying the sols at 60 °C in air for 2 days, followed by calcination at 150 °C in nitrogen for 12 h. The results are shown in Figure 5.6. All of these gel powders showed the nitrogen isotherms of type II characteristics. The PASiNP gel powders exhibited interaction with nitrogen even in the low-pressure region, which was increased as SiO<sub>2</sub> nanoparticle content increased, suggesting an increase in micropore volume. The BET surface areas and the micropore volumes of these gel powders are listed in Table 5.2. The BET surface area of the BTESPA gel powder was 176 m<sup>2</sup>/g. On the other hand, the BET surface areas of the PASiNP gel powders exhibited an increase with increasing SiO<sub>2</sub> nanoparticle content and peaked at 500 m<sup>2</sup>/g, which was approximately three times higher than that of the BTESPA gel powder. Although the BET surface area was decreased by the further introduction of SiO<sub>2</sub> nanoparticles (PASI NP10), it was still higher than that of the BTESPA gel powder. The first increase in BET surface areas was likely due to the introduction of SiO<sub>2</sub> nanoparticles bringing additional micropore volumes between the



BTESPA polymer chains and nanoparticles. However, excess nanoparticles will be packed and leading to a decrease in BET surface area. The results of RO experiments were in agreement with these observations with respect to water permeability. (*vide infra*)

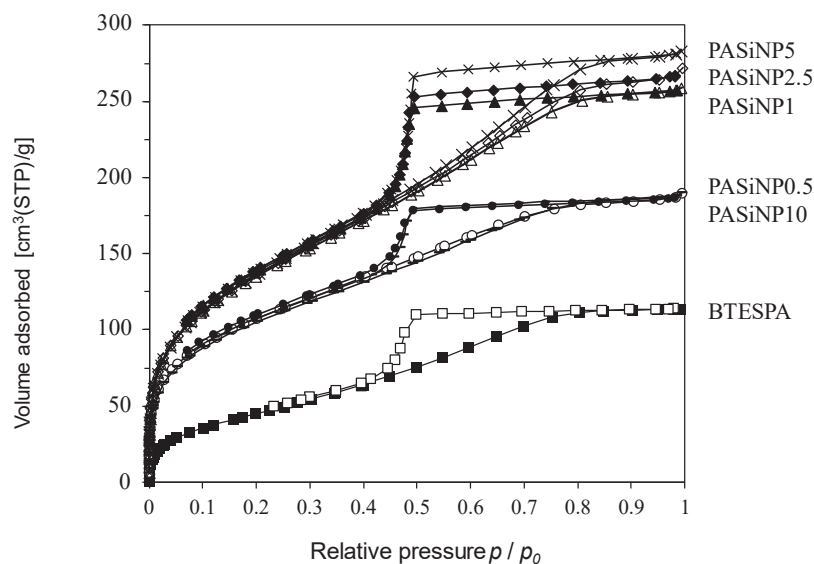


Figure 5.6. N<sub>2</sub> adsorption/desorption isotherms of PASiNP0.5, 1, 2.5, 5, and 10 gel powders and BTESPA gel powder.

Table 5.2. Surface areas and micropore volumes.

Sample	BET surface area (m <sup>2</sup> /g)	Micropore volume (cm <sup>3</sup> /g)
BTESPA	176	0.1762
PASiNP0.5	385	0.2909
PASiNP1	485	0.3996
PASiNP2.5	498	0.4173
PASiNP5	500	0.4366
PASiNP10	275	0.2924

### RO performance

A summary of the RO performance is shown in Figure 5.7. RO experiments of PA and PASiNP membranes were carried out using a 2000 ppm NaCl aqueous solution

under the feed pressure of 1.5 MPa at room temperature. The PA membrane exhibited the lowest water permeability of  $1.3 \times 10^{-13} \text{ m}^3/\text{m}^2\text{sPa}$  among these membranes and the highest water permeability of  $1.2 \times 10^{-12} \text{ m}^3/\text{m}^2\text{sPa}$  was obtained for the PASiNP2.5 membrane, which is approximately 10 times higher than that of the PA membrane. As the author used hydrophobic  $\text{SiO}_2$  nanoparticles, the membrane hydrophilicity would have been rather suppressed. However, the water contact angles of the PASiNP cast film surfaces prepared on glass substrates were lower than that of the PA film (Figure 5.8). The improved porosity seems to be also a reason for the high water permeability. In addition, salt rejection exhibited a slight increase as a result of the introduction of  $\text{SiO}_2$  nanoparticles. Compared with the PA membrane which exhibited a salt rejection of 95.8%, the PASiNP0.5 membrane showed a salt rejection of 96.6%. On the other hand, the PASiNP1, 2.5, and 5 membranes exhibited increased salt rejection of 98.2%, 97.8%, and 98.1%, respectively. However, both liquid permeability and salt rejection were decreased by the further increase in  $\text{SiO}_2$  nanoparticle content, namely, the PASiNP10 membrane exhibited liquid permeability of  $6.5 \times 10^{-13} \text{ m}^3/\text{m}^2\text{sPa}$  and salt rejection of 97.1%. A similar trend was reported for silica-poly(dimethylsiloxane) composite membranes with respect to gas separation, which showed an increase of gas permeance at a low loading ratio of silica up to 15 wt% and then a decrease at 20 wt%. The author also prepared a membrane with 1wt% of hydrophilic  $\text{SiO}_2$  nanoparticles under the same conditions as those for PASiNP1 called PASiNP1', except for using methanol/ethanol mixed solvent instead of ethanol for the sol formation. The membrane water permeability was  $1.12 \times 10^{-12} \text{ m}^3/\text{m}^2\text{sPa}$  as high as that of PASiNP1. However, the salt rejection was 94.0 %, which is lower than that of PASiNP1. It seems likely that the lower salt rejection may be due to the poor miscibility of hydrophilic  $\text{SiO}_2$  nanoparticles, which cannot form a homogeneous separation layer by aggregation in the PSQ separation layer.

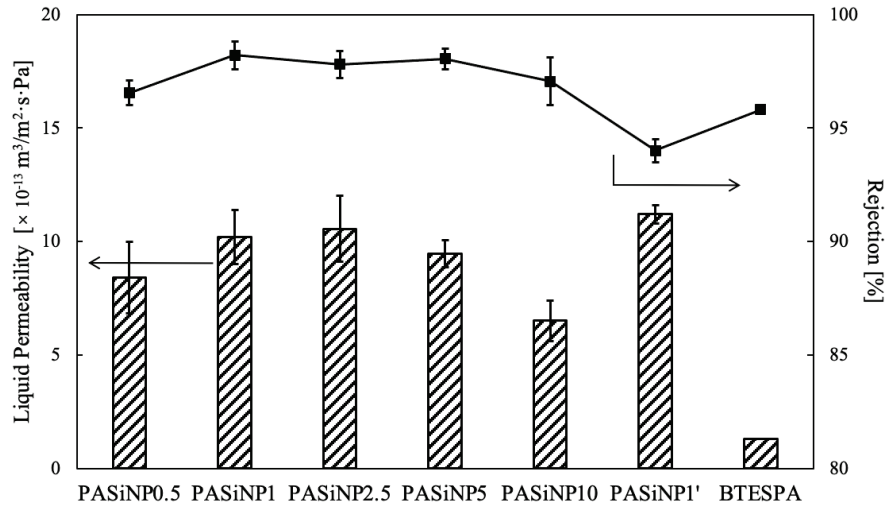


Figure 5.7. RO performance of PASiNP0.5, 1, 2.5, 5, and 10 membranes and PA membrane.

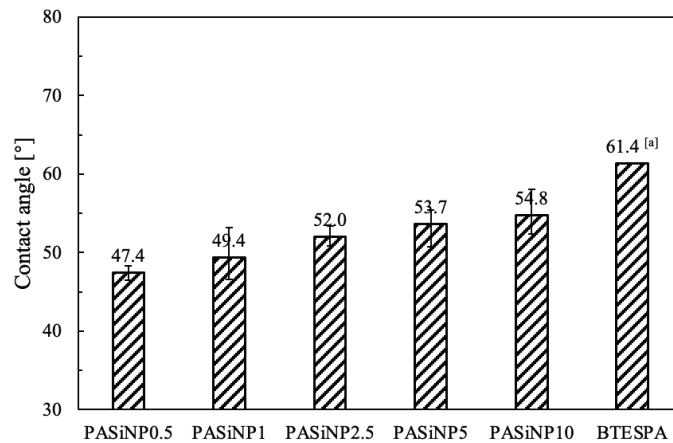


Figure 5.8. Water contact angle of membranes PASiNP0.5, 1, 2.5, 5, 10 and BTESPA.

#### *Resistance to chlorine and thermal stability*

For practical seawater separation, sodium hypochlorite (NaOCl) is widely used in the disinfection process to remove biofilms [3, 4]. To investigate the chlorine resistance of the PASiNP membranes, the author performed chlorine resistance experiments. The membranes were immersed in 1000 ppm NaOCl aqueous solution for 10 h at room temperature. The PA membrane demonstrated excellent resistance to chlorine: no obvious changes in water permeability and salt rejection were apparent up to 10,000 ppm·h NaClO exposure, as presented in Figure 5.9. The PASiNP membranes also exhibited favorable resistance to chlorine exposure; salt rejection decreased by only

0.2–1.8% after 10,000 ppm·h NaClO exposure, which indicates that the introduction of SiO<sub>2</sub> nanoparticles has no significant influence on chlorine resistance.

In addition, thermal stability measurements of the PA and PASiNP membranes were carried out with a stepwise increase in feed temperature from 25 to 95 °C, in which the feed temperature was kept at each temperature for 3 h. The results are shown in Figure 5.10. Compared with the water permeability and the salt rejection at 25 °C, water permeability of the PA membrane was increased by approximately 9-fold at 95 °C. This may be due to the thermal vibration of the polymer network. At the same time, salt rejection was decreased by 4.7% from 95.8% to 91.1%. Upon lowering the operation temperature again to room temperature, the performance could not be recovered as shown in Figure 5.13. This seems to indicate that performance changes at elevated temperature for PA membrane is due to not only enhanced thermal vibration of the polymer network, but also degradation of the polymer structure. PASiNP membranes exhibited much higher thermal stability with smaller changes in the performance, showing a decrease in salt rejection less than 2.5% and an increase of water permeability by approximately two times as the operating temperature was elevated to 95 °C. When the temperature was lowered to room temperature, salt rejection was recovered, although the water permeability was decreased to an extent ( $3.8 \times 10^{-13} \text{ m}^3/\text{m}^2\text{sPa}$ ), as illustrated in Figure 5.11, in contrast to the PA membrane. Compared to other high-performance PSQ-RO membranes reported previously with water permeability and salt rejection higher than  $1 \times 10^{-12} \text{ m}^3/\text{m}^2\text{sPa}$  and 95%, respectively [5, 6], the PASiNP2.5 membrane exhibits the highest thermal stability. Other high-performance PSQ-RO membranes exhibited thermal stability only up to 70-80 °C [5, 6]. To further investigate the thermal stability of the membranes, the author examined the performance changes of PASiNP1 membrane on repetitive heating and cooling cycles from room temperature to 95 °C. As presented in Figure 5.12, the PASiNP1 membrane exhibited gradual decreases in both water permeability and salt rejection. However, it is still noteworthy that the membrane showed only slight decreases in these parameters even after heating at 95 °C and reached stable states after the third cycle.

The improvement in thermal stability of these modified membranes seems to be due to the robust and rigid inorganic SiO<sub>2</sub> nanoparticles stabilizing the organically bridged PSQ structure by immobilization, thus increasing the thermal stability of the RO membranes. The modified membranes demonstrated high water permeability and high salt rejection at high temperatures. Compared with commercial polyamide-based membranes for which the operating temperature limit is 45 °C [7], the PASiNP membranes show high potential for high-temperature operation.

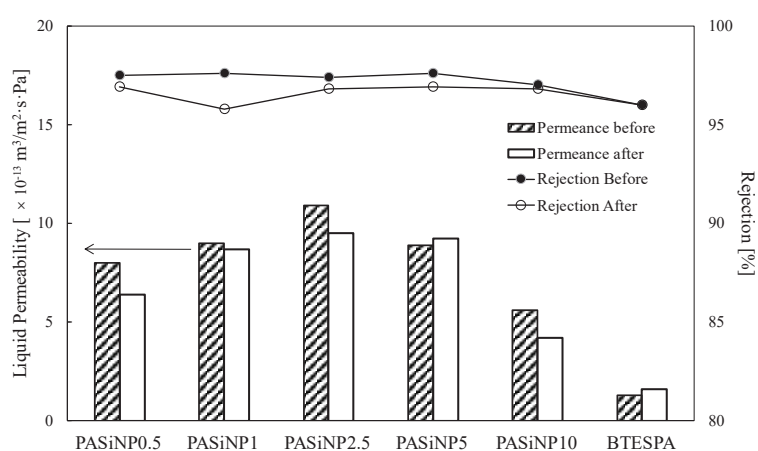


Figure 5.9. RO performance of PASiNP0.5, 1, 2.5, 5, and 10 membranes and PA membrane before and after 10,000 ppm·h NaClO exposure.

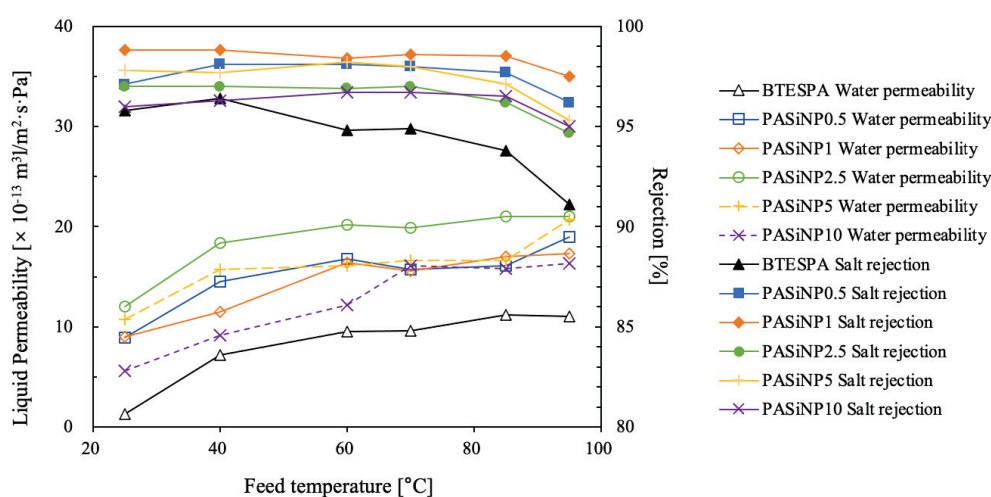


Figure 5.10. Thermal stability measurement of (a) BTESPA, (b) PASiNP0.5, (c) PASiNP1, (d) PASiNP2.5, (e) PASiNP5, and (f) PASiNP10 membranes using 2000 ppm NaCl aqueous solution.

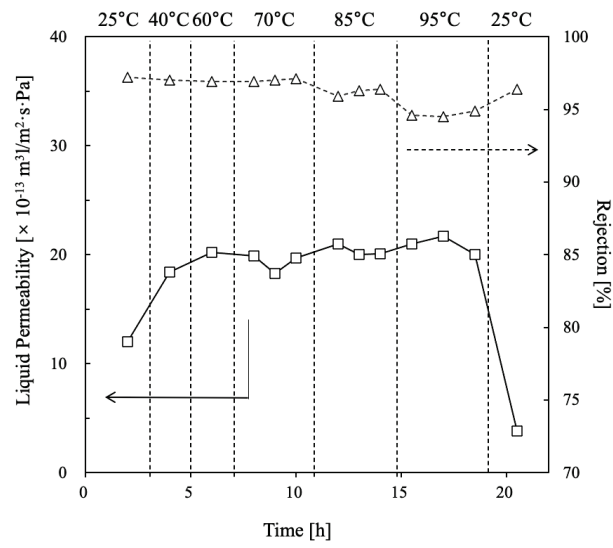


Figure 5.11. Thermal stability measurement of PASiNP2.5 membrane.

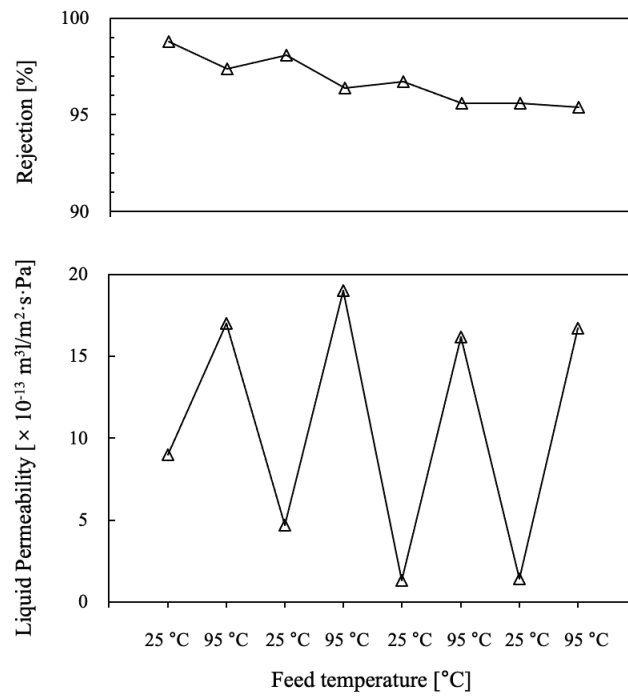


Figure 5.12. Thermal stability measurement of PASiNP1 membrane, by heating up to 95 °C and cooling down to room temperature for 4 cycles.

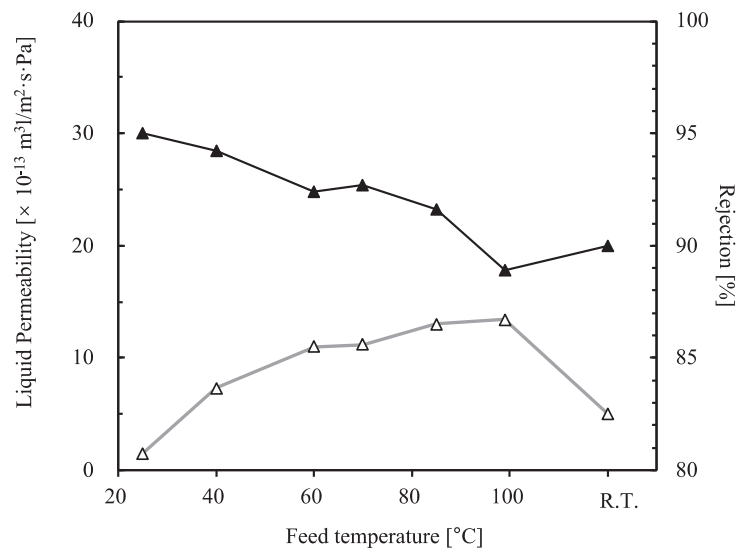


Figure 5.13. Thermal stability measurement of PA membrane.

## Conclusions

In conclusion, the author has modified BTESPA-based PSQ-RO membranes with  $\text{SiO}_2$  nanoparticles. The introduction of  $\text{SiO}_2$  nanoparticles significantly increased the BET surface area, thereby increasing membrane porosity and permeability. The modified membranes exhibited favorable water permeability and high salt rejection. The water permeability of  $1.2 \times 10^{-12} \text{ m}^3/\text{m}^2\text{sPa}$  for the PASiNP2.5 membrane is approximately 10 times higher than the water permeability of the membrane without  $\text{SiO}_2$  nanoparticles and similar to that of commercially available organic RO membrane SW30HR (water permeability  $1.1 \times 10^{-12} \text{ m}^3/\text{m}^2\text{sPa}$ , salt rejection  $98.5 \pm 0.7\%$ ) [8]. In addition, the PASiNP2.5 membrane exhibited a high salt rejection of 97.8%, which is slightly higher than that of the PA membrane. In addition, the modified membranes showed excellent performance in terms of chlorine resistance and favorable thermal stability up to 95 °C, indicating their potential application as robust membranes. This work is the first on PSQ-RO membranes modified by  $\text{SiO}_2$  nanoparticles, which may be applicable to other PSQ-based membranes. Despite our efforts, the author cannot fully understand the mechanism for improved performance of BTESPA membrane by

the introduction of SiO<sub>2</sub> nanoparticles, although interface structure between PSQ polymer and SiO<sub>2</sub> nanoparticles, void formation, and changes of PSQ morphology may affect the performance as proposed for mixed matrix membranes that consist of composites of base polymers and nanofillers. However, the increased water permeability, the high salt rejection, the improved thermal stability, and the excellent chlorine resistance clearly indicate that this method has great potential for the preparation of PSQ-RO membranes for practical use.

## **Experimental**

### *General*

Bis[3-(triethoxysilyl)propyl]amine with 95% purity was purchased from Gelest Inc. Hydrophobic SiO<sub>2</sub> nanoparticle powder (10 nm) was purchased from Admatechs Inc, while hydrophilic SiO<sub>2</sub> nanoparticle (12 nm) was obtained as a 10wt% methanol sol from Nissan Chemical Corporation. All chemicals were used without further purification. Ethanol used as the reaction solvent during the SG process was distilled from Mg and stored over activated molecular sieves in the dark until use. TGA was conducted using an SII EXSTAR TG-DTA6200 thermal analyzer in the temperature range of 50 °C to 1000 °C at the heating rate of 10 °C/min under a gentle nitrogen flow. Contact angle measurements were performed with a Kyowa DM300 contact angle meter. AFM measurements were carried out on an AFM-5500 HITACHI atomic force microscope. Nitrogen adsorption/desorption isotherm measurements were performed using a BELSORP-MAX II 034VP-MZ (MicrotracBEL). TEM images were obtained by using a JEOL model JEM-2010 microscope (200 kV) at N-BARD Hiroshima University on samples prepared by coating copper mesh grids with PSQ gel suspensions and then evaporation of the solvent.

### *Sol-gel process for membrane preparation and evaluation of RO performance*

The SG process and membrane preparation process were conducted as described in chapter 1. The measurement method of two RO performance parameters, water



permeability ( $L_p$ ) and salt rejection ( $R$ ), is the same as described in Chapter 1, which were determined by using equations (1) and (2) [9], respectively.

$$L_p = J_v / (\Delta P - \Delta \pi) \quad (1)$$

$$R = \left(1 - \frac{c_p}{c_f}\right) \times 100\% \quad (2)$$

## References

- [1] J.-F. Li, Z.-L. Xu, H. Yang, L.-Y. Yu, M. Liu, Effect of TiO<sub>2</sub> nanoparticles on the surface morphology and performance of microporous PES membrane, *Appl. Surf. Sci.*, 255 (2009), 4725-4732.
- [2] K. Yamamoto, S. Koge, K. Sasahara, T. Mizumo, Y. Kaneko, M. Kanezashi, T. Tsuru, J. Ohshita, Preparation of bridged polysilsesquioxane membranes from bis[3-(triethoxysilyl)propyl]amine for water desalination, *Bull. Chem. Soc. Jpn.*, 90 (2017), 1035-1040.
- [3] J. Glater, S.-k. Hong, M. Elimelech, The search for a chlorine-resistant reverse osmosis membrane, *Desalination*, 95 (1994), 325-345.
- [4] R. Wang, Z.-X. Low, S. Liu, Y. Wang, S. Murthy, W. Shen, H. Wang, Thin-film composite polyamide membrane modified by embedding functionalized boron nitride nanosheets for reverse osmosis, *J. Membr. Sci.*, 611 (2020), 118389.
- [5] D. Zhang, M. Kanezashi, T. Tsuru, K. Yamamoto, T. Gunji, Y. Adachi, J. Ohshita, Development of PSQ-RO membranes with high water permeability by copolymerization of bis [3-(triethoxysilyl) propyl] amine and triethoxy (3-glycidylxypropyl) silane, *J. Membr. Sci.*, 644 (2022), 120162.
- [6] D. Zhang, J. Ohshita, Preparation of robust RO membranes for water desalination by interfacial copolymerization of bis[(triethoxysilyl)propyl]amine and bis(triethoxysilyl)ethane, *Polym. J.*, 51 (2019), 1231-1234.
- [7] P. Karami, B. Khorshidi, M. McGregor, J.T. Peichel, J.B. Soares, M. Sadrzadeh, Thermally stable thin film composite polymeric membranes for water treatment: A review, *Journal of Cleaner Production*, 250 (2020), 119447.

- [8] E.S. Hatakeyama, C.J. Gabriel, B.R. Wiesenauer, J.L. Lohr, M. Zhou, R.D. Noble, D.L. Gin, Water filtration performance of a lyotropic liquid crystal polymer membrane with uniform, sub-1-nm pores, *J. Membr. Sci.*, 366 (2011), 62-72.
- [9] M.L. Lind, D. Eumine Suk, T.-V. Nguyen, E.M. Hoek, Tailoring the structure of thin film nanocomposite membranes to achieve seawater RO membrane performance, *Environ. Sci. Technol. Lett.*, 44 (2010), 8230-8235.

## Chapter 6 Conclusions

In conclusion, the author proposed four strategies to improve the water permeability of PSQ-RO membranes, including the design and synthesis of new precursors, the introduction of hydroxyl groups and hydrophilic water channels, and the composite formation with SiO<sub>2</sub> nanoparticles. The author also discussed the membranes preparation process of the sol-gel process and interfacial polymerization.

In Chapter 1, the author examined TTESPA, TTESMA, TDEMSPA, TTESP2A, and TTESP3A as new precursors for PSQ-RO membrane preparation by both interfacial polymerization and the sol-gel process. The TTESPA-based membranes exhibited good RO performance of  $7.3 \times 10^{-13} \text{ m}^3/\text{m}^2\text{sPa}$  and  $1.7 \times 10^{-13} \text{ m}^3/\text{m}^2\text{sPa}$  water permeance and 95.6 % and 96.6 % NaCl rejection for those prepared by the interfacial polymerization and the sol-gel process, respectively. The difference of RO performance of membranes prepared from sol-gel process and the interfacial polymerization has also been discussed. The interfacial polymerization can form a sparser but thicker membrane than the sol-gel process, and as a result, water permeability is improved, but salt rejection is slightly lowered.

In Chapter 2, the author successfully introduced epoxy groups into PSQ-RO membranes. The epoxy groups significantly improved membrane hydrophilicity through the formation of hydroxy groups by the ring opening reactions, thereby increasing membrane permeability. The author conducted studies on the condensation/hydrolysis of the C–O–Si group. The surface C–OH group content increased as the immersion time increased, resulting in the improvement of membrane permeability. PA-TEG2-based membrane exhibited high water permeability of  $9.6 \times 10^{-13} \text{ m}^3/\text{m}^2\text{sPa}$  and excellent salt rejection of 97.5%, which were close to those of commercially available polyamide RO membrane SW30HR. In addition, this membrane showed resistance to chlorine and excellent thermal stability up to 60 °C, indicating potential application as a robust membrane.

In Chapter 3, the author successfully introduced hydroxyethylurea groups to PSQ-based RO membranes to increase the permeability of water. The hydroxyethylurea

groups tended to cause aggregation through hydrogen bonding during the gelation process, which formed hydrophilic water channels that significantly increased the permeability of the RO membranes. PAHE25- and PAHE2-25- based membranes exhibited the highest RO performance so far obtained from PSQ RO membrane with permeability of water being  $1.86 \times 10^{-12}$  and  $1.94 \times 10^{-12} \text{ m}^3/\text{m}^2\text{sPa}$  and with NaCl rejection being 95.9% and 96.8 %, respectively. The author also found that the membrane exhibited much higher thermal stability and chlorine resistance than polyamide-based membranes. This is a new molecular design of PSQ-based membranes. The introduction of hydrogen bonding forms a hydrophilic water channel, improving the water permeability.

In Chapter 4, the author has modified BTESPA-based PSQ-RO membranes with  $\text{SiO}_2$  nanoparticles. The BET surface area was significantly increased after the introduction of  $\text{SiO}_2$  nanoparticles, thereby increasing membrane porosity and permeability. The water permeability of  $1.2 \times 10^{-12} \text{ m}^3/\text{m}^2\text{sPa}$  for the PAsiNP2.5 membrane is approximately 10 times higher than the water permeability of the BTESPA-based membrane without  $\text{SiO}_2$  nanoparticles. In addition, the PAsiNP2.5 membrane exhibited a high salt rejection of 97.8%, which is slightly higher than that of the BTESPA-based membrane. In addition, the modified membranes showed excellent performance in terms of chlorine resistance and favorable thermal stability up to 95 °C, indicating their high potential as robust membranes.

On the basis of the above-mentioned results, all of these strategies exhibited significant improvement in RO performance. The resultant membranes showed favorable resistance to heat treatment and chlorine exposure, suggesting these PSQ-RO membranes have high potential application as robust membranes.

## List of publications

### Chapter 2.

Preparation of polysilsesquioxane reverse osmosis membranes for water desalination from tris [(ethoxysilyl) alkyl] amines by sol–gel process and interfacial polymerization.

Dian Zhang, Masakoto Kanezashi, Toshinori Tsuru, Kazuki Yamamoto, Raku Yakuwa, Takahiro Gunji, Yohei Adachi, Joji Ohshita

Applied Organometallic Chemistry, **2021**, *35(11)*, e6374.

### Chapter 3.

Development of PSQ-RO membranes with high water permeability by copolymerization of bis[3-(triethoxysilyl)propyl]amine and triethoxy (3-glycidyoxypropyl)silane

Dian Zhang, Masakoto Kanezashi, Toshinori Tsuru, Kazuki Yamamoto, Takahiro Gunji, Yohei Adachi, Joji Ohshita

Journal of Membrane Science, **2022**, *644*, 120162.

### Chapter 4.

Development of Highly Water-Permeable Robust PSQ-Based RO Membranes by Introducing Hydroxyethylurea-Based Hydrophilic Water Channels

Dian Zhang, Masakoto Kanezashi, Toshinori Tsuru, Kazuki Yamamoto, Takahiro Gunji, Yohei Adachi, Joji Ohshita

ACS Applied Materials & Interfaces, **2022**, *14(18)*, 21426-21435

### Chapter 5.

Development of robust and high-performance polysilsesquioxane reverse osmosis membranes modified by SiO<sub>2</sub> nanoparticles for water desalination

Dian Zhang, Masakoto Kanezashi, Toshinori Tsuru, Kazuki Yamamoto, Takahiro Gunji, Yohei Adachi, Joji Ohshita

Separation and Purification Technology, **2022**, *296*, 121421

This doctoral thesis includes contents reproduced from the papers listed above with permission of the publishers.

Other papers not included in this thesis

Preparation of robust RO membranes for water desalination by interfacial copolymerization of bis[(triethoxysilyl)propyl]amine and bis(triethoxysilyl)ethane

Dian Zhang, Joji Ohshita

Polymer Journal, **2019**, *51(11)*: 1231-1234.

## **Acknowledgements**

This thesis is a summary of my studies from 2019 to 2022 under the direction of Professor Joji Ohshita at Hiroshima University.

I would like to express my sincere gratitude to my supervisor Professor Joji Ohshita for his kind and helpful advice and encouragement. I also would like to thank Professor Toshinori Tsuru, Associate Professor Masakoto Kanezashi, Assistant Professor Yohei Adachi, Lecturer Takashi Hamada, Professor Takahiro Gunji, Lecturer Kazuki Yamamoto for their useful advices and helps.

I would like to thank Mr. Katsuhiro Horata, Mr. Daiji Katsura, Ms. Sakino Takase, Mr. Tetsuya Maeda, Mr. Sun Weipeng, Ms. Wang Conghuan, Mr. Takashi Kai, Mr. Keigo Kawakami, Mr. Kei Oshima, Ms. Maho Kurihara, Mr. Mitsuru Sakabe, Mr. Tetsuya Sugimoto, Mr. Kohei Yamada, Mr. Arata Tanaka, Mr. Takumi Hasegawa, Mr. Tsubasa Yoshio, Mr. Lin Zhixin, Mr. Shota Terao, Mr. Ryuji Matsuura, Mr. Ryuto Miyazaki for their kindness and collaboration. We also thank Mr. Toshiyuki Kawashima in Nitto Denko Corporation for performing the SEM measurements in part.